

Fig. D.V.2. Electron-diffraction patterns of M_4C_3 : (a) [001] zone, (b) [110] zone, and (c) [112] zone. (Dyson and Andrews.)

to [111] which divide the reciprocal lattice distance 220 into three. In this case the weak maxima are not along this [220] vector. A well-defined row of subsidiary spots is, however, found along a line parallel to [351].

The replica was known to be composed primarily of vanadium carbide which has a variable composition and could contain nitrogen or oxygen atoms. The streaking appears to be due to the existence of ordered domains or stacking faults, and extra spots in the same directions would also fit ordering or hexagonal-cell formation. The one-third separations are believed to be due to a separate epitaxial oxide phase analogous to the titanium phase as described by Vere and Smallman.

Dr. H. MCL. CLARK (University of Illinois, U.S.A.): I notice that Professor Rao found a maximum drop in resistivity at 40% Ag in the Ag-Pd alloy, but at 50% Ag there is an increase. I wonder if there is an explanation for this effect. I know that in Cu-Pd the ordered phase is situated on the copper-rich side. The second point is why was such a small deformation—9% reduction in area—used? Would it not be possible to increase this a little?

Professor K. KRISHNA RAO (University of Nebraska, U.S.A.): In this system the maximum resistivity change corresponds to ~ 15 or 16% reduction in area. Further cold work causes the resistivity to increase.

Dr. CLARK: My point is that the maximum decrease in resistivity was found; that corresponds to short-range order.

Dr. J. KITTL (Argentine Atomic Energy Commission, Buenos Aires, Argentine): I would like to ask Professor Rao how he separates the contribution of recovery from the order contribution when changing the temperature.

Professor RAO: One of the ways to deal with this is to look at an alloy that does not show a sharp recovery, and then study both contributions.

Dr. D. H. WARRINGTON (University of Sheffield): I would like to ask Dr. Southworth whether it is possible to distinguish between the end of short-range order and the start of long-range order.

Dr. H. N. SOUTHWORTH (University of Cambridge): I do not think there is any distinction between these two cases; long-range order is an extension of short-range order. All one can say is that in the field-ion microscope the image gets more and more regular. I would state, however, that there is a change in symmetry. While the image is still showing cubic symmetry, there may be either short-range or partial long-range order. When it begins to exhibit tetragonal symmetry I would say it is certainly a case of long-range order.

Dr. B. RALPH (University of Cambridge): One point I should like to add here in answer to Dr. Warrington's question is that in a small volume you can, in fact, state the absolute order parameter within that volume. In other words you can work out how many atoms are in their correct positions.

Dr. H. I. AARONSON (Ford Motor Co. Research Laboratories, Dearborn, U.S.A.): Newkirk *et al.** indicated that both coherent and incoherent growth can occur at the same reaction temperature in the same part of the specimen. I wonder if the authors' explanation of the transformation sequence in the system can accommodate such an arrangement.

* J. B. Newkirk, A. H. Geisler, D. L. Martin, and R. Smoluchowski, *Trans. Amer. Inst. Min. Met. Eng.*, 1950, **188**, 1249.

Dr. SOUTHWORTH: I believe that you are referring to the occurrence of a different ordering process at the grain boundaries. We have not actually observed any grain boundaries in this study. You will appreciate that in the field-ion microscope such a tiny volume is studied that we have not hit on one. I think this would be a separate nucleation event.

Professor R. B. NICHOLSON (University of Manchester): Concerning the ordering that took place at the low temperature, the whole interface looked extremely diffuse, which at first sight is a rather surprising result.

Dr. SOUTHWORTH: This is really part of the basis of our explanation of ordering up to 500° C. By having a diffuse interface one avoids the interface-energy terms. The interface can afford to be diffuse because the free energy of ordering at these temperatures is high. Consequently, even with a

partial-long-range ordered diffuse interface a fairly high free energy is still released when atoms cross this interface.

Professor NICHOLSON: If I understand the explanation correctly, it is very similar to that for the formation of a transition precipitate in an ordinary precipitation system whereby you sacrifice the volume energy to get a structure that is more similar to the matrix, but even in this situation you still try to minimize what interfacial free energy there is by minimizing the area of the interface. In this case it looks as though the area is very large.

Dr. RALPH: I think the point is that it is diffuse in two senses. It is diffuse in the sense that it does not have a regular habit plane and it is also diffuse in the sense that it does not represent a sharp change in order, i.e. there is a wide region over which the order is changing. There is not just a one-atom-diameter interface between order and disorder.

The Role of Interfaces in Phase Transformations

M. Hillert

Some effects of interfaces on solid-state phase transformations are examined using a simple model where the interface is regarded as a thin film of boundary "phase" having its own molar free-energy function for binary alloys. The free-energy losses during the movement of such an interface are evaluated from free-energy diagrams. Two mechanisms of free-energy dissipation are found, caused by diffusion ahead of the interface and inside the interface. The force necessary for moving the grain boundaries in a single-phase binary alloy at a given rate is estimated from this model and the result agrees with the impurity-drag effect treated by Cahn. In particular, the force decreases at high rates as a result of an increasing deviation from local equilibrium at the interface. For discontinuous precipitation, the deviation from local equilibrium at the interface results in a force pulling the grain boundary along with the precipitating phase, thus supplying a force necessary for this kind of reaction. It is suggested that discontinuous precipitation can occur only when there is a deviation from local equilibrium. A detailed calculation of the diffusional process during discontinuous precipitation is carried out and compared with equivalent calculations for a eutectoid transformation under volume or grain-boundary diffusion. The dissipation of free energy under "zero-growth-rate" conditions is examined and Zener's optimum-spacing hypothesis is discussed. The conditions for diffusionless transformation are examined in some detail. The effect of alloying elements on the transformation of austenite is discussed considering the behaviour of an alloying element in and close to the moving interface. The simple pile-up model for the effect is accepted at high temperatures. At lower temperatures two new effects occur; first an increasing free-energy loss due to diffusion inside the interface and, secondly, an increasing deviation from local equilibrium at the interface. As an application, the *TTT* diagram for the ferrite formation in a molybdenum steel is explained, making use of Hultgren's concept of paraequilibrium.

Grain boundaries and phase boundaries are often considered as mathematically sharp boundaries, although they have important physical properties. As an example of such a property, the specific interfacial energy, σ , may give rise to a pressure difference if the surface is curved

$$P = \sigma \left(\frac{1}{\rho_1} + \frac{1}{\rho_2} \right)$$

ρ has dimensions of stress, or energy/volume
... (1)

The mathematically sharp boundary model was used, e.g. by Becker,¹ in deriving an expression for σ in a binary alloy. On the other hand, it has been shown that important properties of σ can be derived by applying a more realistic model of the boundary where it is treated as a transition region of some width.²⁻⁴

Another property of considerable importance for phase transformations is the mobility M that relates the velocity of a boundary v to the pulling force,

$$P = v/M \quad \dots (2)$$

M is sometimes assumed to be a constant; in other cases it varies with v . In particular, the theory of the mobility of grain boundaries in alloys has been based on a model where the boundary is treated as a thin film of some thickness.^{5,6}

A third property of great importance for phase transformations is the enhanced diffusion along boundaries. In the treatments of boundary diffusion the predominant model is that the boundary can be regarded as a thin film of grain-boundary material of thickness δ and diffusivity D^B . The grain boundary is thus treated as a film of a separate phase having its own properties. This crude model will be applied in the present paper, and the grain-boundary material will be assumed to have its own molar free-energy function. Free-energy changes in and close to the boundary will be considered and expressions will be derived for the forces acting on the boundary due to such free-energy changes.

Such expressions are based on the fundamental relation

$$P = \Delta G_m / V_m \quad \dots (3)$$

where V_m is the molar volume of the new phase. Depending on the sign of ΔG_m , the force may act in either direction. For the case of boundary migration in single-phase alloys, equation (3) will be used to derive the retarding force due to the so-called impurity-drag effect. For the case of discontinuous precipitation, it will be shown that equation (3) will yield the force necessary for pulling the grain boundary along as the new phase precipitates. Without this force, which has been overlooked in previous theories of discontinuous precipitation, this process may not be possible.

Free-Energy Diagram of Binary Alloys

The chemical equilibrium between two phases may be displaced by a pressure difference caused by a curved interface. The well-known Thomson-Freundlich equation describes this effect quantitatively for a simple case. Under more complicated conditions, the mathematics of the thermodynamic calculation may be very complex and quite difficult to penetrate. However, the situation can be presented quite

Manuscript received 25 April 1968. Professor M. Hillert, Sc.D., is at the Royal Institute for Technology, Stockholm, Sweden.

quantitatively by using a free-energy diagram and the derivation of mathematical expressions may thus be reduced to a matter of arithmetic.

To simplify the discussion in this paper, we shall always assume that the original matrix phase, γ , is under ordinary pressure and any pressure difference according to equation (1) will thus be situated in the growing phase, α or β . Fig. 1 shows an example of the well-known free-energy diagram for a binary system containing two phases. A γ phase with the composition X_1 is supersaturated with respect to the β phase. There is a driving force ΔG^β for the formation of the β phase and β may thus form even under a high pressure P^β , caused by a curved interface. The critical value of this pressure is easily calculated using equation (3). $P^\beta = \Delta G^\beta/V_m$, thus allowing us to evaluate the critical size of a nucleus or the critical curvature of the interface during growth.

To carry out a numerical calculation, the shape of the free-energy curves must be known. Such calculations may be quite complex, in particular if the molar volume V_m of the β phase is not constant but must be represented by the expression

$$V_m = (1 - X) \cdot \bar{V}_A + X \cdot \bar{V}_B \quad \dots (4)$$

The broken curve in Fig. 1 shows that the free-energy curve of the β phase is distorted when raised a distance $P^\beta V_m$. However, it has been shown⁷ that the composition of the β phase in such a case is simply obtained by the point of tangency if a tangent to the β curve is drawn in such a way that the distances between the intercepts at the two sides of the diagram are related as \bar{V}_A to \bar{V}_B .

Numerical calculations are greatly simplified if the free-energy curve of the β phase is so narrow that the composition X^β can be treated as a constant. For instance, using the equation

$$\Delta G^\beta = (1 - X^\beta) (\mu_A^1 - \mu_A^e) + X^\beta (\mu_B^1 - \mu_B^e) \dots (5)$$

where μ represents the chemical potentials, i.e. the level of the intercepts of a tangent on the sides of the diagram (see Fig. 2), and e represents the equilibrium between the two phases, and approximating the γ phase as an ideal or dilute solution, we get

$$\Delta G^\beta = RT \left[(1 - X^\beta) \ln \frac{1 - X_1^\gamma}{1 - X_e^\gamma} + X^\beta \ln \frac{X_1^\gamma}{X_e^\gamma} \right] \dots (6)$$

If $X_1^\gamma - X_e^\gamma \ll X_e^\gamma$, we get approximately

$$\Delta G^\beta = RT \left[\frac{1 - X^\beta}{1 - X_e^\gamma} - \frac{X^\beta}{X_e^\gamma} \right] (X_e^\gamma - X_1^\gamma) \dots (7)$$

It is often of interest to calculate the total driving force for the complete reaction. This quantity is represented by ΔG_{total} in Fig. 2 and using the same approximation, equation (6) (with X_1^γ substituted for X^β) will now give us

$$\Delta G_{total} = RT \frac{(X_e^\gamma - X_1^\gamma)^2}{2X_1^\gamma} \dots (8)$$

Free-Energy Sinks

All the free energy available for a transformation cannot always be used to overcome the pressure difference according to equation (1), if the transformation takes place with a measurable speed. Some energy may be used to overcome the friction according to equation (2) and, if diffusion occurs, this process will also require free energy. Consider the formation of β phase from a supersaturated γ matrix with composition X_1 (Fig. 3). Let us assume that a concentration

difference of $X_1 - X_i$ is needed in the matrix to make the diffusion sufficiently rapid. X_i will then be the matrix composition close to the growing β phase. Fig. 3 demonstrates that the driving free energy for moving the boundary, ΔG^β , is lowered by the diffusion process. Of the total free energy available for the complete transformation, the quantity ΔG_d is used up by the diffusion process. Its size is easily estimated in the same way as equation (8), yielding

$$\Delta G_d = RT \frac{(X_i^\gamma - X_1^\gamma)^2}{2X_1^\gamma} \dots (9)$$

Application of Boundary Model to Grain-Boundary Migration

We shall assume that a grain boundary in a single-phase binary alloy can be regarded as a thin film of a special phase with a free-energy curve such that equilibrium with a γ grain is established when the concentrations are related by

$$X^B = K \cdot X^\gamma \dots (10)$$

Fig. 4 demonstrates this case with a K value larger than unity. Equilibrium is obtained from any pair of parallel tangents and it is a true, stable equilibrium, since the amount of the grain-boundary phase is constant as the width of the film δ is constant. The vertical position of the free-energy curve for the grain-boundary film was chosen arbitrarily in Fig. 4, this position not being of any importance for the present discussion. On the other hand, it is important if one wants to discuss the value of the interfacial free energy.

The concentration profile is shown at the bottom of Fig. 4. In spite of the high concentration inside the boundary, it should be realized that X_1 will be the average composition of the material flowing down through the boundary, if the boundary is slowly migrating upward with a constant velocity. At the upper side of the boundary, the material entering the boundary is transferred to a higher free-energy state, as illustrated by the arrow ΔG_u , and at the lower side of the boundary the same amount of material is leaving the boundary and thus being transferred to a lower state as illustrated by the arrow ΔG_l . However, no net force is acting on the boundary since

$$P = (\Delta G_u - \Delta G_l)/V_m = 0 \dots (11)$$

The concentration profile will change somewhat if the boundary is moving with a constant measurable velocity, (Fig. 5). In each phase the profile must be of the exponential form with the value X_1 as the limiting value.

$$X^\gamma = X_1 + (X_u^\gamma - X_1) \exp[-vy/D^\gamma] \dots (12)$$

$$X^B = X_1 + (X_l^B - X_1) \exp[-v(y + \delta)/D^B] \dots (13)$$

Assuming chemical equilibrium to be established locally at each side of the boundary, equation (10) will yield

$$X_l^B = KX_l^\gamma = K \cdot X_1 \dots (14)$$

$$X_u^B = KX_u^\gamma \dots (15)$$

and the application of equation (13) at $y = 0$ yields

$$X_u^B = X_1 [1 + (K - 1) \exp(-v\delta/D^B)] \dots (16)$$

The quantity X_u^γ in equation (12) can now be substituted to yield

$$X^\gamma = X_1 \left[1 + \frac{K - 1}{K} (\exp(-v\delta/D^B) - 1) \exp - vy/D^\gamma \right] \dots (17)$$

But there is no equality of chemical potentials, Fig. 4?

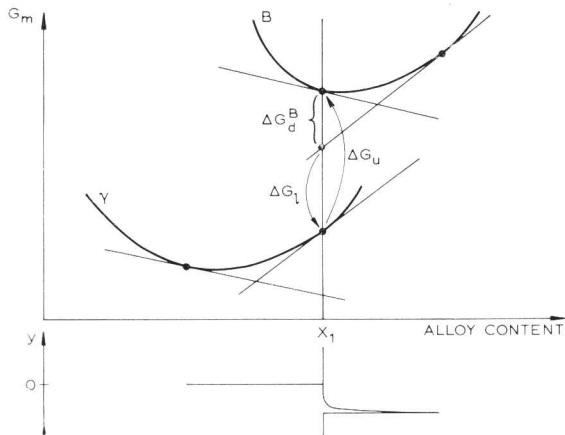


Fig. 7 Free-energy diagram without local equilibrium at the upper side of the boundary.

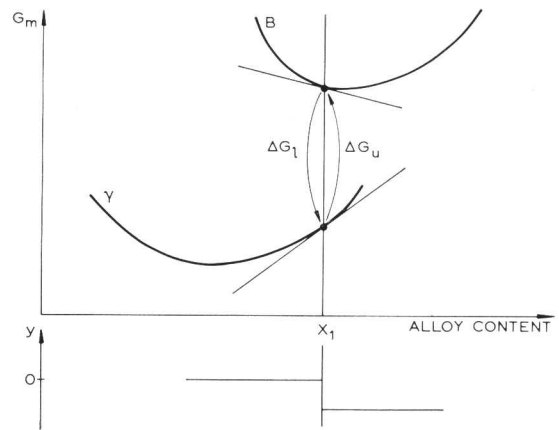


Fig. 8 Free-energy diagram with no local equilibrium at the sides of the boundary.

It is interesting to note that all the compositions at the two sides of the boundary are independent of the diffusivity in the grain, D^γ . The compositions at the upper side X_u^γ and X_u^B are dependent on the diffusivity inside the boundary D^B .

The concentration profiles in Fig. 5 should give rise to diffusion and one should thus expect a loss of free energy in each phase, ΔG_d^γ and ΔG_d^B , i.e. a retarding force on the boundary motion. This fact is also illustrated by the difference in length of the two arrows ΔG_u and ΔG_l in Fig. 5 and, as expected, one finds

$$P = (\Delta G_u - \Delta G_l)/V_m = (\Delta G_d^\gamma + \Delta G_d^B)/V_m \quad \dots (18)$$

Using equation (9) we find

$$\begin{aligned} \Delta G_d^\gamma &= \frac{RT}{2X_1} (X_1 - X_u^\gamma)^2 \\ &= \frac{RT}{2} \left(\frac{K-1}{K} \right)^2 [1 - \exp(-v\delta/D^B)]^2 \cdot X_1 \dots (19) \end{aligned}$$

$$\begin{aligned} \Delta G_d^B &= \frac{RT}{2X_1} [(X_1 - X_l^B)^2 - (X_1 - X_u^B)^2] \\ &= \frac{RT}{2} (K-1)^2 [1 - \exp(-2v\delta/D^B)] \cdot X_1 \dots (20) \end{aligned}$$

For low velocities, v , and K not much less than unity, the exponential functions can be expanded in series and inserting equations (19) and (20) in equation (18) we obtain

$$P = \frac{RT\delta(K-1)^2 X_1}{D^B V_m} \cdot v \quad \dots (21)$$

We have thus derived an expression for the effect of an alloy element on the mobility M of a boundary. Hypothesizing an interaction force between the alloy atoms and the grain boundary, Lücke and Detert⁵ were able to derive a similar expression for the same effect, the only difference being that they obtained $(K-1)$ to the first power instead of squared. Their expression thus seemed to predict a negative friction force P for an alloy element with $K < 1$, an unreasonable result as pointed out by Cahn.⁶ Cahn carried out a very ambitious treatment of the problem assuming a continuous variation of the attraction energy and diffusivity through the boundary, and was able to resolve the difficulty. For low velocities his result seems to be in agreement with our equation (21).

For high velocities the concentration profiles will change to the situation demonstrated in Fig. 6. The concentrations at the upper side of the boundary have reached their limits, $X_u^B = X_1$ and $X_u^\gamma = X_1/K$ and the friction force has reached its maximum value

$$P = \frac{RT(K-1)^2 X_1}{2V_m} \quad \dots (22)$$

On the other hand, at high velocities we must consider a new effect; the concentration profiles may become so narrow that they only exist mathematically but not physically. This will first occur in the γ phase because $D^\gamma \ll D^B$ (Fig. 7), and finally in the boundary phase as well (Fig. 8). The difference between the two arrows, ΔG_u and ΔG_l , will decrease and go to zero.

Owing to the atomistic nature of the system, it may never be realistic to treat the extreme value at the tip of a profile as existing physically. Instead we shall choose to use the value existing at a distance of $\delta/4$ from the tip of the profile. This is an arbitrary choice but should be fairly realistic considering the fact that the width of the grain boundary, δ , is probably a few atomic distances. Fig. 9 demonstrates this model and yields the following result:

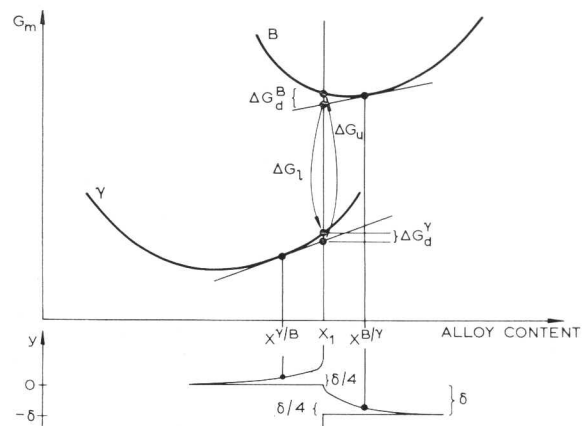


Fig. 9 Realistic free-energy diagram for rapidly moving boundary.

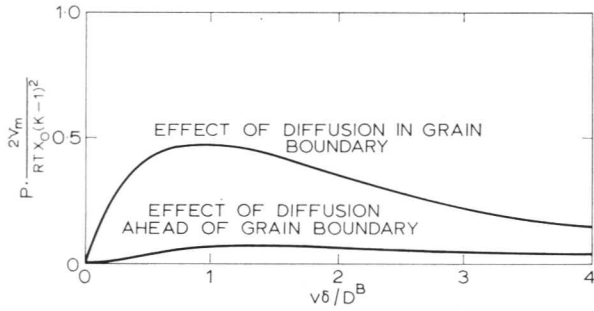


Fig. 10 Impurity-drag effect on the movement of a grain boundary calculated with $D^B = D^\gamma$. The lower curve will be negligible for $D^B \gg D^\gamma$.

$$X^\gamma(y = \delta/4) = X_1 \left[1 - \frac{K-1}{K} [1 - \exp(-v\delta/D^B)] \cdot \exp(-v\delta/4D^\gamma) \right] \dots (23)$$

$$X^B(y = -3\delta/4) = X_1 [1 + (K-1) \exp(-v\delta/4D^B)] \dots (24)$$

$$\Delta G_d^\gamma = \frac{RT}{2} \left(\frac{K-1}{K} \right)^2 [1 - \exp(-v\delta/D^B)]^2 \cdot \exp(-v\delta/2D^\gamma) \cdot X_1 \dots (25)$$

$$\Delta G_d^B = \frac{RT}{2} (K-1)^2 [\exp(-v\delta/2D^B) - \exp(-2v\delta/D^B)] \cdot X_1 \dots (26)$$

$$P = \frac{RT}{2V_m} (K-1)^2 \left[\exp\left(-\frac{v\delta}{2D^B}\right) - \exp\left(-\frac{2v\delta}{D^B}\right) + \left[1 - \exp\left(-\frac{v\delta}{D^B}\right)\right]^2 \cdot \exp\left(-\frac{v\delta}{2D^\gamma}\right) \frac{1}{K^2} \right] \cdot X_1 \dots (27)$$

This expression holds for all values of the velocity, low and high. Fig. 10 shows the result of a numerical calculation carried out with $D^\gamma = D^B$ and $K = 2$. The very low curve represents the effect due to diffusion in the γ phase ahead of the boundary. With values of $D^\gamma \ll D^B$ this curve will be even smaller and can be completely neglected for practical purposes. The main effect causing the friction force is thus due to the diffusion process inside the boundary.

In principle, Fig. 10 shows the same result as obtained by Cahn⁶ using a more ambitious model. An advantage of the present model may be that it yields simpler mathematics and a final expression in closed form for all values of velocity.

It is interesting to note that the decrease in the friction force occurs as a result of a growing deviation from local equilibrium at the sides of the boundary. In the next section we shall find that such a deviation from local equilibrium may even result in a force pulling the boundary.

Mechanism of Discontinuous Precipitation

Discontinuous precipitation resembles a eutectoid transformation, although the phase diagram indicates that only one new phase should form. However, this phase forms as parallel lamellae growing together with a new grain of the matrix phase

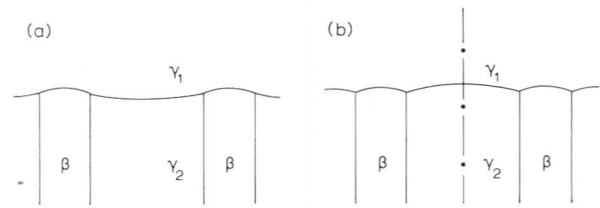
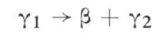


Fig. 11(a) and (b) Possible shapes of the interface of discontinuous precipitation during growth.



The new γ_2 grain has a much lower alloy content than the original, supersaturated γ_1 grain. The loss of supersaturation thus occurs discontinuously as the γ_1/γ_2 grain boundary advances and it has been suggested that the reaction is controlled by grain-boundary diffusion.⁸

The growth process has been treated theoretically by Turnbull⁸ and Cahn.⁹ They calculated the rate of grain-boundary diffusion necessary to lower the alloy content in front of the new γ_2 grain but neglected to consider the force actually pulling the grain boundary. As a consequence, their treatments give no indication why discontinuous precipitation occurs. Cahn simply assumed that the grain boundary will move with a rate proportional to the available free energy, without considering by what mechanism part of this energy could be transformed into a force.

To resolve this difficulty, Kirkaldy¹⁰ suggested the existence of a metastable miscibility gap in the γ phase. The reaction could then be treated as a eutectoid transformation where there is a chemical driving force acting on the growth of both the new phases. Shapiro¹¹ has worked out this theory in detail. On the other hand, it may be argued that discontinuous precipitation occurs in such regions of temperature and composition that it is difficult to imagine that suitable miscibility gaps would exist in all necessary cases.

Another mechanism has been proposed by Sulonen,¹² who suggested that the difference in atomic size would give rise to strain energy in the concentration gradient ahead of the growing γ_2 grain. This effect would result in a force on the boundary because the strains would be released as the new grain advances. This model has not been worked out in detail.

A further possibility is that the interfacial energies at the three-phase junctions balance each other in such a way that the γ_1/γ_2 grain boundary is actually pulled by the growing β phase, (Fig. 11(a)). This mechanism has been observed occasionally during precipitation of cementite from austenite but may not be a mechanism characteristic of precipitation controlled by grain-boundary diffusion. On the contrary, evidence from electron microscopy^{11,13} strongly indicates that the γ_1/γ_2 grain boundary is convex, as illustrated by Fig. 11(b).

To derive an expression for the force acting on the γ_1/γ_2 grain boundary, we should examine the free-energy diagram. The concentration profile at the bottom of Fig. 12 holds along a line perpendicular to the grain boundary (e.g. the line at the centre of the γ_2 lamella in Fig. 11(b)). The concentration across the assumed grain-boundary film is almost constant because of the high value of D^B in relation to the growth rate. On the other hand, there may be a very rapid change in the matrix grain in front of the boundary because

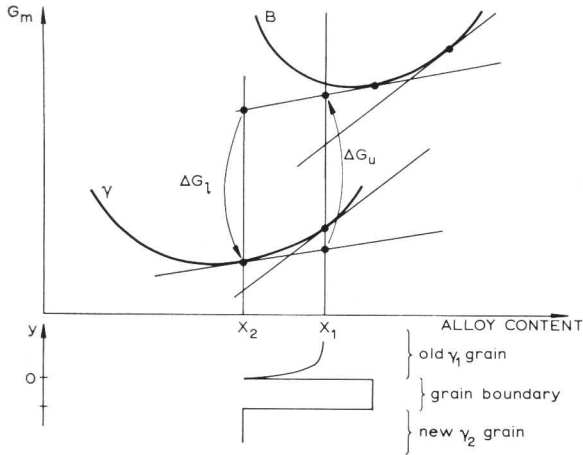


Fig. 12 Free-energy diagram for the grain boundary in discontinuous precipitation assuming local equilibrium.

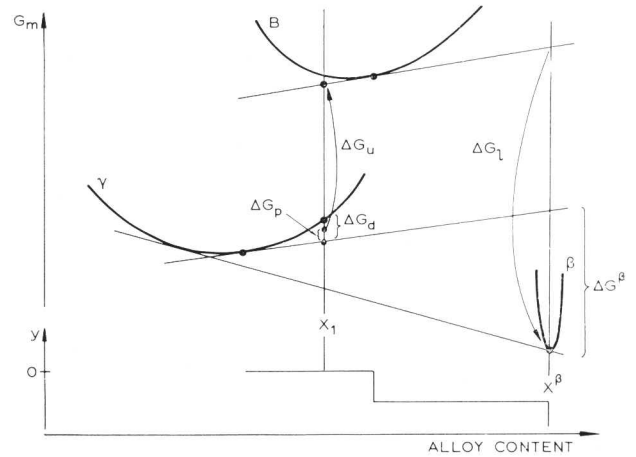


Fig. 15 Free-energy diagram for the γ/β interface in discontinuous precipitation.

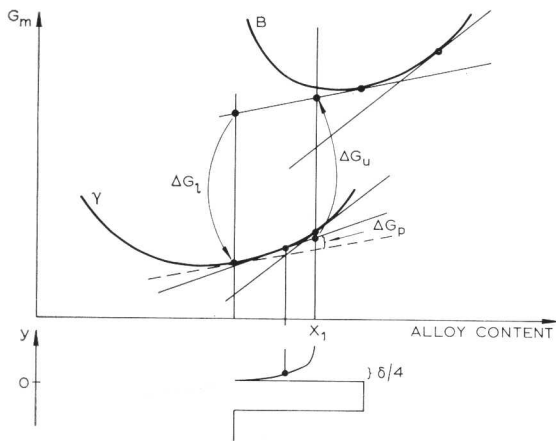


Fig. 13 Free-energy diagram for the grain boundary in discontinuous precipitation with deviation from local equilibrium.

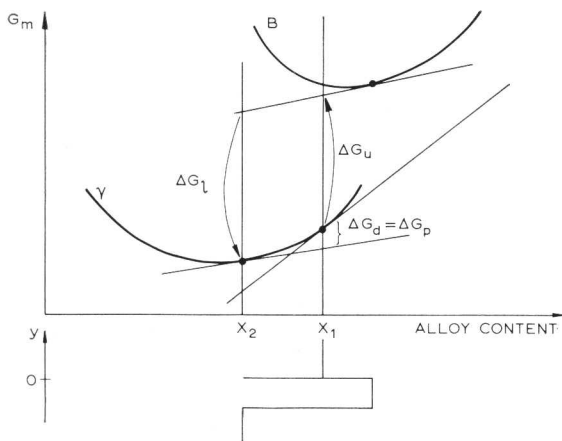


Fig. 14 Free-energy diagram for the grain boundary in discontinuous precipitation with maximum force on the boundary.

$D\gamma$ is much smaller. When using the free-energy diagram in this case, it must be realized that the average composition of the material entering the grain boundary is not the same as that of the material leaving the grain boundary to form the new γ_2 grain. The two composition values are X_1 and X_2 , respectively. The difference is caused by the sidewise diffusion along the grain boundary necessary for the growth of the β phase. The arrows ΔG_u and ΔG_l at the top of Fig. 12 represent the free-energy changes accompanying the transfer of material. They have the same length and will thus give no net force on the grain boundary.

If the growth rate is high enough in relation to $D\gamma$, the profile may be so sharp that it is not realistic to assume full chemical equilibrium at the upper side of the grain boundary. Fig. 13 shows such a situation using the same approach as in the previous section. The two arrows will now have different lengths, the difference being equal to the free energy that is no longer used on diffusion in the γ phase. In this case we find a force pulling the grain boundary upwards

$$P = (\Delta G_l - \Delta G_u)/V_m = \Delta G_p/V_m \dots (28)$$

This force will reach its maximum value when the transformation is so rapid that no diffusion occurs in the matrix ahead of the grain boundary (Fig. 14).

$$P_{max.} = \Delta G_d/V_m \dots (29)$$

From this model we may predict that discontinuous precipitation would occur only when the grain-boundary diffusion is so much higher than lattice diffusion that the profile will be steep enough. Equation (17) shows that the shape of the profile is determined by the ratio $D\gamma/v$. As an example, Speich¹³ has evaluated $D\gamma = 7 \times 10^{-16}$ cm/sec at 500°C in the Fe-Zn system and the lowest growth rate observed for discontinuous precipitation at that temperature is 1.15×10^{-7} cm/sec. We thus find

$$D\gamma/v = 7 \times 10^{-16}/1.15 \times 10^{-7} \text{ cm} = 0.6 \times 10^{-8} \text{ cm}.$$

It may thus be safe to conclude that the force is very close to its maximum value in all Speich's experiments.

A detailed theory of the growth of discontinuous precipitation will be worked out in a later section of this paper. It will then be assumed that some fraction, f , of ΔG_d will not be spent on diffusion but give rise to a force

$$P = f \cdot \Delta G_d/V_m \dots (30)$$

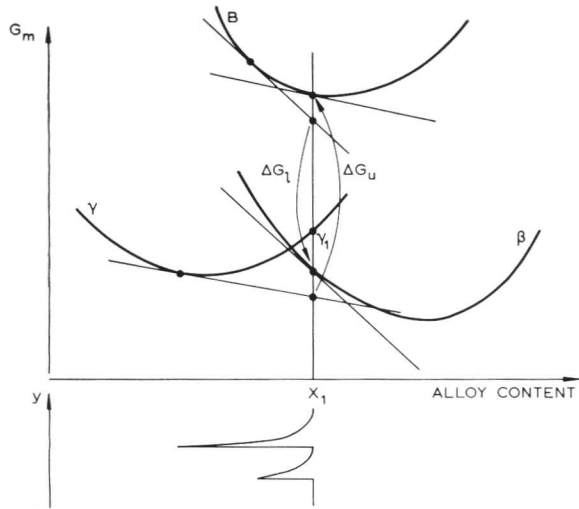


Fig. 16 Diffusionless transformation $\gamma_1 \rightarrow \beta$ is not possible with complete local equilibrium.

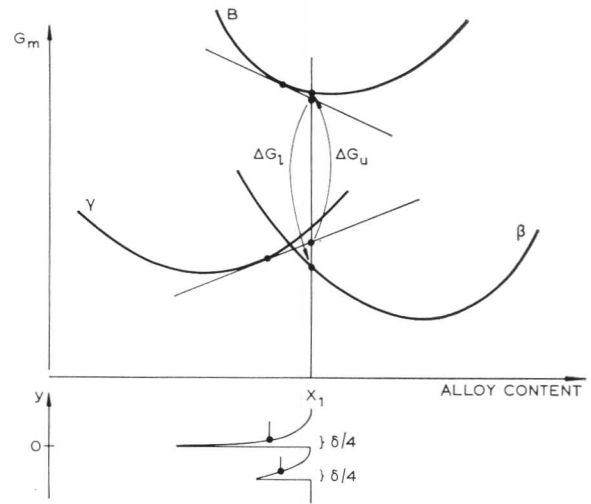


Fig. 17 Diffusionless transformation $\gamma_1 \rightarrow \beta$ is possible with deviation from local equilibrium.

In applying this theory to a specific case, it is necessary to estimate the value of f from the predicted value of v , using the parameter D^γ/v to estimate the steepness of the profile. As in the previous section, this value of f may be estimated from Fig. 13 using the composition of the mathematical shape of the profile at the distance $\delta/4$ from the boundary or the concentration at some other distance, e.g. one atomic distance.

Fig. 15 illustrates the force acting on the movement of the γ_1/β interface

$$P = (\Delta G_l - \Delta G_u)/V_m = (\Delta G^\beta + \Delta G_p)/V_m = (\Delta G^\beta + f\Delta G_d)V_m \dots (31)$$

Diffusionless Transformation in Alloys

If the free-energy curve of the β phase in Fig. 15 was much wider, a diffusionless transformation $\gamma \rightarrow \beta$ might be possible. A necessary condition is that the composition of the matrix γ phase lies to the right of the intersection of the two free-energy curves, as illustrated in Fig. 16. However, this condition is not sufficient as shown by the fact that $\Delta G_u > \Delta G_l$. These arrows have been constructed assuming local equilibrium at both sides of the boundary. For the reaction to proceed, we must have $\Delta G_u < \Delta G_l$. This may occur if the rate of reaction is high enough to result in a deviation from local equilibrium at the upper side of the boundary. This situation is illustrated by Fig. 17. We can conclude that a diffusionless transformation may occur if there is some mechanism by which its speed is initially raised to a high value. The critical speed appears to depend upon the free-energy curve of the boundary.

The same free-energy diagram can be used to show that there is no critical speed if the original composition lies to the right of the composition of β phase in stable equilibrium with γ phase. In such an alloy, the precipitation of β phase should automatically develop into a diffusionless growth.

Balance of Forces in Lamellar Structures

We shall now consider the formation of lamellar structures and assume that they are completely regular and contain perfectly parallel lamellae. The radius of curvature at any point on the advancing interface should be such that all the

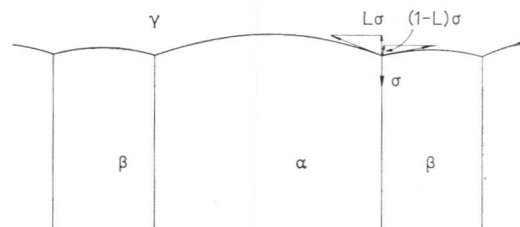


Fig. 18 Balance of forces at three-phase junctions.

forces will balance each other. Equations (1)–(3) give

$$\frac{\sigma}{\rho} = \frac{\Delta G_m}{V_m} - \frac{v}{M} \dots (32)$$

The three-phase junctions deserve particular attention. The three surface tensions should here balance each other and thus control the size of the three angles. As demonstrated by Fig. 18, the surface tension of the newly formed α/β interface, σ , is carried partly by the α lamella and partly by the β lamella. The two parts of σ may be denoted as $L\sigma$ and $(1-L)\sigma$, where L can easily be calculated from information on the three angles or the three surface tensions.

Balancing the forces acting on the whole edge of the α lamella, we find

$$2L\sigma = \int_{-S^\alpha/2}^{S^\alpha/2} (\Delta G_m/V_m - v/M) dz \dots (33\alpha, \beta)$$

By the number (33 α, β) we indicate that a similar equation holds for the β lamella. To use this equation, it is necessary to know how ΔG_m varies along the edge of the lamella, i.e. to know the variation in composition along the edge. This kind of information can be obtained from a calculation of the diffusion.

Diffusion during Growth of Lamellar Structures

We shall neglect the possibility of diffusion occurring in the growing phases, thus assuming that they retain the composition obtained at the moment of formation. When treating the diffusion ahead of a growing lamella, it is useful

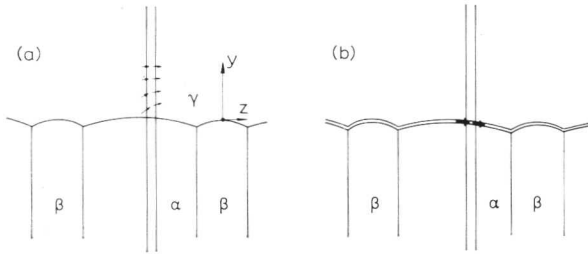


Fig. 19 Growth of lamellar structures by (a) volume diffusion and (b) boundary diffusion.

to consider a thin, long volume element as shown in Fig. 19(a). As the phase boundary moves upwards within this volume element, its change in composition must be balanced by sidewise diffusion

$$-\int_{-\infty}^{\infty} D \frac{d^2x}{dz^2} dy = v(X_1^\gamma - X^\alpha) \dots (34\alpha, \beta)$$

To solve this equation in the general case, we must know the shape of the interface. As a consequence, equation (34 α, β) must be solved simultaneously with equation (33 α, β). However, in a previous paper⁷ it was shown that the procedure is greatly simplified if the edges of the lamellae can be approximated as flat. A representation of the composition in the matrix by a series

$$X^\gamma - X_1^\gamma = \sum_0^\infty A_n \exp(-\lambda_n y) \cdot \cos 2\pi n z/S \dots (35)$$

will then reduce to a simple Fourier series at the edge, $y = 0$. To satisfy Fick's law

$$\lambda_n = \frac{v}{2D} (1 + \sqrt{1 + 16\pi^2 n^2 D^2 / v^2 s^2}) \dots (36)$$

The application of equation (34 α, β) yields the values of the Fourier coefficients

$$A_n = \frac{4\lambda_n v S^2}{D(2\pi n)^3} (X^\beta - X^\alpha) \sin n\pi S^\alpha / S \text{ for } n > 0 \dots (37)$$

At low temperatures, the volume diffusion may be very slow and boundary diffusion may instead dominate. This situation is described by Fig. 19(b), where the thickness of the boundary has been greatly exaggerated in order to illustrate the effect. Treating the boundary as a thin film of thickness δ and diffusivity D^B , we can easily integrate equation (34 α, β), again approximating the interface as flat

$$-\int_{-\infty}^{\infty} D \frac{d^2x}{dz^2} dy = D^B \frac{d^2x^B}{dz^2} \cdot \delta = v(X_1^\gamma - X^\alpha) \dots (38\alpha, \beta)$$

Integrating (38 α, β) for the case of constant X^α we obtain

$$\frac{X^B - X_3^B}{X_1^\gamma - X^\alpha} = \frac{v(S^\alpha)^2}{8KD^B\delta} \left[1 - \left(\frac{2z}{S^\alpha} \right)^2 \right] \dots (39)$$

X_3^B is the composition in the boundary at the three-phase junction, i.e., at $z = S^\alpha/2$ and X_1^γ is the original matrix composition.

Assuming a constant distribution coefficient between the boundary phase and the γ phase according to equation (10), we can represent the concentration in the boundary by an equivalent composition that would hold in the γ phase at equilibrium. We shall denote such values by X^b . Equation (39) can thus be transformed,

$$\frac{X^b - X_3^b}{X_1^\gamma - X^\alpha} = \frac{v(S^\alpha)^2}{8KD^B\delta} \left[1 - \left(\frac{2z}{S^\alpha} \right)^2 \right] \dots (40)$$

In discontinuous precipitation, the growing α phase is actually a grain of the same phase as the γ matrix. As long as the α phase is formed in local equilibrium with the grain-boundary material, we have $X^\alpha = X^b$. The composition X^α will then vary along the interface. Cahn⁹ has shown that equation (38) will then have the following solution

$$\frac{X^b - X_1^\gamma}{X_3^b - X_1^\gamma} = \frac{\cosh z \sqrt{a}/S^\alpha}{\cosh \sqrt{a}/2} \dots (41)$$

where

$$a = v(S^\alpha)^2 / KD^B\delta \dots (42)$$

Again, the properties of the boundary are expressed by a single quantity ($KD^B\delta$).

Eutectoid Transformation at Zero Growth Rate

Some essential features of the eutectoid transformation can be demonstrated by a very simple model where the two growing phases are supposed to be in full equilibrium with the adjacent matrix. Naturally, the growth rate must be zero in this hypothetical case. There will be no sidewise diffusion and the composition of the adjacent matrix can be represented by a single value X^γ . It may be tempting to assume that X^γ is identical to the original matrix composition X_1^γ but this point will require further discussion.

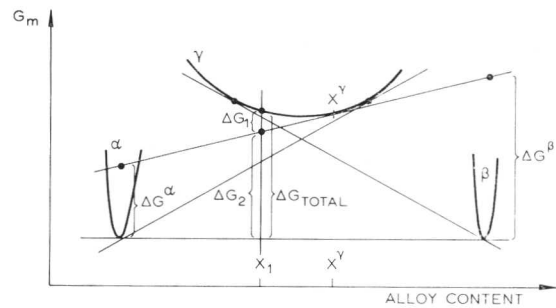


Fig. 20 Free-energy diagram for eutectoid reaction.

Fig. 20 shows a free-energy diagram and ΔG_{total} is the available free energy. If all this energy would go into the interfaces between the lamellae in the eutectoid structure, we would have

$$S_{rev.} = 2\sigma V_m / \Delta G_{total} \dots (43)$$

where rev. stands for reversible, indicating that no free energy is lost irreversibly on diffusion or on any other rate process.

We shall now apply equation (33 α, β) using the expression of ΔG^β given by equation (7). The integration can easily be carried out since X^γ is constant

$$L\sigma V_m = \int_0^{S^{\alpha/2}} \Delta G^{\alpha} dz = RT \left[\frac{1 - X^{\alpha}}{1 - X_e^{\gamma/\alpha}} - \frac{X^{\alpha}}{X_e^{\gamma/\alpha}} \right] \int_0^{S^{\alpha/2}} (X_e^{\gamma/\alpha} - X^{\gamma}) dz$$

$$= RT \left[\frac{1 - X^{\alpha}}{1 - X_e^{\gamma/\alpha}} - \frac{X^{\alpha}}{X_e^{\gamma/\alpha}} \right] (X_e^{\gamma/\alpha} - X^{\gamma}) S^{\alpha/2} \quad \dots (44)$$

$$(1 - L)\sigma V_m = RT \left[\frac{X^{\beta}}{X_e^{\gamma/\beta}} - \frac{1 - X^{\beta}}{1 - X_e^{\gamma/\beta}} \right] (X^{\gamma} - X_e^{\gamma/\beta}) S^{\beta/2} \quad \dots (45)$$

The lever rule relates S^{α} , S^{β} , and S . Assuming a constant molar volume for all the phases, we obtain

$$(X_1^{\gamma} - X^{\alpha})S^{\alpha} = (X^{\beta} - X_1^{\gamma})S^{\beta} = (X^{\beta} - X^{\alpha})S^{\alpha}S^{\beta}/S \quad \dots (46)$$

Equations (44) and (45) may thus be said to contain two unknown quantities, X^{γ} and S , and they can be solved easily. We shall denote this particular S value by S_0 because it is characteristic of zero growth rate.

Dividing equations (44) and (45) will give

$$\frac{X_e^{\gamma/\alpha} - X^{\gamma}}{X^{\gamma} - X_e^{\gamma/\beta}} = \frac{L}{1 - L} \frac{S^{\beta}}{S^{\alpha}} \left[\frac{X^{\beta}}{X_e^{\gamma/\beta}} - \frac{1 - X^{\beta}}{1 - X_e^{\gamma/\beta}} \right] \left/ \left[\frac{1 - X^{\alpha}}{1 - X_e^{\gamma/\alpha}} - \frac{X^{\alpha}}{X_e^{\gamma/\alpha}} \right] \right. \quad \dots (47)$$

It is shown that the composition X^{γ} depends upon the relative values of the three interfacial energies involved (through L) and upon the asymmetry of the phase diagram (through the values of the two brackets). Even for the completely symmetric case, equation (47) predicts $X^{\gamma} = X_1^{\gamma}$ only for $X_1^{\gamma} = 1/2$. In spite of the fact that we set out to treat the case where no sidewise diffusion occurs, we find that lengthwise diffusion cannot be prevented in the general case. We should thus expect some loss of free energy, i.e. we should expect to find $S_0 \neq S_{rev}$.

Adding equations (44) and (45) will give

$$S_0 = \frac{2\sigma V_m}{RT(X_e^{\gamma/\alpha} - X_e^{\gamma/\beta})} \left\{ \frac{LS/S^{\alpha}}{\left[\frac{1 - X^{\alpha}}{1 - X_e^{\gamma/\alpha}} - \frac{X^{\alpha}}{X_e^{\gamma/\alpha}} \right]} + \frac{(1 - L)S/S^{\beta}}{\left[\frac{X^{\beta}}{X_e^{\gamma/\beta}} - \frac{1 - X^{\beta}}{1 - X_e^{\gamma/\beta}} \right]} \right\} \quad \dots (48)$$

The relation between S_0 and the composition at the front X^{γ} is best demonstrated by the free-energy diagram. Direct integration of equation (44) for the case of ΔG^{α} constant will give

$$L\sigma V_m = \Delta G^{\alpha} S^{\alpha}/2 \quad \dots (49\alpha)$$

and in the same way for the β phase

$$(1 - L)\sigma V_m = \Delta G^{\beta} S^{\beta}/2 \quad \dots (49\beta)$$

Adding (49 α) and (49 β) and using the lever rule,

$$\Delta G^{\alpha} S^{\alpha} + \Delta G^{\beta} S^{\beta} = \Delta G_2 S \quad \dots (50)$$

we obtain

$$S_0 = 2\sigma V_m / \Delta G_2 \quad \dots (51)$$

Fig. 20 demonstrates that part of the total free energy available will be spent on diffusion, ΔG_1 , and the rest will go into interfacial energy, ΔG_2 . As a consequence, we find that

$S_0 > S_{rev}$. However, the difference is not very great, ΔG_1 being only a minor part of ΔG_{total} .

Eutectoid Transformation by Volume Diffusion

This case has been treated by Zener,¹⁴ using a method based on dimensional arguments, and by the present author⁷ and by Jackson and Hunt¹⁵ in a more rigorous way, which will now be followed.

We shall apply the same procedure as with zero growth rate in the preceding section. If the friction term v/M in equation (33 α , β) is neglected, we again find the same expression as the first part of equation (44) but the integration will be more complicated because X^{γ} now varies along the edge of the lamella. For volume diffusion we can express X^{γ} by means of the Fourier coefficients given by equation (37) and after integration of equation (44) we obtain

$$L\sigma V_m = RT \left[\frac{1 - X^{\alpha}}{1 - X_e^{\gamma/\alpha}} - \frac{X^{\alpha}}{X_e^{\gamma/\alpha}} \right] \cdot \left[(X_e^{\gamma/\alpha} - X_1^{\gamma} - A_0) \frac{S^{\alpha}}{2} - \frac{vS^2(X^{\beta} - X^{\alpha})}{2D\pi^3} \cdot B \right] \quad \dots (52)$$

$$(1 - L)\sigma V_m = RT \left[\frac{X^{\beta}}{X_e^{\gamma/\beta}} - \frac{1 - X^{\beta}}{1 - X_e^{\gamma/\beta}} \right] \cdot \left[(X_1^{\gamma} - X_e^{\gamma/\beta} + A_0) \frac{S^{\beta}}{2} - \frac{vS^2(X^{\beta} - X^{\alpha})}{2D\pi^3} \cdot B \right] \quad \dots (53)$$

where

$$B = \sum_1^{\infty} \frac{\lambda_n S}{2\pi n^4} (\sin \pi n S^{\alpha}/S)^2 \quad \dots (54)$$

Again equation (46) relates S^{α} , S^{β} , and S . Equations (52) and (53) may thus be said to contain three unknown quantities, A_0 (defining the average composition at the front), S , and v . Adding equations (52) and (53) will give

$$\left[X_e^{\gamma/\alpha} - X_e^{\gamma/\beta} - \frac{vS(X^{\beta} - X^{\alpha})S^2}{D\pi^3 S^{\alpha} S^{\beta}} \cdot B \right] \cdot S = \frac{2\sigma V_m}{RT} \left[\frac{LS/S^{\alpha}}{\left[\frac{1 - X^{\alpha}}{1 - X_e^{\gamma/\alpha}} - \frac{X^{\alpha}}{X_e^{\gamma/\alpha}} \right]} + \frac{(1 - L)S/S^{\beta}}{\left[\frac{X^{\beta}}{X_e^{\gamma/\beta}} - \frac{1 - X^{\beta}}{1 - X_e^{\gamma/\beta}} \right]} \right] \quad \dots (55)$$

The right-hand side can be expressed in terms of S_0 according to equation (48) and we obtain

$$v = \frac{D\pi^3 S^{\alpha} S^{\beta} (X_e^{\gamma/\alpha} - X_e^{\gamma/\beta})}{BS^2(X^{\beta} - X^{\alpha})} \cdot \frac{1}{S} \left(1 - \frac{S_0}{S} \right) \quad \dots (56)$$

This relation is equivalent to the expression derived by Zener. The numerical value of B can easily be calculated for any S^{α}/S and shows good agreement with Zener's estimate.⁷

As pointed out by Zener, a relation such as equation (56) can be satisfied by any value of S larger than S_0 . Consequently, it does not directly predict that the lamellar structure should form with a constant spacing S . However, Zener suggested that there should be some self-regulating mechanism by which the spacing would be adjusted close to the value that maximizes the growth rate

$$S_{optimum} = 2S_0.$$

شاهد في
الجزء
الأسفل

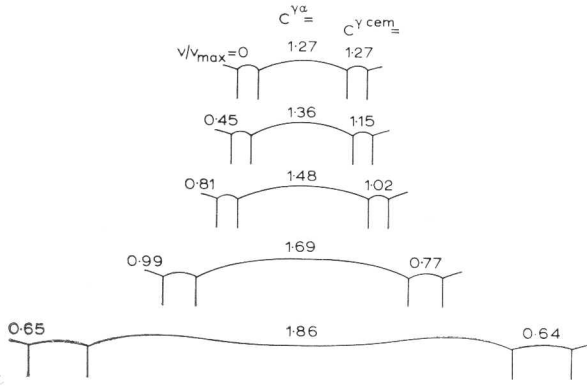


Fig. 21 Calculated shape and growth rate of pearlite with different interlamellar spacings.

Equations (48) and (56) predict

$$S_{\text{optimum}} \propto (X_e^{\gamma/\alpha} - X_e^{\gamma/\beta})^{-1}$$

$$v_{\text{maximum}} \propto (X_e^{\gamma/\alpha} - X_e^{\gamma/\beta})^2$$

For any value of S one can calculate v as well as A_0 and the concentration is then known in detail along the front. The derivation of our basic equations (44) and (45) was based on the assumption of local chemical equilibrium at all points of the growth front. We can now calculate what shape the front should have in order to be in local equilibrium, using equation (32) but again neglecting the term v/M . The radius of curvature ρ is related to the shape of a lamella by

$$\frac{1}{\rho} = -\frac{d^2y}{dz^2} \left/ \left[1 + \left(\frac{dy}{dz} \right)^2 \right]^{3/2} \right. \quad \dots (57)$$

A detailed calculation of the shape of the edges was carried out by Hillert⁷ and by Jackson and Hunt.¹⁵ Fig. 21 shows the result for the case $S^\alpha/S = 7/8$ which holds for pearlite in the Fe-C system. It is very interesting to note that the interface is rather flat, thus justifying the assumption used in deriving the concentration profile. It is also interesting to note that the interface will bend back for large S values. The critical S value for this phenomenon can be directly calculated by putting $X^\gamma = X_e^{\gamma/\alpha}$ at the middle of the edge of the α lamella ($z = 0$; $y = 0$). Equation (35) yields

$$X_e^{\gamma/\alpha} - X_1^\gamma = A_0 + \sum_1^\infty A_n = A_0 + \frac{vS(X^\beta - X^\alpha)}{D\pi^2} \cdot C \quad \dots (58)$$

where

$$C = \sum_1^\infty \frac{\lambda_n S}{2\pi n^3} \cdot \sin n\pi S^\alpha/S \quad \dots (59)$$

Inserting this in equation (52) and eliminating v by means of equation (56), yields

$$S = S_0 + \frac{2L\sigma V_m S^2/S^\alpha S^\beta}{RT \left[\frac{1 - X^\alpha}{1 - X_e^{\gamma/\alpha}} - \frac{X^\alpha}{X_e^{\gamma/\alpha}} \right] (X_e^{\gamma/\alpha} - X_e^{\gamma/\beta}) (\pi C S^\alpha/S^\beta - 1)} \quad \dots (60\alpha, \beta)$$

For the case of a symmetric phase diagram and symmetric conditions at the three-phase junctions, $L = 1/2$, we obtain approximately

$$S = 3S_0 \quad \dots (61)$$

For all other cases, the bending back of the edge will occur even sooner either for the α lamellae or for the β lamellae. The fact that this phenomenon is not usually observed experimentally seems to indicate that $S < 3S_0$ and it seems justified to conclude that the spacing is automatically adjusted to a value close to $S = 2S_0$ as suggested by Zener's optimizing principle. On the other hand, experimental data in many cases seem to indicate strongly that S is \gg than S_{rev} . As discussed in the previous section, the free-energy loss due to lengthwise diffusion gives an effect in that direction but it is rather small. It is conceivable that there are other, more important free-energy losses that have not yet been considered. It may, for instance, be pointed out that according to the present approach the two new phases in general form under different pressures at the three-phase junction, in spite of the fact that they have a flat interface which cannot support any pressure difference. This may lead to complications and a free-energy loss of some kind.

Eutectoid Transformation by Boundary Diffusion

This case was treated by Cahn⁹ assuming that the composition of the two growing phases would vary with the concentration in the boundary. Equation (41) was thus employed to describe the diffusion. However, we are mainly interested in the same kind of system as in the preceding section, where X^α and X^β are regarded as constants and equation (40) will thus be applied when the transformation is controlled by boundary diffusion rather than volume diffusion. The similar case of monotectoid reaction has been treated by Shapiro¹¹ in an attempt to explain discontinuous precipitation.

Expressing the composition in front of the edge of a growing lamella by equation (40) we can integrate equation (44), obtaining

$$L\sigma V_m = RT \left[\frac{1 - X^\alpha}{1 - X_e^{\gamma/\alpha}} - \frac{X^\alpha}{X_e^{\gamma/\alpha}} \right] \cdot \left[X_e^{\gamma/\alpha} - X_3^\beta - \frac{v(S^\alpha)^2(X_1^\gamma - X^\alpha)}{12KD^B\delta} \right] \cdot \frac{S^\alpha}{2} \quad \dots (62)$$

$$(1 - L)\sigma V_m = RT \left[\frac{X^\beta}{X_e^{\gamma/\beta}} - \frac{1 - X^\beta}{1 - X_e^{\gamma/\beta}} \right] \cdot \left[X_3^\beta - X_e^{\gamma/\beta} - \frac{v(S^\beta)^2(X^\beta - X_1^\gamma)}{12KD^B\delta} \right] \cdot \frac{S^\beta}{2} \quad \dots (63)$$

Again equation (46) relates S^α , S^β , and S and can be used to replace $(X_1^\gamma - X^\alpha)$ and $(X^\beta - X_1^\gamma)$ by $(X^\beta - X^\alpha)$. We shall now simplify the calculations by assuming that the two kinds of boundary have the same value of $(KD^B\delta)$. Adding equations (62) and (63) would then yield

$$\left[X_e^{\gamma/\alpha} - X_e^{\gamma/\beta} - \frac{v(X^\beta - X^\alpha)S^\alpha S^\beta}{12KD^B\delta} \right] \cdot S = \frac{2V_m\sigma}{RT} \left[\frac{LS/S^\alpha}{\left(\frac{1 - X^\alpha}{1 - X_e^{\gamma/\alpha}} - \frac{X^\alpha}{X_e^{\gamma/\alpha}} \right)} + \frac{(1 - L)S/S^\beta}{\left(\frac{X^\beta}{X_e^{\gamma/\beta}} - \frac{1 - X^\beta}{1 - X_e^{\gamma/\beta}} \right)} \right] \quad \dots (64)$$

and inserting S_0 from equation (48) we obtain

$$v = \frac{12KD^B\delta S^2(X_e^{\gamma/\alpha} - X_e^{\gamma/\beta})}{S^\alpha S^\beta (X^\beta - X^\alpha)} \cdot \frac{1}{S^2} \left(1 - \frac{S_0}{S} \right) \quad \dots (65)$$

Except for the factor S^2 , instead of S , this result is very similar to that which was obtained with volume diffusion. The maximum growth rate is now obtained at

$$S_{\text{optimum}} = \frac{3}{2} S_0$$

and the dependence of supersaturation becomes

$$S_{\text{optimum}} \propto (X_e^{\gamma/\alpha} - X_e^{\gamma/\beta})^{-1}$$

$$v_{\text{maximum}} \propto (X_e^{\gamma/\alpha} - X_e^{\gamma/\beta})^3$$

As before, we can calculate the critical spacing where the edge would start to bend back by putting $X^\gamma = X_e^{\gamma/\alpha}$ at $z = 0$, $y = 0$. Equation (40) then yields

$$X_e^{\gamma/\alpha} - X_3^b = (X_1^\gamma - X^\alpha) \frac{v(S^\alpha)^2}{8KD^B\delta} \quad \dots (66)$$

and inserting this in equation (62) combined with equation (65), we obtain

$$S = S_0 + \frac{4L\sigma V_m(S/S^\alpha)^2}{RT \left[\frac{1 - X^\alpha}{1 - X_e^{\gamma/\alpha}} - \frac{X^\alpha}{X_e^{\gamma/\alpha}} \right] (X_e^{\gamma/\alpha} - X_e^{\gamma/\beta})} \quad \dots (67\alpha, \beta)$$

The symmetric case again yields $S = 3S_0$, and the fact that bending back is not normally observed experimentally seems to support the view that Zener's optimizing principle may be fairly correct whether boundary or volume diffusion is the rate-controlling process.

At low temperatures it may be reasonable to expect a eutectoid transformation to take place by means of boundary diffusion with such a high rate that the volume diffusion in the matrix ahead of the interface is too slow to allow local equilibrium between the matrix and the interface. Equation (44) should then be modified by adding $f \cdot \Delta G_I$ to ΔG^α and ΔG^β . However, this will make only a slight change, as demonstrated by the fact that ΔG_I is a small fraction of ΔG_{total} .

NOTE ADDED IN PROOF: Eutectoid transformation by boundary diffusion has recently been treated by Shapiro and Kirkaldy (*Acta Met.*, 1968, 16, 579) and by Sundquist (personal communication). Their approaches are somewhat different but their results are essentially in agreement with the present result.

Discontinuous Precipitation

This reaction will only be treated assuming rate control by boundary diffusion, since we have not found any driving force for the grain-boundary movement unless there is a deviation from local equilibrium between the γ matrix and the boundary. The new γ grain that grows together with the β phase will be denoted α , to emphasize the similarity with the eutectoid reaction. This case of growth of a lamellar structure does not seem to have been treated adequately before. As pointed out earlier, the treatments by Turnbull⁸ and Cahn⁹ have a severe limitation.

The concentration in the boundary at the edge of the β lamellae is described by equation (40) as in the eutectoid transformation, but equation (41) must be used for the α lamellae because their composition will vary as X^b . We now get the following result by applying equation (33 α), neglecting the term v/M , expressing ΔG_a by equation (9) and integrating

$$\begin{aligned} L\sigma V_m &= \int_0^{S^\alpha/2} f \cdot \Delta G_a dz = \frac{fRT}{2X_1^\gamma} \int_0^{S^\alpha/2} (X_1^\gamma - X^b)^2 \\ &= \frac{fRT(X_1^\gamma - X_3^b)^2}{2X_1^\gamma (\cosh \sqrt{a/2})^2} \int_0^{S^\alpha/2} (\cosh z \sqrt{a/S^\alpha})^2 dz \\ &= \frac{fRT(X_1^\gamma - X_3^b)^2}{8X_1^\gamma} (1 + \sqrt{a/\sinh \sqrt{a}}) \cdot \frac{\tanh \sqrt{a/2}}{\sqrt{a/2}} \cdot S^\alpha \quad \dots (68) \end{aligned}$$

For the β lamellae there is also a force due to the deviation from local equilibrium (equation (31)). However, the force due to the chemical change, ΔG^β , may be much larger. The term $f \cdot \Delta G_a$ will therefore be neglected and we then obtain exactly the same result as for the β lamellae in a eutectoid transformation (equation (63)).

$$\begin{aligned} (1-L)\sigma V_m &= \int_0^{S^\beta/2} (\Delta G^\beta + f\Delta G_a) dz \\ &\simeq RT \left[\frac{X^\beta}{X_e^{\gamma/\beta}} - \frac{1 - X^\beta}{1 - X_e^{\gamma/\beta}} \right] \\ &\left[X_3^b - X_e^{\gamma/\beta} - \frac{v(S^\beta)^2 (X^\beta - X_1^\gamma)}{12KD^B\delta} \right] \cdot \frac{S^\beta}{2} \quad \dots (69) \end{aligned}$$

Again we have two equations and three unknowns, now X_3^b , S , and v . The calculation will be somewhat more complicated than for the eutectoid transformation, mainly because the relation between S^α , S^β , and S depends upon the growth rate, the composition of the α phase not being constant.

The average composition of the α phase can be calculated by means of equation (41) using $X^\alpha = X^b$, i.e. assuming local equilibrium between the boundary and the growing α grain in agreement with the earlier discussion.

$$\begin{aligned} X_1^\gamma - \bar{X}^\alpha &= \frac{2}{S^\alpha} \int_0^{S^\alpha/2} (X_1^\gamma - X^b) dz = \frac{2(X_1^\gamma - X_3^b)}{S^\alpha \cosh \sqrt{a/2}} \\ \int_0^{S^\alpha/2} \cosh z \sqrt{a/S^\alpha} dz &= (X_1^\gamma - X_3^b) \cdot \frac{\tanh \sqrt{a/2}}{\sqrt{a/2}} \quad \dots (70) \end{aligned}$$

The composition of the β phase is constant and the lever rule will thus yield

$$\frac{S^\beta}{S^\alpha} = \frac{X_1^\gamma - \bar{X}^\alpha}{X^\beta - X_1^\gamma} = \frac{X_1^\gamma - X_3^b}{X^\beta - X_1^\gamma} \cdot \frac{\tanh \sqrt{a/2}}{\sqrt{a/2}} \quad \dots (71)$$

A similar expression was derived by Cahn⁹ using the equilibrium value $X_e^{\gamma/\beta}$ instead of X_3^b . This was a serious and unnecessary approximation.

Numerical calculations can now in principle be performed using equations (68), (69), and (71), in combination with the definitions $S = S^\alpha + S^\beta$ and $a = v(S^\alpha)^2/KD^B\delta$ from equation (42). However, for low amounts of β phase, equation (69) can be simplified by neglecting the third term in the bracket. By dividing equation (68) with (69) and using equation (71), we would then obtain

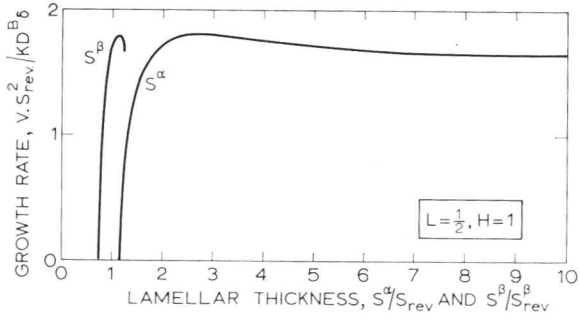


Fig. 22 Growth rate as a function of lamellar thickness for discontinuous precipitation.

$$\frac{1-L}{L} = \frac{X_3^b - X_e^{\gamma/\beta}}{X_1^\gamma - X_3^b} \cdot \frac{\left[\frac{X^\beta}{X_e^{\gamma/\beta}} - \frac{1 - X^\beta}{1 - X_e^{\gamma/\beta}} \right]}{\left[\frac{X^\beta}{X_1^\gamma} - 1 \right]} \cdot \frac{4}{f(1 + \sqrt{a/\sinh \sqrt{a}})} \quad \dots (72)$$

By introducing a new quantity H ,

$$H = \frac{1-L}{L} \cdot f \cdot \left[\frac{X^\beta}{X_1^\gamma} - 1 \right] / \left[\frac{X^\beta}{X_e^{\gamma/\beta}} - \frac{1 - X^\beta}{1 - X_e^{\gamma/\beta}} \right] \quad \dots (73)$$

we can now write

$$\frac{X_3^b - X_e^{\gamma/\beta}}{X_1^\gamma - X_3^b} = \frac{H}{4} (1 + \sqrt{a/\sinh \sqrt{a}}) \quad \dots (74)$$

$$\frac{X_1^\gamma - X_3^b}{X_1^\gamma - X_e^{\gamma/\beta}} = 1 / \left[1 + \frac{H}{4} (1 + \sqrt{a/\sinh \sqrt{a}}) \right] \quad \dots (75)$$

Inserting equation (75) in equation (68), we get a relation between S^α and v (through the parameter a).

$$S^\alpha = \frac{4L\sigma V_m X_1^\gamma}{fRT(X_1^\gamma - X_e^{\gamma/\beta})^2} \cdot \frac{\sqrt{a}}{\tanh \sqrt{a/2}} \cdot \frac{\left[1 + \frac{H}{4} (1 + \sqrt{a/\sinh \sqrt{a}}) \right]^2}{1 + \sqrt{a/\sinh \sqrt{a}}} \quad \dots (76)$$

For any value of a , we can directly calculate S^α and, through the definition of a , we can then obtain the corresponding growth rate v . In expressing the value of S^α it is convenient to use the spacing of the hypothetical structure that would form if all the free energy available went into interfacial energy

$$S_{rev.} = \frac{2\sigma V_m}{\Delta G_{total}} = \frac{4\sigma V_m X_1^\gamma}{RT(X_1^\gamma - X_e^{\gamma/\beta})^2} \quad \dots (77)$$

It is justifiable to compare S^α directly with this value because the amount of β phase is assumed to be small. The thickness of the β lamellae should be compared with their thickness in the same hypothetical structure,

$$S_{rev.}^\beta = \frac{X_1^\gamma - X_e^{\gamma/\beta}}{X^\beta - X_e^{\gamma/\beta}} \cdot \frac{4\sigma V_m X_1^\gamma}{RT(X_1^\gamma - X_e^{\gamma/\beta})^2} = \frac{4\sigma V_m X_1^\gamma}{RT(X_1^\gamma - X_e^{\gamma/\beta})(X^\beta - X_e^{\gamma/\beta})} \quad \dots (78)$$

Using equation (71) we now obtain

$$\frac{S^\alpha}{S_{rev.}} = \frac{L}{f} \cdot \frac{\sqrt{a}}{\tanh \sqrt{a/2}} \cdot \frac{\left[1 + \frac{H}{4} (1 + \sqrt{a/\sinh \sqrt{a}}) \right]^2}{1 + \sqrt{a/\sinh \sqrt{a}}} \quad \dots (79)$$

$$\frac{S^\beta}{S_{rev.}^\beta} = \frac{2L}{f} \cdot \frac{1 + \frac{H}{4} (1 + \sqrt{a/\sinh \sqrt{a}})}{1 + \sqrt{a/\sinh \sqrt{a}}} \quad \dots (80)$$

In view of the definition of the quantity a (equation (42)), it is convenient to express calculated values of v in terms of $KD\delta/(S_{rev.})^2$.

Whatever relation we shall find between S^α , S^β , and v , we can immediately see that for any set of values of the parameters L , f , and H the following dependency of the original supersaturation could be expected

$$S_{optimum}^\alpha \propto (X_1^\gamma - X_e^{\gamma/\beta})^{-2}$$

$$S_{optimum}^\beta \propto (X_1^\gamma - X_e^{\gamma/\beta})^{-1}$$

$$v_{maximum} \propto (X_1^\gamma - X_e^{\gamma/\beta})^4$$

Such a strong variation of the growth rate with supersaturation seems to be confirmed by Speich's experimental data.¹³ Unfortunately, it is difficult to test the theory quantitatively with those data because the solid solution in the Fe-Zn system is far from ideal and the amount of β phase was as high as 30% in Speich's experiments.

Equations (79) and (80) show that the spacing expected for zero growth rate will in general be different from $S_{rev.}$ and $S_{rev.}^\beta$. At the limit $v \rightarrow 0$ we get $a \rightarrow 0$ and equations (79) and (80) are simplified to

$$\frac{S_0^\alpha}{S_{rev.}} = \frac{L}{f} \left(1 + \frac{H}{2} \right)^2 \quad \dots (81)$$

$$\frac{S_0^\beta}{S_{rev.}^\beta} = \frac{L}{f} \left(1 + \frac{H}{2} \right) \quad \dots (82)$$

For eutectoid transformations we found that, in general, $S_0 > S_{rev.}$ owing to the occurrence of some diffusion in a direction normal to the growth front. Some free energy is then lost irreversibly. For discontinuous precipitation, we have the same situation. The factor $(1-f)$ represents the amount of ΔG_a in Fig. 14 that is spent on diffusion in the matrix ahead of the boundary and, as expected, equation (81) predicts that S_0^α will grow larger with larger $(1-f)$, i.e. smaller f . For this transformation it can be a very large effect and in the limit all ΔG_a is spent on diffusion, and the spacing will be infinite. For eutectoid reactions the corresponding effect had minor importance only.

In the other extreme, $f = 1$, no free energy is lost irreversibly at $v = 0$ but, nevertheless, the spacing may become very large depending on the L value. Contrary to the eutectoid transformation, discontinuous precipitation seems to be very sensitive to the interfacial energies that determine the angles at the three-phase junctions and thus the value of L . For $L = 0$, equation (81) in combination with equation (73) predicts an infinitely large spacing and equation (75) reveals that $X_3^b = X_1^\gamma$. No decomposition is taking place and all the free energy available is saved in the "growing α phase". As expected, equation (80) predicts that the fraction of β phase will be negligible in this extreme. S_0^β can increase only as a result of small f values. Keeping f constant, equation

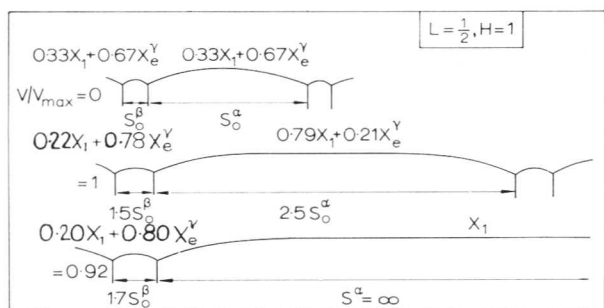


Fig. 23 Shape of the interface of discontinuous precipitation as a function of spacing and growth rate. Numbers give the local concentration at the centre of the edge of each lamella.

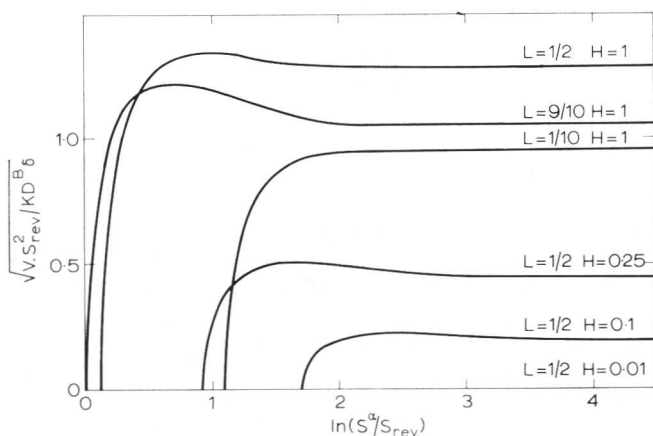


Fig. 24 Growth rate as a function of spacing under various conditions.

(81) predicts that S_0^β will decrease towards a value of $S_{rev}^\beta/2$ for $L = 0$ as a result of the decreasing degree of decomposition. In fact, this effect will also dominate when we consider the case $v > 0$ and study the variation of spacing with growth rate. Fig. 22 presents the result of a numerical calculation based on equations (79) and (80) and using $f = 1, L = 1/2, H = 1$. The curve of v versus S^α is similar to the same curve for a eutectoid transformation. The growth rate starts at zero at a critical value S_0^α , it increases rapidly towards a maximum at $\sim 2S_0^\alpha$, and decreases slowly as the spacing is further increased. In this transformation, however, the growth rate does not decrease towards zero but towards a value only slightly lower than the maximum value. This difference from a eutectoid transformation is explained by the curve of v versus S^β . Again the growth rate starts at zero at a critical value S_0^β , but as the growth rate increases S^β increases only by a factor of 2. From the viewpoint of a β lamella, the situation does not change much as the spacing S^α increases from the optimum value towards infinity. Fig. 23 illustrates the shape of the growth front and should be compared to Fig. 21 for the eutectoid transformation. In addition to the differences already discussed, Fig. 23 also shows that the edge of the α lamella is not predicted to bend back at large spacings. This result is formally a consequence of the expression for the composition in the boundary (equation (41)), which does not allow the composition to pass through the value of X_1^Y . The composition at the middle of the edges is also given in Fig. 23 as calculated from equations (75) and

TABLE I
Growth Characteristics of Lamellar Structures

	Eutectoid		Discontinuous Precipitation by Boundary Diffusion
	Volume Diffusion	Boundary Diffusion	
v_{max} prop.	$(\Delta T)^2$	$(\Delta T)^3$	$(\Delta T)^4$
$S_{optimum}$ prop.	$(\Delta T)^{-1}$	$(\Delta T)^{-1}$	$(\Delta T)^{-2}$
$S^\beta_{optimum}$ prop.	$(\Delta T)^{-1}$	$(\Delta T)^{-1}$	$(\Delta T)^{-1}$
$S_{optimum}/S_0$	2	1.5	~ 2
S_0/S_{rev}	close to 1	close to 1	from 1 to ∞
$S_{bending\ back}/S_0$	~ 3	~ 3	∞

(41) and demonstrates clearly that the situation for the β lamellae does not change appreciably after the maximum in growth rate.

In view of these results, one could expect almost any spacing S^α to form from the optimum at $\sim 2S_0$ to infinity. For Zener's optimizing principle to work, there must be a very effective mechanism for the formation of new β lamellae that is sensitive to a small deviation of the growth rate from its maximum value. It appears difficult to visualize such a mechanism. On the other hand, the experimental information seems to indicate strongly that the spacing is fairly constant, thus suggesting that the curve of v vs. S^α should show a more pronounced maximum. This would happen if the growth rate decreases more at large spacings, e.g. by the effect of the term v/M neglected in our calculation. Such a term may also lead to a drastic change in shape of the growth front at large spacings.

Fig. 24 shows the results calculated for a series of L values and for a series of f values. With the approximations used in the present calculations, the L value will mainly influence the position of S_0^α relative to S_{rev} , whereas the value of f will also affect the growth rate at large spacings.

Some of the results obtained for the various lamellar structures are summarized in Table I. To allow comparison, the different supersaturations have here been represented by the undercooling ΔT , assuming proportionality.

The Effect of Alloying Elements on the Transformation of Austenite

When studying the transformations of austenite in alloyed steels, Hultgren¹⁶ noticed that the kinetic data on the ferrite formation could often be represented by two C-curves in the TTT diagram, instead of one. This indicates that there are two different modes of formation. He also found that the two transformation products sometimes show a difference in appearance under the microscope. Hultgren concluded that the difference was due to the behaviour of the alloying elements during the transformation. At high temperature it is natural to expect that complete chemical equilibrium exists at the phase interfaces and a partitioning of the alloying elements between the matrix and the growing phases could be expected. At low temperatures, the sluggish alloying element may not have sufficient time for diffusion since the growth rate depends on the rate of carbon diffusion. The growing phases may then inherit the alloy content of the matrix. Such transformation products were called para-ferrite, paracementite, and parapearlite by Hultgren, who also

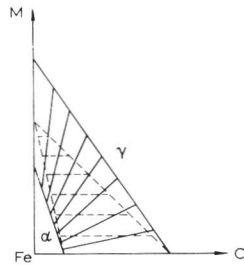


Fig. 25 Isothermal section of ternary phase diagram. Broken lines represent true paraequilibrium.

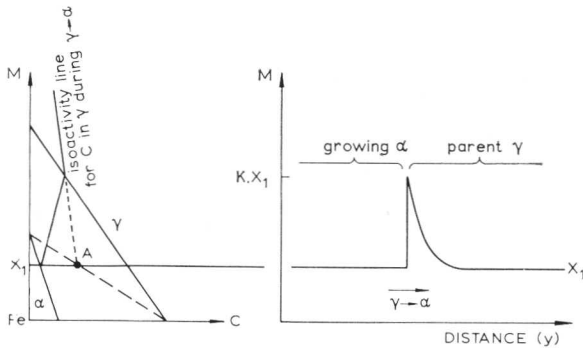


Fig. 26 Pile-up of M ahead of growing α . The original alloy content is X_1 . The original composition must lie to the left of A if the growing α is to inherit the alloy content X_1 .

discussed the equilibrium at the phase interfaces, introducing the term paraequilibrium to designate the case of partial equilibrium where the two adjoining phases are in equilibrium with respect to carbon only, the iron and the alloying element being too sluggish for redistribution. The case of complete equilibrium at interfaces was called orthoequilibrium. Hillert¹⁷ and Rudberg¹⁸ discussed in detail the position of the paraequilibrium phase boundaries in ternary phase diagrams and Aaronson *et al.*¹⁹ recently presented detailed calculations of such phase boundaries under the name of no-partition equilibrium curves. Fig. 25 presents a simple case of an isothermal phase diagram for iron-rich alloys in a system Fe-C-M where the alloying element M may stand for Mn and the temperature could be 800° C. The solid lines represent the stable phase diagram and the dashed lines the paraequilibrium. The tie-lines in the paraequilibrium phase diagram are of course directed towards the C corner because they hold under the condition of no partitioning of M between the two phases.

The conditions at the moving interface during transformation of an alloy system were considered in further detail by the present author,²⁰ who pointed out that the new phase might form with the same alloy composition as the parent phase even if there was complete chemical equilibrium at the interface. This may occur as a result of the formation of a pile-up of the alloying element ahead of the interface, as illustrated in Fig. 26. It was also pointed out that the carbon activity at the interface was controlled by this situation and a method was published by means of which quantitative estimates of the carbon activity could be made.²¹ For low alloy contents, it was possible to calculate the change in

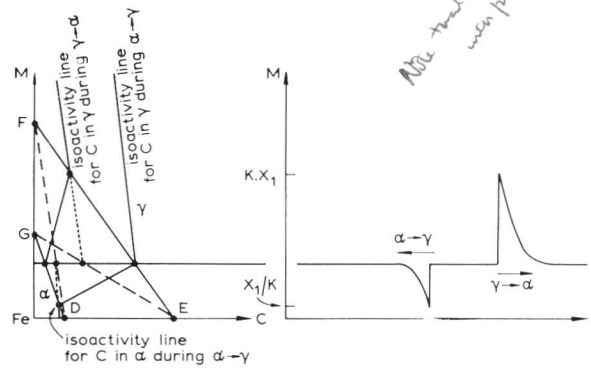


Fig. 27 Difference between the reaction $\gamma \rightarrow \alpha$ and the reverse reaction $\alpha \rightarrow \gamma$. The difference in carbon activity represents a hysteresis.

carbon activity at the two-phase boundary from the equilibrium partition coefficient $K^{\gamma/\alpha}$ of the element between the two phases

$$\ln a_C^1/a_C^0 = - \frac{K^{\gamma/\alpha} \cdot X_{Fe}^\alpha - X_{Fe}^\gamma}{X_C^\gamma - X_C^\alpha} \cdot X_M^\alpha \dots (83)$$

a_C^0 and a_C^1 are the carbon activity values without and with the alloy content X_M^α , respectively. It was suggested that the main part of the effect of alloying elements on the transformation of austenite to ferrite, cementite, pearlite, and bainite was due to this change in carbon activity which affects the carbon-activity difference available to drive the diffusion of carbon. The same pile-up model has independently been suggested by Popov and Mikhalev,²² Kirkaldy,²³ and Darken.²⁴

The pile-up model predicts that the rate of the reaction $\gamma \rightarrow \alpha$ should be controlled by the rate of carbon diffusion away from the moving interface into the interior of the γ grain. This can occur only if the carbon activity is higher at the interface than in the interior of the γ grain. The model may thus work only if the parent phase has an original carbon content to the left of the point A in Fig. 26. The dashed line describes the position of this critical carbon content for various alloy contents. If the original composition lies to the right of this line but inside the equilibrium two-phase field, the reaction can still take place but only by long-range diffusion of the alloy element. The reaction will then be very much slower and the new phase will not inherit the original composition of the parent phase.

The triangle DGE in Fig. 27 may be regarded as the operating two-phase field during the reaction $\gamma \rightarrow \alpha$ as long as it is rate-controlled by carbon diffusion. For the reverse reaction $\alpha \rightarrow \gamma$ the operating two-phase field is the triangle DFE under the same condition. It is important to note that these are two different triangles. The difference may be described as a kind of hysteresis, considering a repeated process of decarburizing and carburizing, and it is due to the free-energy loss connected with the diffusion of the alloying element in the pile-up. At very low temperatures, or high growth rates, the pile-up may become so thin that it exists only mathematically. No free energy will then be lost for diffusion of the alloying element and the hysteresis has disappeared. The two triangles of Fig. 27 have now moved together and have finally coincided to form the broken-line triangle in Fig. 25, representing the true paraequilibrium. The effect of a given alloy addition on the transformation should thus be expected to decrease con-

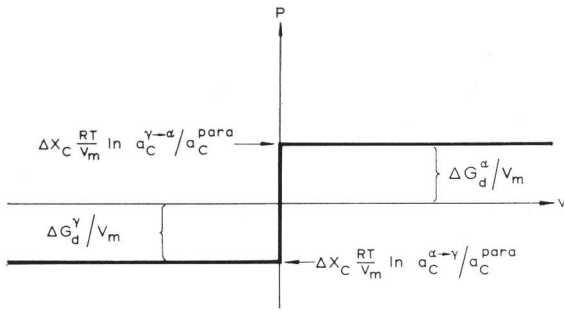


Fig. 28 The force necessary for moving an α/γ interface at a rate v .

siderably when this situation is established at low temperature.

To use the pile-up model in a particular case, where long-range diffusion of the alloying element can be excluded, one simply has to calculate the carbon activity at the α/γ interface, e.g. from the approximate equation (83), and to use this value in the proper kinetic equation. However, there is an alternative method of treating this problem, which uses the true paraequilibrium as a starting point. To introduce this method, we shall consider a hypothetical experiment with a small piece of an Fe- M alloy that is originally in a two-phase state ($\alpha + \gamma$) with no partitioning of the alloy element and a constant carbon activity. The temperature is assumed to be low enough to prevent any long-range diffusion of M . The specimen is then subjected to an atmosphere of another carbon activity. The difference in carbon activity gives rise to a force acting on the α/γ phase boundary. A higher carbon activity in the atmosphere would result in a force pulling the boundary in the direction of the α grain, thus causing the reaction $\alpha \rightarrow \gamma$. A lower carbon activity would have the opposite effect. The value of the force supplied by a certain atmosphere can easily be estimated using the basic equation (3)

$$P = -\Delta G_m/V_m = -\Delta X_C \frac{RT}{V_m} \ln \frac{a_C^{\text{para}}}{a_C^{\text{atm}}} \dots (84)$$

The quantity ΔX_C is the number of moles of carbon absorbed by the specimen during the transformation of one mole of material. a_C^{para} is the carbon activity of the true paraequilibrium according to Fig. 25. To use this type of equation, it may in general be necessary first to calculate a_C^{para} .

Fig. 28 illustrates the growth rate v as a function of P , neglecting the limiting kinetic factors due to the necessity of carbon transport. (In the following diagrams, P will be directly defined as the force caused by the local carbon activity at the interface, in order to avoid the discussion of such kinetic factors.) As the carbon activity of the atmosphere decreases below a critical level $a_C^{\gamma \rightarrow \alpha}$, the growth of α can suddenly start and the growth rate will be limited only by kinetic factors such as the rate of transfer of carbon from the specimen or the rate of carbon diffusion inside the specimen. If the carbon activity of the atmosphere is increased, the reverse transformation does not start until the carbon activity is above another critical value $a_C^{\alpha \rightarrow \gamma}$. The two critical carbon-activity values are caused by the free-energy losses due to the diffusion in the pile-up and can easily be calculated by estimating these losses. The relation between

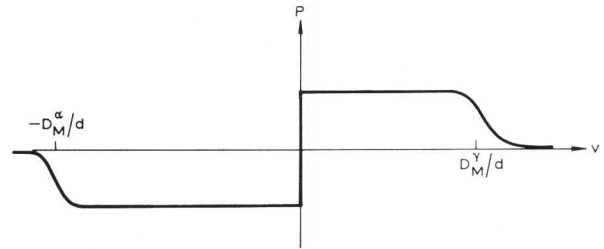


Fig. 29 The decrease of the force at high growth rates where a deviation from local equilibrium begins to develop.

these ΔG_d and a_C is given by Fig. 28. For low contents of M and C and for $K^{\gamma/\alpha}$ close to unity, we obtain approximately from equation (9)

$$\Delta G_d^{\gamma} = RT \left(\frac{X_1}{K} - X_1 \right)^2 / 2X_1 \simeq RT(1-K)^2 X_1 / 2 \dots (85)$$

$$\Delta G_d^{\alpha} = RT(X_1 - KX_1)^2 / 2X_1 \simeq RT(1-K)^2 X_1 / 2 \dots (86)$$

where X_1 is the original alloy content. A more accurate calculation based on an equation such as (6) must be carried out if K is not close to unity.

The size of the hysteresis is obtained by adding equations (85) and (86) and applying the relationships shown in Fig. 28.

$$(X_C^{\gamma} - X_C^{\alpha}) RT \ln a_C^{\text{para}} / a_C^{\gamma \rightarrow \alpha} - (X_C^{\gamma} - X_C^{\alpha}) RT \ln a_C^{\text{para}} / a_C^{\alpha \rightarrow \gamma} = \Delta G_d^{\alpha} + \Delta G_d^{\gamma} \dots (87)$$

$$\ln a_C^{\alpha \rightarrow \gamma} / a_C^{\gamma \rightarrow \alpha} = (K-1)^2 X_1 / (X_C^{\gamma} - X_C^{\alpha}) \dots (88)$$

The size of the hysteresis can also be estimated from the phase diagram (Fig. 27) using equation (83)

$$\ln a_C^{\gamma \rightarrow \alpha} / a_C^0 = -\frac{K-1}{X_C^{\gamma} - X_C^{\alpha}} X_1 \dots (89)$$

$$\ln a_C^{\alpha \rightarrow \gamma} / a_C^0 = -\frac{K-1}{X_C^{\gamma} - X_C^{\alpha}} \cdot X_1 / K \dots (90)$$

Subtracting equation (89) from (90) yields

$$\ln a_C^{\alpha \rightarrow \gamma} / a_C^{\gamma \rightarrow \alpha} = \frac{K-1}{X_C^{\gamma} - X_C^{\alpha}} \left(1 - \frac{1}{K} \right) X_1 \simeq (K-1)^2 X_1 / (X_C^{\gamma} - X_C^{\alpha}) \dots (91)$$

in agreement with equation (88). This is a demonstration of the fact that the two methods of calculation are equivalent. The following discussion of the effect of alloying elements can thus be based on a consideration of the free-energy loss, ΔG_d , instead of the carbon activity.

If the kinetic factors connected with the transport of carbon are rapid enough in comparison with the rate of diffusion of the alloying element, the growth rate may be so high that the thickness of the pile-up decreases below some measure of the atomic dimensions, d . Exactly as in the case of the impurity-drag effect on the motion of a grain boundary considered earlier, we now find that the free-energy loss decreases and goes to zero. We would then obtain the curve shown in Fig. 29. The effect of the alloying element will now be quite small once the threshold has been overcome.

As in the case of grain-boundary migration, we should consider a further effect: as the growth rate increases a

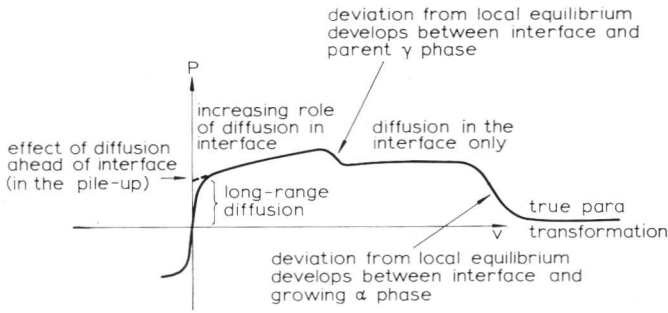


Fig. 30 Hypothetical diagram demonstrating the variation of the force on the interface as function of the growth rate.

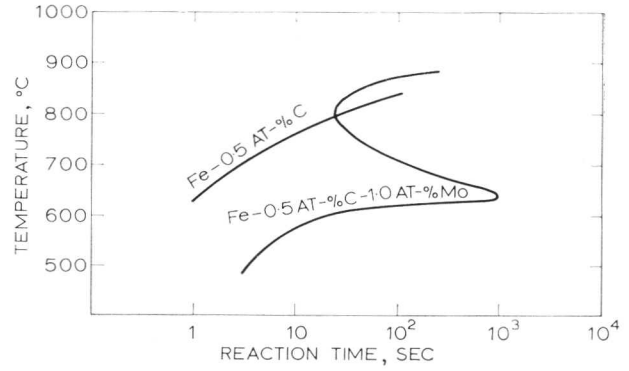


Fig. 32 Isothermal transformation diagrams for the formation of ferrite (Ref. 25).

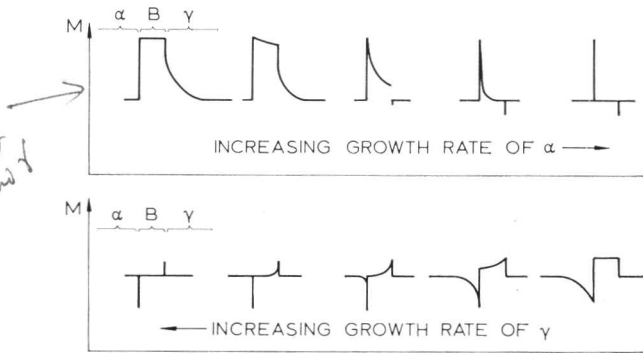


Fig. 31 Concentration profile inside and ahead of α/γ interface.

concentration gradient inside the boundary film may form and increase in importance and we then obtain a new loss of free energy. An even higher carbon activity is then necessary to further increase the growth rate. This effect may very well build up considerably before the first effects starts to decline. Fig. 30 shows a possible shape of the curve, taking both the effects into account and also considering the fact that the alloying element can diffuse over large distances if the growth rate is low enough. A detailed calculation of the two effects can be carried out in the same way as for grain-boundary migration. The shape in Fig. 30 is obtained if the alloy content at equilibrium is higher in the boundary than in γ , which in turn is higher than in α . Fig. 31 demonstrates the concentration profiles at a series of growth rates in the two directions. It is evident that the net effect will be rather different for the two reactions $\gamma \rightarrow \alpha$ and $\alpha \rightarrow \gamma$.

Depending upon the choice of partition coefficients between α , γ , and the boundary, a great variety of behaviour will be found. The effect due to diffusion inside the boundary may be large or small as compared to the first effect and it may also influence the first effect in such a way that there will be a net decrease of the total effect.

A certain set of conditions will in general result in a definite growth rate where the kinetic factors for the carbon transport are in balance with the carbon activity required at the moving interface. In particular, this is true as long as the curve in Fig. 30 has a positive slope. Cases of instability are theoretically conceivable only if the slope of the curve has negative values, large enough to dominate over the rate of increase of the kinetic resistance with growth rate. This may not be a common case.

At high temperature and low supersaturations the transformation of austenite occurs close to the origin in Fig. 30 where the rate is determined by long-range diffusion of M . At higher supersaturations, the growth rate may be high enough to prevent long-range diffusion of M . The effect of the alloying element may now be well accounted for by the simple pile-up model, yielding the extrapolated value on the P axis, using the local carbon-activity value at the interface for the calculation of P .

At lower temperatures of transformation, (and at higher growth rates), we move further to the right in Fig. 30 because D^γ and D^B decrease relative to the growth rate. The increase of the curve now becomes more and more important. At even lower temperatures we may reach the descending parts of the curve where the effect of the alloying element decreases rapidly.

By the use of a diagram like Fig. 30 we might understand the effect of molybdenum on the TTT diagram, which shows two C-curves for the formation of α .¹⁶ Fig. 32 shows a direct comparison made by Kinsman and Aaronson,²⁵ who also proved that the effect of molybdenum was not only on the rate of nucleation but also on the growth rate. At high temperature we should expect a higher growth rate with molybdenum because it is a ferrite stabilizer. The retarding effect that starts at $\sim 800^\circ\text{C}$ and reaches its maximum at $\sim 630^\circ\text{C}$ can be explained as caused by the growing importance of the free-energy loss inside the boundary. To explain the large size of this effect, we must assume that molybdenum has a strong tendency to segregate to the α/γ interface (i.e. a large value of K). In fact, Kinsman and Aaronson, after examining several possibilities without finding the explanation for the existence of the bay in this TTT diagram, also concluded that it may be due to an "impurity-drag" effect.

At even lower temperatures, the concentration profiles in front of the boundary and inside the boundary grow steep enough to give an increasing deviation from local equilibrium. The free-energy losses now decrease and the effect of molybdenum grows weaker. If this description is correct, the upper C-curve holds for the formation of ferrite under complete local equilibrium between the moving boundary and the growing α grain. The lower C-curve should hold for ferrite formed under some deviation from local equilibrium and, at a low enough temperature, for ferrite formed under true paraequilibrium conditions. The original suggestion by Hultgren may thus be essentially correct, although he did not develop his hypothesis in sufficient detail.

Acknowledgement

This study is part of a research project supported financially by the Swedish Council for Applied Research.

References

1. R. Becker, *Z. Metallkunde*, 1937, **29**, 245.
2. S. Ono, *Mem. Fac. Eng. Kyushu Univ.*, 1947, **10**, 195.
3. M. Hillert, *Acta Met.*, 1961, **9**, 525.
4. J. W. Cahn and J. E. Hilliard, *J. Chem. Physics*, 1958, **28**, 258.
5. K. Lücke and K. Detert, *Acta Met.*, 1957, **5**, 628.
6. J. W. Cahn, *ibid.*, 1962, **10**, 789.
7. M. Hillert, *Jernkontorets Ann.*, 1957, **141**, 757.
8. D. Turnbull, *Acta Met.*, 1955, **3**, 55.
9. J. W. Cahn, *ibid.*, 1959, **7**, 18.
10. J. S. Kirkaldy, "Decomposition of Austenite by Diffusional Processes", p. 39. **1962**: New York and London (Interscience Publishers).
11. J. M. Shapiro, Ph.D. Thesis, McMaster Univ., **1966**.
12. M. S. Sulonen, *Acta Met.*, 1964, **12**, 748.
13. G. Speich, "Cellular Precipitation in Fe-Zn Alloys", to be published.
14. C. Zener, *Trans. Amer. Inst. Min. Met. Eng.*, 1946, **167**, 550.
15. K. A. Jackson and J. D. Hunt, *Trans. Met. Soc. A.I.M.E.*, 1966, **236**, 1129.
16. A. Hultgren, *Jernkontorets Ann.*, 1951, **135**, 403.
17. M. Hillert, *ibid.*, 1952, **136**, 25.
18. E. Rudberg, *ibid.*, 1952, **136**, 91.
19. H. I. Aaronson, H. A. Domian, and G. M. Pound, *Trans. Met. Soc. A.I.M.E.*, 1966, **236**, 768.
20. M. Hillert, *Internal Rep., Swedish Inst. Metal Research*, **1953**.
21. M. Hillert, *Acta Met.*, 1955, **3**, 34.
22. A. A. Popov and M. S. Mikhalev, *Physics Metals Metallography*, 1959, **7**, 36.
23. J. S. Kirkaldy, *Canad. J. Physics*, 1958, **36**, 907.
24. L. S. Darken, *Trans. Met. Soc. A.I.M.E.*, 1961, **221**, 654.
25. K. R. Kinsman and H. I. Aaronson, "Symposium on Transformation and Hardenability in Steel, 1967", to be published.

Phase Transformations in U-Cr Alloys

A. Bar-Or and G. Kimmel

Rates of growth of pearlite, bainite, and martensite in U-Cr alloys have been determined. Good agreement between Turnbull's theoretical formulae for growth rate and the bainite experimental results indicated that the growth of bainite is controlled by the interface atom jumps, for both lateral and longitudinal directions. Extrapolation of the growth-rate results from the bainite into the pearlite range showed surprisingly close agreement with growth-rate measurements of pearlite, suggesting that an identical mechanism controls both. The good agreement between Turnbull's formulae for rate of growth and the experimental results in martensite leads also to the proposal that the rate of growth for martensite plates in U-Cr alloys is controlled by interface movement, itself controlled by individual atom jumps. It is suggested that growth of martensite takes place in two steps: the rate-controlling step and an intermittent second step in which a certain proportion of atoms cross the interface by a co-operative process.

The existence of three modes of transformation in dilute uranium-chromium alloys, namely pearlite transformation in the high-temperature range, bainite in the medium range, and martensite at the lower temperatures, was recognized in White's¹ classical work and later, even more clearly, in the studies summarized by Burke.² Both White and the investigators after him who studied the U-Cr system examined mainly the mechanism of the overall transformation. To gain a deeper insight into the various individual transformations, it was decided to take growth-rate measurements with the aid of which it was hoped to clarify the growth-controlling mechanisms.

Experimental

Measurements of the Growth Rate of Pearlite^{3,4}

It was evident that in the U-Cr system growth-rate measurements could conveniently be carried out only very high in the α range where nucleation does not interfere with the measurements. In this temperature range it is interesting to note that a rim of columnar pearlite grains grew from the specimen surfaces (Fig. 1). By following the change in width of this rim with time, the growth rate of pearlite was determined accurately and with great ease. As finer grains were found

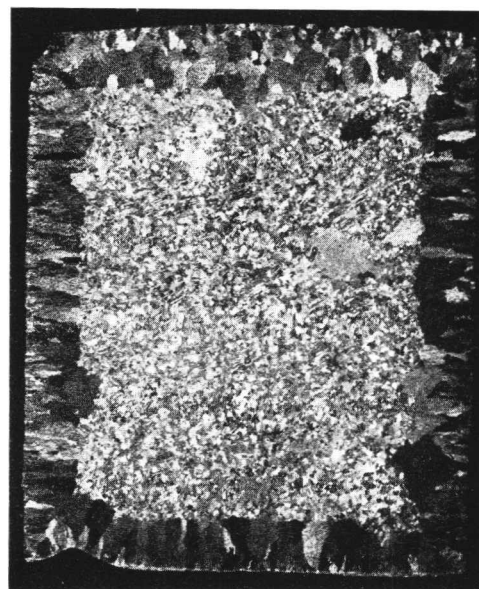


Fig. 1 Growth of rim of columnar grains in U-1.35 at.-%Cr, isothermally treated at 620 °C. $\times \sim 2\frac{1}{2}$.

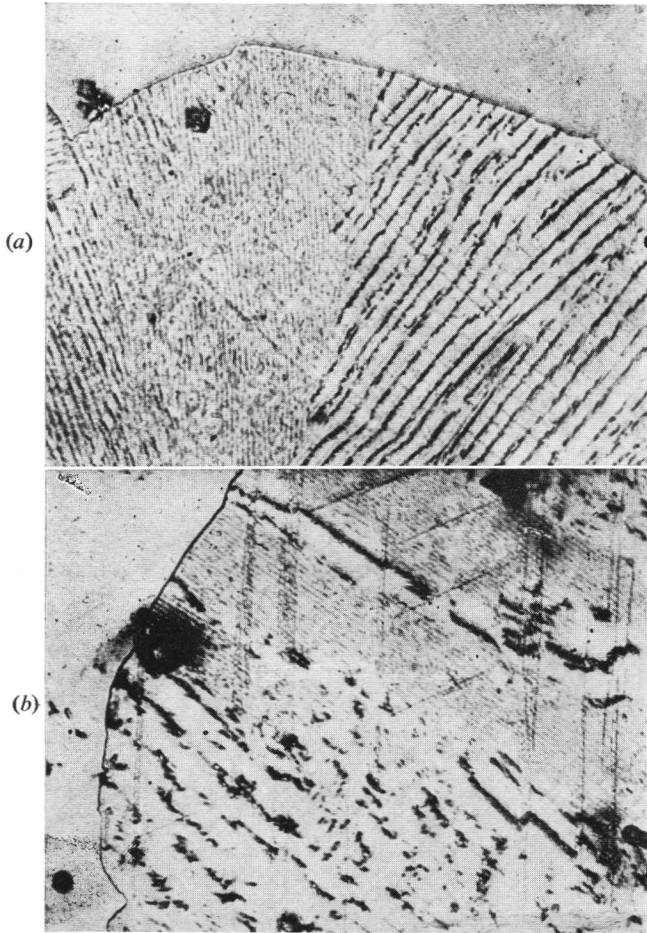
on the surfaces of the specimens than in their interiors, it was concluded that the higher rate of surface nucleation was responsible for the rim formation.⁵

On the assumption that the transformation in the upper α range is pearlitic, the structure was examined for characteristic pearlite lamellae. However, the precipitate found in the matrix did not resemble any known pearlitic structure and it was discovered that distinct lamellae appear only in alloys made from electrolytic-purity uranium (E.P.U.) melted in ceramic crucibles (Figs. 2(a) and (b)). In alloys made from nuclear-purity uranium (N.P.U.), which contains ~ 700 ppm carbon, or in E.P.U. alloys to which 700 ppm carbon was added, only a degenerate structure appeared.

Once the lamellar structure was revealed in E.P.U. alloys, it was decided to re-examine the growth rate in these alloys and to determine interlamellar spacings. Representative results of growth-rate measurements are given in Fig. 3. It is evident that, after an incubation period, growth rate is a linear function of time until impingement occurs.

Various specimens were examined metallographically to ascertain whether there is a correlation between change in interlamellar spacing and growth rate. It was found that in some grains the interlamellar spacings change appreciably, yet growth rate is almost unaffected (Fig. 2(b)).

Manuscript received 20 March 1968. A. Bar-Or, Ph.D., and G. Kimmel, B.Sc., are with the Israel Atomic Energy Commission, Nuclear Research Center, Negev.



Figs. 2(a) and (b) Chromium lamellae in electrolytic-purity uranium alloy (E.P.U.) containing 0.67 at.-% Cr. $\times 1500$.

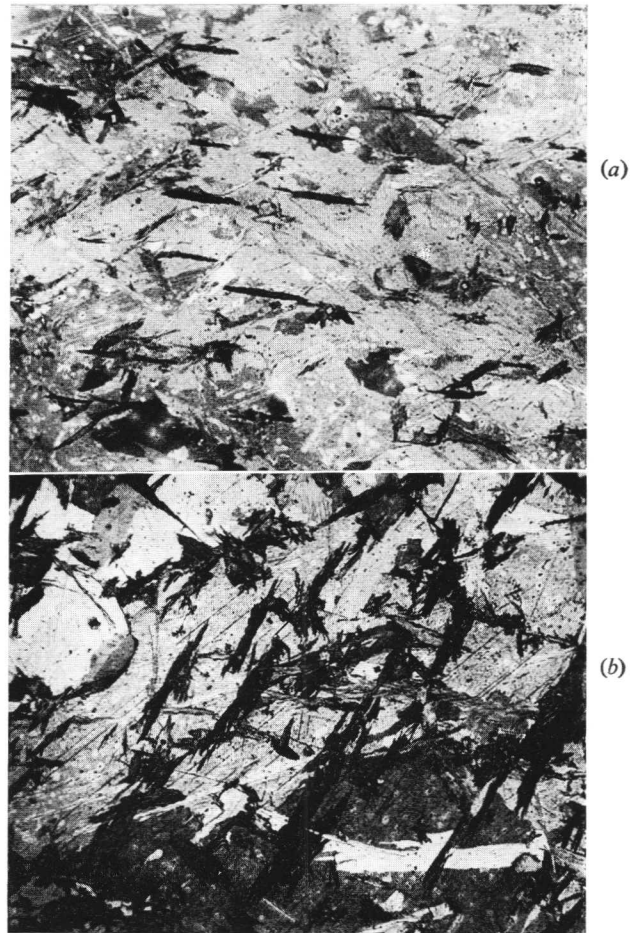


Fig. 4 Bainite plates in U-0.61 at.-% Cr alloy after different periods of isothermal heat-treatment at 448 °C. (a) 10 min; (b) 20 min. $\times 100$.

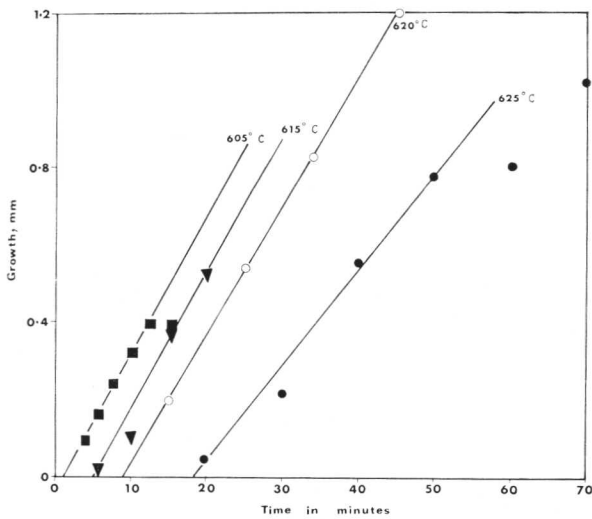


Fig. 3 Growth rate of pearlite in E.P.U.-1.1 at.-% Cr at various temperatures.

Measurements of the Growth Rate of Bainite⁶

Growth rates of bainite plates were determined in both transverse and longitudinal directions by following statistically the change in width and length of the largest plates (Fig. 4) in the U-0.61 at.-% Cr and U-0.70 at.-% Cr alloys.

The growth-rate results in U-0.61% Cr are presented in Fig. 5, from which linear growth in both lateral and longitudinal directions is clearly evident. Also it is apparent that the growth of bainite plates is a thermally activated process. The activation energy for lateral growth is the same as that for longitudinal growth to the degree of accuracy of the measurements. On comparing the growth rates for the two alloys, it can be seen that chromium retards the growth rate of bainite plates.

Measurement of the Growth Rate of Martensite⁷

The isothermal growth rates in both the lateral and longitudinal directions of individually identified plates (Fig. 6) were determined in a series of U-Cr alloys at various temperatures.

To eliminate the interference of β grain boundaries with the growth of plates, all measurements were conducted on specimens that were pretreated by slow cooling from γ to β , to allow the growth of large β grains up to a few mm in dia. It was also ascertained that there was no interference by athermal growth with the rate measurements

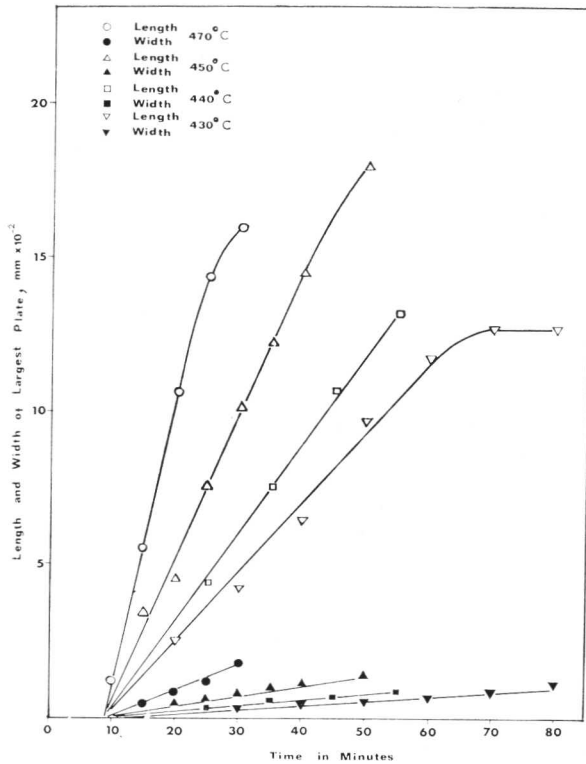


Fig. 5 Lateral and longitudinal growth rates of bainite plates in U-0.61 at-% Cr alloy.

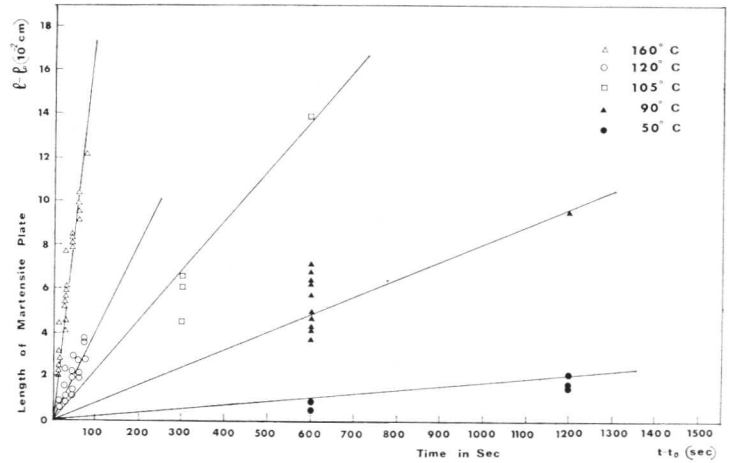


Fig. 7 Growth-rate measurements of martensite plates in U-0.73 at-% Cr alloy.

Representative results for both lateral and longitudinal growth for the U-0.73 at-% Cr alloy are given in Fig. 7; the linear growth rate is clearly evident. Similar results were recorded for the U-0.45 and U-0.95 at-% Cr alloys. Growth in both directions is thermally activated, having the same activation energy.

Discussion

Growth of Pearlite

With quantitative information on the growth rate in the pearlite range and on the interlamellar spacing, it becomes possible to use Cahn and Hagel's⁸ criteria to ascertain whether or not the mechanism controlling growth is long-distance diffusion of Cr. The results indicate that long-range diffusion of Cr does not control pearlite growth. Two other experimental results support this finding:

(a) Profound changes in lamellar structure occur when carbon is added which have very little effect on the growth rate.

(b) The marked change in the lamellar structure in individual grains has no noticeable effect on growth rate.

It is therefore thought that growth is controlled by interface migration, as suggested by Picklesimer *et al.*⁹ for pearlite in some iron-carbon alloys. The lamellar structure is a subsidiary effect that follows interface movement but does not control it.

Growth of Bainite

By comparing the experimental diffusion coefficient for Cr in U with that calculated by the aid of the Zener-Hillert formula, it could be shown that this model does not apply in the present case. There are two other observations to support this deduction:

(a) The radius of the tip of the bainite plates varies appreciably from one plate to another, while their sizes are comparable.

(b) The activation energy should be temperature-dependent, in contradiction to our findings.

Interface Movement of Pearlite and Bainite

In view of the negative results of the Cahn criterion for the growth-controlling step of pearlite and of the Zener-Hillert criterion for bainite, it was considered whether the alternative mechanism of interface mobility might control pearlite as well as bainite.

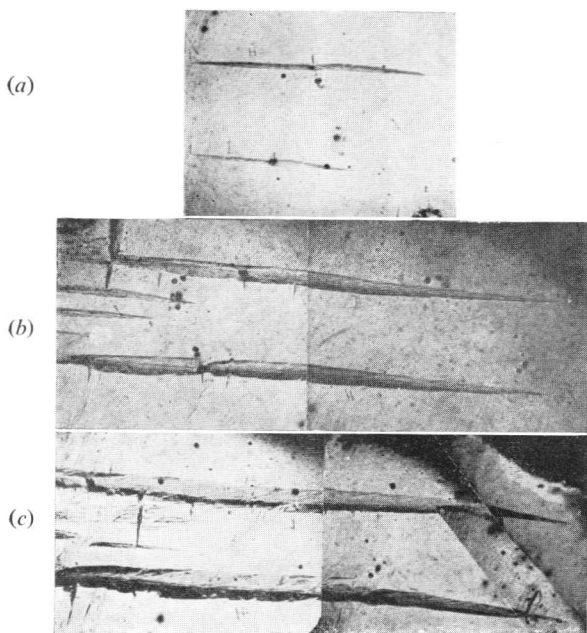


Fig. 6 Growth of martensite plates in U-0.73 at-% Cr at 200°C. (a) 5 min; (b) 10 min; (c) 15 min. x 25.

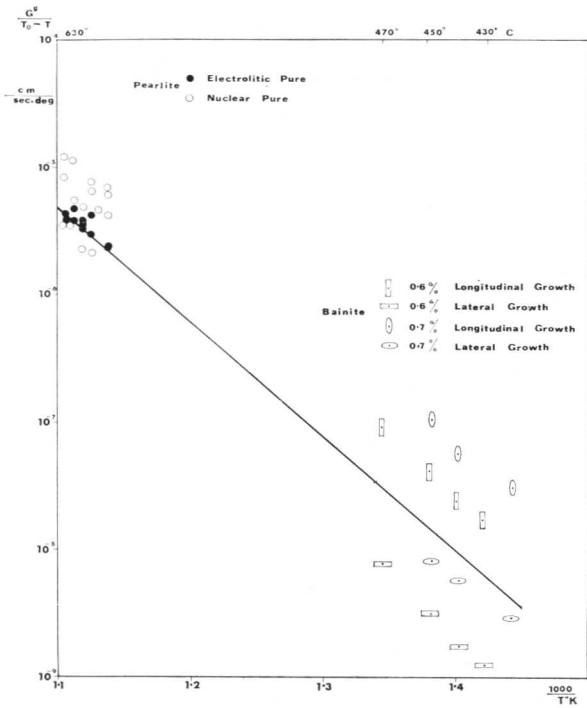


Fig. 8 Comparison between growth-rate values calculated with the aid of Turnbull's equation and experimental growth-rate results for pearlite and bainite.

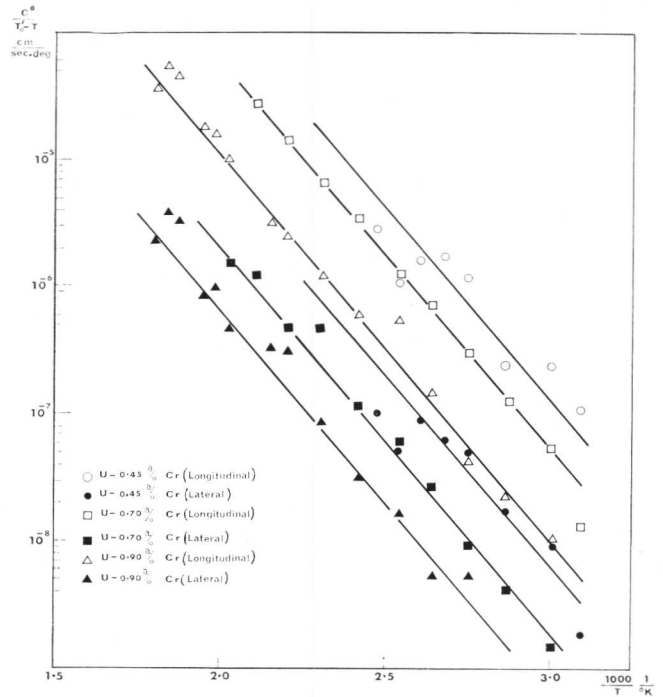


Fig. 9 The activation energies for lateral and longitudinal growth for martensite plates.

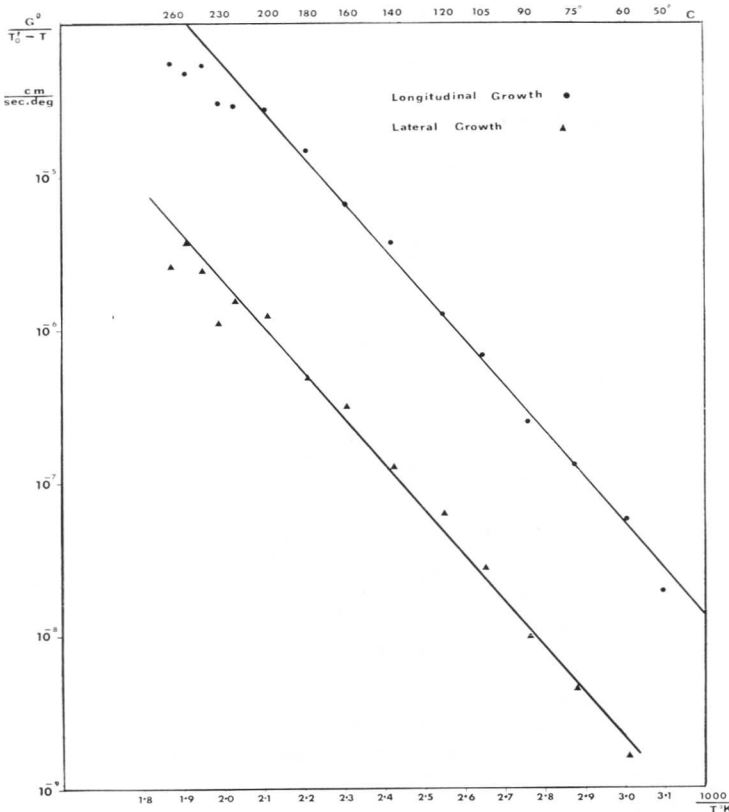


Fig. 10 Comparison between lateral and longitudinal growth rates of martensite in U-0.73 at.% Cr alloy.

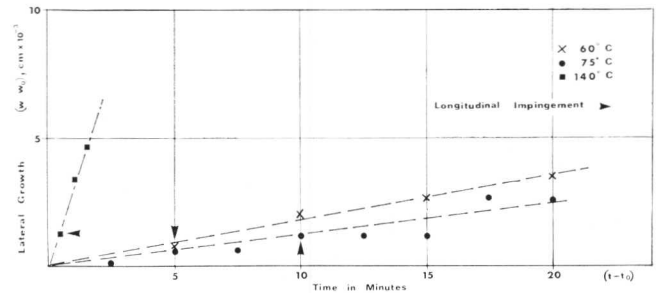


Fig. 11 Lateral-growth rate of martensite plates before and after impingement with β grain boundary in U-0.73 at.% Cr.

TABLE I			
Comparison between Various Pre-Exponential Terms for Different U-Cr Alloys			
Alloy, at.-%	$L_0, \text{cm} \cdot \text{sec}^{-1} \cdot \text{K}^{-1}$		T_0', K
	Longitudinal	Lateral	
0.45	200	15	723
0.73	100	5	673
0.95	70	3	643

We have followed Turnbull¹⁰ and used absolute-rate theory for describing the growth of the two transformations. Turnbull showed that \dot{G} , the rate at which an interface moves, is given by

$$\dot{G} = \lambda \frac{\Delta F}{hN} \exp\left(\frac{\Delta S^*}{R}\right) \exp\left(-\frac{\Delta H}{RT}\right)$$

where λ is the displacement (i.e. distance moved) to adjust the atomic positions on passing from $\beta \rightarrow \alpha$; $\Delta F = F^\alpha - F^\beta$ is the driving force for growth; F^α, F^β are the free energies of α and β , respectively; ΔS^* is the entropy of the activated state; h is Planck's constant; and N is Avogadro's number. λ is estimated to be one interatomic distance, 3×10^{-8} cm. ΔF can be estimated from the relation

$$\Delta F = \frac{\Delta H_{\alpha\beta}}{T_0} (T_0 - T)$$

where $T_0 = 907^\circ \text{K}$, the eutectoid temperature, taken between the values given by Daane and Wilson¹¹ and by Aubert;¹² $\Delta H_{\alpha\beta} = 695$ cal/mole, the heat of transformation taken from Holden;¹³ and ΔS^* is estimated from the Zener¹⁴ relation

$$\Delta S^* \simeq b \frac{\Delta H}{T_{mp}}$$

where b is a constant equal to 0.35; ΔH , the activation energy, is measured experimentally⁶ from the growth rate of bainite plates and equals 42 kcal. mole⁻¹.

From these values ΔS^* is found to be 10.5 cal. mole⁻¹ °K⁻¹.

Inserting the various values into Turnbull's equation written in the following way

$$\dot{G} = L_0 (T_0 - T) \exp\left(-\frac{\Delta H}{RT}\right)$$

one obtains

$$L_0 = \frac{\lambda}{hN} \frac{\Delta H_{\alpha\beta}}{T_0} \exp\left(\frac{\Delta S^*}{R}\right) = 4.6 \times 10^4 \text{ cm. sec}^{-1} \text{ } ^\circ\text{K}^{-1}$$

On plotting the theoretical line $\dot{G} = 4.6 \times 10^4 (T_0 - T) \exp(-42,000/RT)$ (Fig. 8) we find that it fits well with the experimental results for the growth of pearlite and is intermediate between the values for lateral and longitudinal growth of bainite. It is therefore deduced that pearlite and the two directions of bainite are controlled by the same interface mobility, itself controlled by individual random atom movements at the interface. The better agreement between calculated and experimental results for alloys made from E.P.U. material is attributed to the variable effect of impurities in the N.P.U. material.

The fact that the pre-exponential term for pearlite is intermediate between those for lateral and longitudinal growth of bainite explains how the radial growth of pearlite as well as plate-like growth of bainite are controlled by the same mechanism.

Growth of Martensite

From the experimental measurements of growth rate of martensite plates we note the following:

(a) The growth of the individual martensite plates is a linear function of time at all temperatures, suggesting that growth is controlled by some interface mechanism.

(b) Growth rate is a thermally activated process.

(c) A clear maximum in the growth rate as a function of temperature is found in the three alloys studied.

From the first two observations we assume that growth of martensite plates is controlled by a process similar to that described previously for growth of pearlite and bainite. To test this assumption we again turn to Turnbull's equation and attempt to compare experimental results with theoretical calculations. The activation energies for both lateral and longitudinal directions for various alloys were found to be 14 ± 1 kcal. mole⁻¹ (Fig. 9).

The pre-exponential term L_0' (all the parameters are given primes in this case) was calculated with the aid of Turnbull's equation in which various parameters need to be estimated as previously

$$\Delta F' = \frac{\Delta H_{\alpha\beta}}{T_0'} (T_0' - T) \quad \text{for } M_s < T_0' < T_E$$

where T_E is the β/α equilibrium temperature, $\simeq T_0$ in pearlite; M_s is the martensite-start temperature taken from Burke;¹⁵

and $\frac{\Delta H_{\alpha\beta}}{T_0'} \simeq 1.0$ cal. mole⁻¹ °K⁻¹.

The value for λ' was taken to be 3×10^{-9} cm, since a minimum of 10% homogeneous strain is needed for one β unit cell to transform into several α' cells, as shown by Lomer.¹⁶ The activation energy of 14 kcal. mole⁻¹ suggests that the atom movements occur only over part of an interatomic distance. ΔS^* is estimated as before using the Zener¹⁴ relation and is found to be ~ 3.5 cal. mole⁻¹ °K⁻¹. Hence L_0' for martensite = 180 cm. sec⁻¹ °K⁻¹. Experimental L_0' values were determined by plotting $\dot{G}/(T_0' - T)$ against $1/T$ (Fig. 9) and are given in Table I.

It can be seen that for longitudinal growth there is an excellent agreement between the calculated and experimental values in the case of the lower-chromium (0.45%) alloy. However, on increasing the Cr content, we find a discrepancy between theory and experiment which increases with Cr content. To understand the reason for this, it is necessary to examine the effect of Cr on the various parameters contained in L_0' . It is clear that Cr cannot affect λ and its effect on ΔF has already been taken into account. A change in Cr content can account for a change of only 0.1 cm. sec⁻¹ °K⁻¹ in ΔS^* , while the experimental discrepancy is an order of magnitude greater than this. (Previously we attempted to correlate experimental results and calculations by changing ΔS^* arbitrarily.⁷) We are therefore inclined to attribute the discrepancy caused by the addition of Cr to its effect on jump frequency at the interface. This factor was considered to be constant in our calculation, but should be taken as a function of Cr content.

The lateral-growth rate is smaller than the longitudinal rate (Fig. 10) by a ratio that is almost independent of Cr content and temperature. It is therefore suggested that either lateral growth is controlled by longitudinal growth or the same mechanism controls both. To distinguish between these two possibilities, longitudinal and lateral rates of growth of identified plates were measured, before and after the plate edge impinged upon a β grain boundary. From the results presented in Fig. 11 it can be seen that the lateral growth is independent of the longitudinal growth. We therefore believe that lateral growth is controlled by the same process as longitudinal growth, and that there is some factor responsible for its being slower by a constant ratio. At the present stage of knowledge it is difficult to identify this factor; we tend to attribute it to differences in jump frequency at the two orientations.

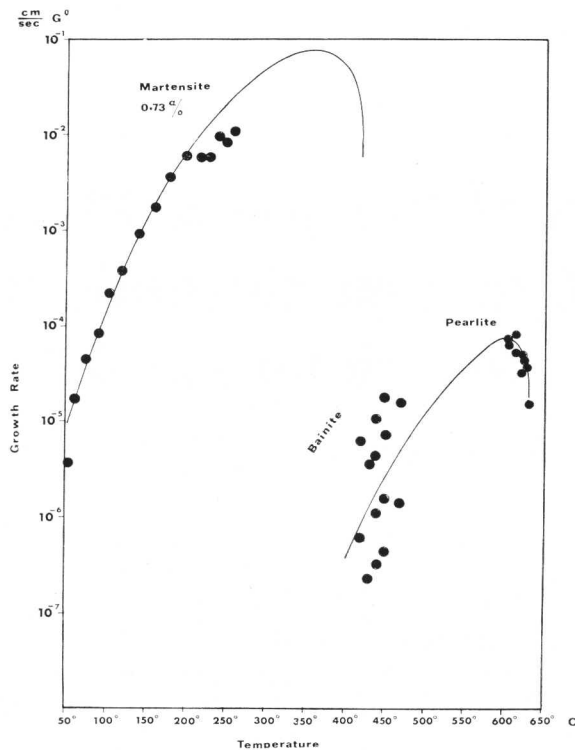


Fig. 12 \dot{G} vs. T for pearlite, bainite, and martensite.

It is evident that the plate growth in the present study causes surface relief but the individual atom jump process suggested to control growth cannot account for it. We assume that growth proceeds in two stages: one of cooperative coherent growth, which explains the surface relief; the other of individual random atom jumps of subatomic distance at the

interface. The latter is the step that controls the rate of growth according to the results of the present study. If such a mechanism is operative, the value found for the pre-exponential term would differ from the calculated one by a factor given by the ratio of numbers of atoms crossing the interface in the two stages. If this ratio is not more than an order of magnitude, the agreement between experiment and theory would still be good.

The results of the present study can best be summarized by Fig. 12, where calculated growth rates for pearlite, bainite, and martensite are compared with the respective experimental values.

References

1. D. W. White, *Trans. Amer. Inst. Min. Met. Eng.*, 1955, **203**, 1221.
2. J. Burke and P. H. Dixon, *J. Nuclear Mat.*, 1962, **7**, 38.
3. A. Bar-Or, P. Wynblatt, and G. Hirsh, *Trans. Met. Soc. A.I.M.E.*, 1965, **233**, 1100.
4. A. Bar-Or, *J. Inst. Metals*, 1966, **94**, 214.
5. A. Bar-Or and P. Wynblatt, *ibid.*, 1963-64, **92**, 183.
6. I. Amity, A. Rosen, and A. Bar-Or, *ibid.*, 1967, **95**, 48.
7. A. Bar-Or and G. Kimmel, *Trans. Met. Soc. A.I.M.E.*, 1967, **239**, 1615.
8. J. W. Cahn and W. C. Hagel, "Decomposition of Austenite by Diffusional Processes", p. 131. 1962: New York and London. (Interscience Publishers).
9. M. L. Picklesimer, D. L. McElroy, T. M. Kegley, E. E. Stansbury, and J. H. Frye, Jr., *Trans. Met. Soc. A.I.M.E.*, 1960, **218**, 473.
10. D. Turnbull, "Thermodynamics in Physical Metallurgy", p. 301. 1950: Cleveland, Ohio (Amer. Soc. Metals).
11. A. H. Daane and A. S. Wilson, *Trans. Amer. Inst. Min. Met. Eng.*, 1955, **203**, 1219.
12. H. Aubert, *Commissariat à l'Energie Atomique Rap.* (2186), 1962.
13. A. N. Holden, "Physical Metallurgy of Uranium". 1958: Reading, Mass. (Addison Wesley).
14. C. Zener, "Imperfections in Nearly Perfect Crystals". 1952: New York and London (John Wiley).
15. J. Burke, "Physical Properties of Martensite and Bainite", (Special Rep. No. 93). 1965: London (Iron Steel Inst.).
16. W. M. Lomer, "The Mechanism of Phase Transformations in Metals". 1955: London (Inst. Metals).

Transformation Kinetics of the $\beta \rightarrow \alpha$ Phase Change in a Uranium–Chromium–Molybdenum Alloy

M. M. Haberman and G. F. Slattery

The $\beta \rightarrow \alpha$ transformation in a uranium–0.25 at.-% chromium–0.5 at.-% molybdenum alloy has been studied at temperatures down to 300° C by dilatometry, metallography, hardness, and X-ray diffraction. A detailed analysis of the kinetics of transformation has been made. The *TTT* diagram was derived by dilatometry and found to consist of two C curves. The upper C curve was predominantly associated with a diffusion-controlled transformation but the associated metallographic, hardness, and X-ray results would suggest a subdivision of this upper C region at a temperature in the range 480–510° C. The intermediate mechanism of transformation is probably of a bainitic type and extends down to $\sim 425^\circ$ C. The low-temperature C curve appears to involve a shear-type transformation.

The phase change $\beta \rightarrow \alpha$ in uranium is of considerable technological interest since it is the basis of the heat-treatment used to refine the grain size of uranium nuclear-fuel rods. This refinement is required to eliminate surface wrinkling under irradiation, a phenomenon ascribed to unrestrained irradiation-growth of surface grains and potentially a source of cladding failures. The β -quenching treatment of Springfield uranium rods produces a small amount of preferred orientation in the transformed α -uranium, leading to an overall irradiation-induced anisotropic growth of the fuel rods.¹

Alloying with 0.5 at.-% chromium retards the $\beta \rightarrow \alpha$ transformation so that the β phase can be caused to transform isothermally at 550° C, yielding a fine-grained α product. Compared to quenching, the isothermal heat-treatment leads to a reduction in the temperature gradient between rim and core of the fuel rod during the transformation. A substantial reduction in preferred orientation also occurs such that the fuel rods are now reasonably random in texture.² The addition of molybdenum confers strength and irradiation stability on uranium;³ hence the presence of small amounts of this element in the dilute U–Cr alloy presents an attractive fuel composition. Some aspects of the transformation character-

istics of such a ternary U–Cr–Mo alloy under continuous cooling have already been reported.⁴

The aim of the present investigation was to study the effects of adding Mo to the U–Cr alloy on the kinetics and mode of the isothermal $\beta \rightarrow \alpha$ transformation. It has been established that the effect of the two alloying elements in combination are more than additive in terms of the incubation period required for the $\beta \rightarrow \alpha$ transformation.^{5,6} Since it is important to minimize reactivity losses due to alloying in a nuclear fuel, the Cr content was reduced to 0.25 at.-% and the Mo addition fixed at 0.5 at.-%. This combination was adequate to ensure the production of a fine-grained α product by isothermal transformation at 550° C.

Previous Work

White⁷ used a dilatometric technique to derive the *TTT* diagrams for several U–Cr alloys. The *TTT* diagrams for alloys containing 0.6, 0.45, and 0.3 at.-% Cr consisted of two C curves: the upper curve between 660 and 400° C was associated with a diffusion-controlled transformation while the lower curve represented a diffusionless shear-type transformation. Jepson *et al.*,⁵ also using dilatometry, found two loops in the *TTT* diagram of the U–0.5 at.-% Cr alloy. There was a well-defined break between the loops and the upper loop was very similar to that found by White.⁷ Similar transformation characteristics were obtained for a wide range of dilute uranium alloys. Metallographic examination showed that the structure produced by transformation above 500° C comprised equiaxed, polygonal grains of α -U whose grain size decreased with decreasing transformation temperature, as expected from a diffusion-controlled transformation. Lowering the temperature further inside the upper C loop produced a fine acicular structure with irregular grain boundaries. Beaudier *et al.*⁸ also showed a distinct change in microstructure between these two regions.

Dixon and Burke⁹ redetermined the *TTT* diagram for the U–0.5 at.-% Cr alloy using an electrical-resistivity technique and produced evidence to suggest that the upper C curve was composed of two overlapping C curves intersecting at $\sim 520^\circ$ C. Analysis of the transformation kinetics¹⁰ indicated that the β phase transformed to α by three distinct mechanisms depending on temperature. As the temperature is lowered in the upper region, the diffusion-controlled nucleation and growth C_1 transformation gives way to one, termed the C_2 region, involving both shear and diffusion

Manuscript received 23 February 1968. M. M. Haberman, B.Sc., and G. F. Slattery, M.Sc., Ph.D., A.I.M., A.Inst.P., are with the U.K.A.E.A. Reactor Group, Springfields Works, Salwick, near Preston, Lancs.

similar to a bainitic transformation. The third mechanism from 420° C downwards became the C_3 transformation, of a martensitic type. Since their evidence was only indirect because of a low sensitivity of the resistivity method in the critical temperature range of interest of $\sim 520^\circ\text{C}$, a further study was made of the U-0.85 at.-% Cr alloy,¹¹ and this established direct evidence for the existence of a C_2 region in this alloy. It was suggested that the mechanism in C_2 was more related to the diffusional reaction of C_1 than the martensitic C_3 , and that the phase change in C_2 involved diffusion as the dominant process. Amity *et al.*¹² have investigated the structure formed in the intermediate C_2 region in the binary U-Cr alloys and found two types of acicular structure, namely a Widmanstätten structure and bainitic plates.

Kitchingman *et al.*¹³ investigated the U-1.0 at.-% Pt alloy and found three mechanisms of transformation by using electrical resistivity, but dilatometric measurements on the same alloy indicated only two transformations since they did not show any subdivision of the high-temperature $\beta \rightarrow \alpha$ phase transformation.

Experimental

The alloy used was in the form of 1-in.-dia. rods prepared by vacuum induction-melting and casting into graphite moulds. The composition (ppm by wt.) was: Mo 1951, Cr 542, Si 27, C 569.

The apparatus consisted of three furnaces, a high-temperature radiation furnace for the β -phase treatment, an intermediate-temperature lead bath, and a lower-temperature lead-tin eutectic bath. The two baths covered transformation ranges from 600 to 200° C. The furnaces were situated in a circular baseplate at equal intervals on a common circle. The silica dilatometer assembly was supported on a central shaft so that the specimen could be transferred from one furnace to another within 3 sec. The system could be evacuated to 10^{-3} mm Hg or used in an inert atmosphere such as argon. A Chromel/Alumel thermocouple was inserted into the dilatometric specimen to record the temperature. A transducer with a linear response accurate to 1% was attached to the specimen to measure the dilation as a function of time.

The specimens were cylindrical pencils 1 in. long $\times \frac{3}{16}$ in. dia. They were held at the soaking temperature of 720° C for 30 min, transferred rapidly to the transformation bath, and a plot made of specimen contraction vs. logarithm of time to give a rate curve. The start and finish of transformation could be determined from the curve. The cooling rates from the β -phase temperature to the transformation temperature were maintained uniform at 20 ± 5 degC/sec. The mean value for the magnitude of the linear length change for the $\beta \rightarrow \alpha$ phase change was 0.32%. A dilatometric trace for this alloy, obtained using a Chevenard-type dilatometer¹⁴ and slow heating and cooling rates of 90 and 170 degC/h, respectively, showed the $\alpha \rightleftharpoons \beta$ transformation on heating at $670 \pm 5^\circ\text{C}$ and on cooling at $570 \pm 5^\circ\text{C}$.

Each of the fully transformed specimens was sectioned and examined metallographically using standard techniques of preparation.¹⁵ The grain sizes were measured by the lineal-intercept method, although sub-graining in the lower C shear region made measurements difficult and the values obtained for this region are approximate. The hardness of transformed specimens was measured on a Reichert microhardness tester. Five readings were taken on each specimen and the results averaged. Back-reflection photographs of transformed specimens were taken using $\text{CuK}\alpha$ radiation and a specimen-to-film distance of 3 cm.

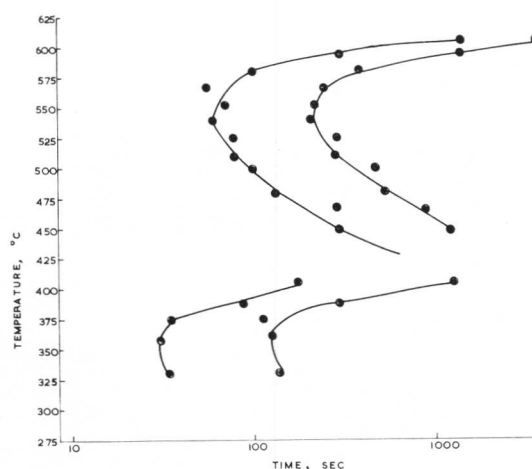


Fig. 1 TTT curve of the U-Cr-Mo alloy.

Results

The isothermal transformation curves obtained from dilatometric measurements are shown in the form of a *TTT* diagram in Fig. 1. All the rate curves were sigmoidal in form. The *TTT* diagram comprised an upper and lower C loop. The break between the two C loops, corresponding to maximum β stability, occurred at $\sim 425^\circ\text{C}$. A minimum value of 60 sec was obtained for the incubation period at 540° C in the upper C loop, while the minimum value in the lower C loop occurred at 350° C. There appeared to be a possible discontinuity in the upper C loop at 525° C where the times for both the start and the finish of the transformation were slightly larger than at neighbouring temperatures, but this effect could be within the experimental scatter. Generally there was scatter in either the start or the finish of the transformation but it is interesting that this 525° C result was the only one where deviations were obtained for both.

Comparing the diagram with the binary U-0.3 at.-% Cr alloy diagram obtained by White,⁷ the effect of the Mo addition was to depress and extend the range of the upper C loop with an increase in incubation period. Similarly, the incubation period was considerably increased for the lower C region.

Metallographic examination of the transformed product showed it to be polygonal, equiaxed and twinned α down to 525° C in the upper C region (Fig. 2(a)), the grain size decreasing as the transformation temperature was reduced (Fig. 2(b)). Below 525° C the equiaxed product changed to a mixture of a feathery structure with some equiaxed-grain regions, and this mixture of products existed over a temperature range of ~ 30 degC. Below 480° C, the structure was duplex acicular consisting of Widmanstätten needles and shear platelets (Fig. 2(c)) and this persisted to the bottom of the upper C loop. Transformation in the lower C loop produced a large, irregular structure with extensive sub-graining (Fig. 2(d)). An approximate estimate of grain size showed an increase with decreasing transformation temperature from 90 μm at 405° C to 160 μm at 310° C (Fig. 3).

Precipitation was observed in the upper C region, but the nature of this varied as the temperature was lowered. Above 525° C the product appeared as a fine lamellar eutectoid decomposition product (Fig. 4(a)). The higher the transformation temperature in this region, the coarser and more abundant were the lamellae. Below 525° C there was a

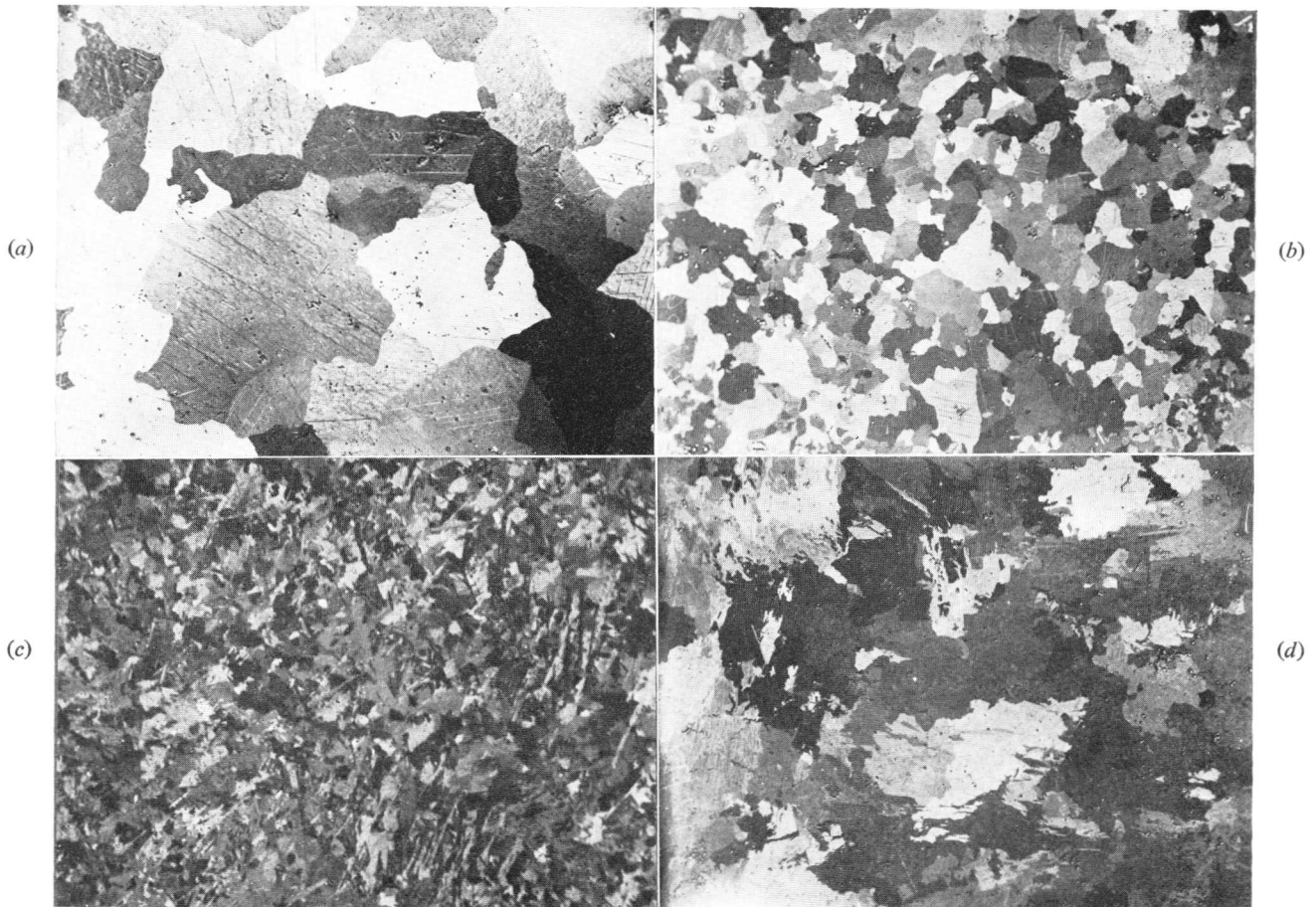


Fig. 2 Polygonal α produced by transformation at (a) 605° C; (b) 540° C. $\times 80$. (c) α produced by transformation at 447° C. $\times 160$. (d) Shear α produced by transformation at 375° C. $\times 80$.

change to a discrete globular precipitate, fairly randomly dispersed (Fig. 4(b)). The precipitate was probably an Mo/Cr/U complex from a supersaturated α solution formed by shear of the β . No precipitate was visible in the specimens transformed in the lower C martensitic region.

The hardness is plotted in Fig. 5 as a function of transformation temperature for the upper C region. The hardness increased with decreasing transformation temperature with a discontinuity in the curve represented by a softening between 510 and 480° C. This region of softening coincided with the region of mixed metallographic structures and suggests that both transformation products coexist over a limited temperature range. In the lower C region there was a decrease in hardness with decreasing transformation temperature, as found for the U-Cr alloy.⁹

The X-ray diffraction patterns from specimens transformed above the nose of the upper C loop were different in appearance from those below the nose (Figs. 6(a) and (b)). Above the nose the diffraction rings were well resolved and typical of a strain-free structure, whereas below the nose the rings were diffuse and continuous, indicative of lattice strain appropriate to a shear-type product.

Discussion

The dilatometric results indicate that the $\beta \rightarrow \alpha$ transformation occurs by two mechanisms, viz. an upper C region down to 425° C and a lower C martensitic-type region. The presence

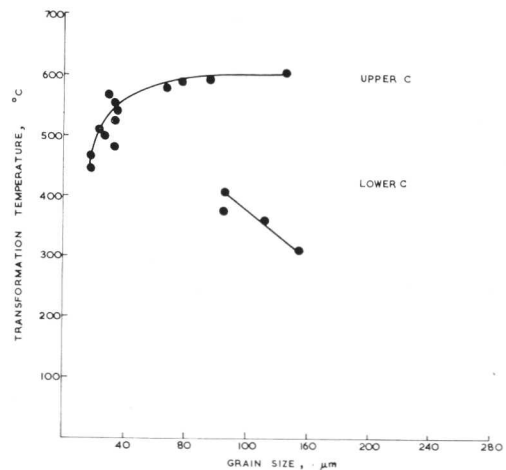


Fig. 3 Variation in grain size of the α transformation product as a function of transformation temperature in the isothermally transformed U-Cr-Mo alloy.

of a softening discontinuity in the hardness curve, coupled with the changes in microstructure and diffraction behaviour, all provide indirect but substantial evidence to suggest a subdivision in the transformation mechanism to give a C_1 and C_2 in the upper region. The slight discontinuity found in

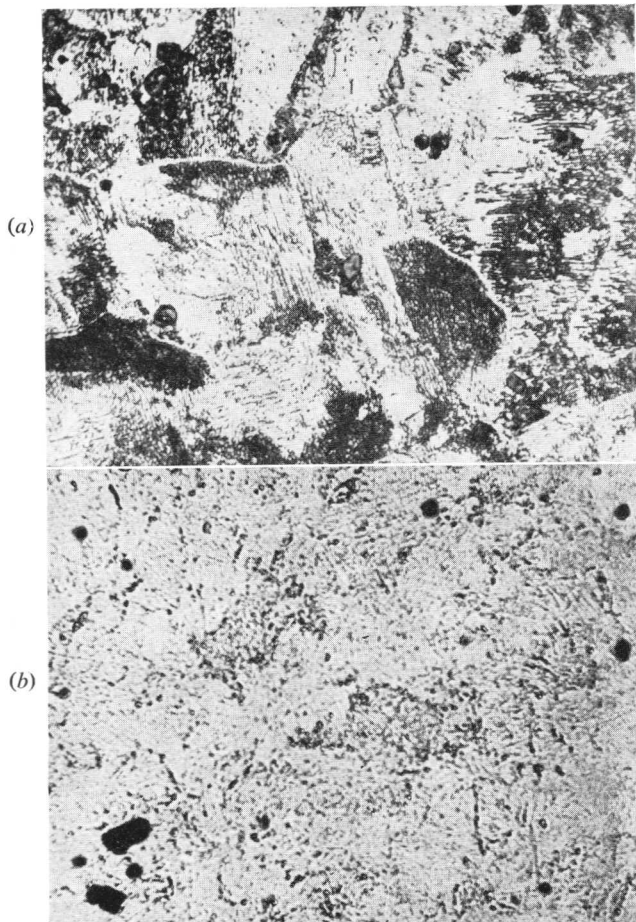


Fig. 4 Microstructure of specimen transformed at (a) 605°C; (b) 465°C. $\times 800$.

the dilatometric results at 525°C may also suggest a subdivision in transformation, but the scatter in the data is of the same order as the discontinuity and so it could not be proved. The microstructures show that C_1 is a diffusion-controlled nucleation and non-coherent growth process, while C_2 is probably a bainitic-type transformation giving a duplex acicular product. Such a subdivision has been confirmed for a U-Cr alloy¹¹ using electrical resistivity. In the U-Pt alloy study,¹³ dilatometric methods did not separate the high-temperature transformation modes whereas electrical resistivity did. This was ascribed to the larger mass of the dilatometric specimens accelerating the formation of the α phase owing to the quenching stresses produced. Further work on a ternary U-Pt-Nb alloy confirmed the separation of the high-temperature C curves in the binary *TTT* curves.¹⁶

To resolve this difference between the dilatometric results and the associated metallographic, hardness, and X-ray data, a detailed analysis of the reaction kinetics was undertaken along similar lines to that made for the U-Cr alloy,¹⁰ to ascertain whether one or two mechanisms of transformation were involved in the upper C region.

Temperature-Dependence of Transformation

Becker's equation^{17,18} for the initial nucleation rate of one phase from another is given as

$$I = k \exp - [(A_0 + Q)/RT]$$

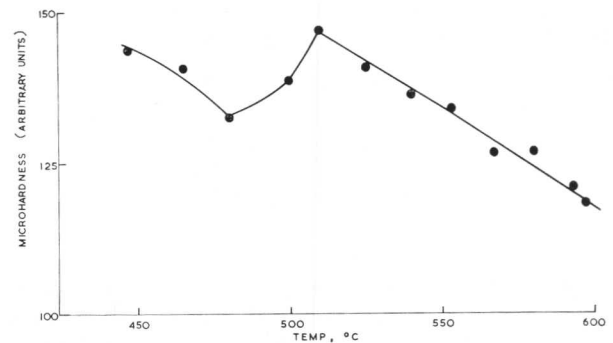


Fig. 5 Variation of microhardness (arbitrary units) with temperature of transformation for the upper C region.

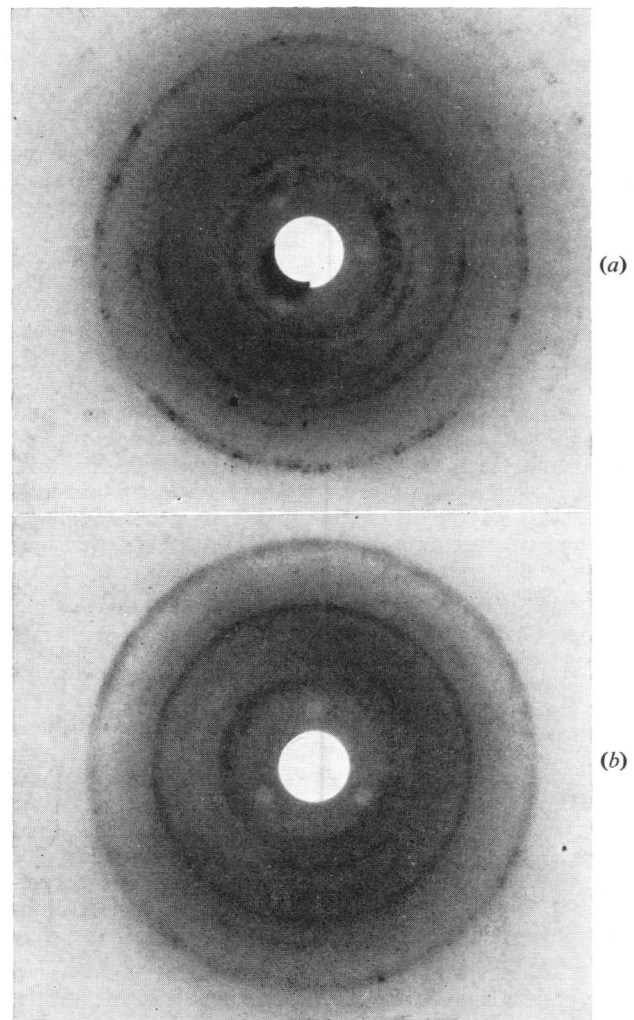


Fig. 6 X-ray diffraction pattern of specimen transformed (a) above the nose of the upper C region; (b) below 480°C in the upper C region.

where k is a constant depending on the frequency of occurrence of the process, A_0 is the activation energy for the formation of a nucleus of critical size, Q is the activation energy for diffusion, and T is the absolute temperature.

This equation may be rewritten in terms of the time t required for the formation of a segregate

$$t = K_1 \exp [(A_0 + Q)/RT]$$

and

$$\ln t = \frac{A_0}{RT} + \frac{Q}{RT} + C$$

where C is a constant.

A plot of $\ln t$ (to some particular stage of the decomposition) vs. $1/T$ is termed a Reciprocal Rate Plot.¹⁹ It is itself in the form of a C curve asymptotic to a maximum temperature, where $A_0 \rightarrow \infty$ corresponds to vanishing driving force, and consists of two separate parts, viz:

- (a) $\ln \frac{Q}{RT}$ which is a straight line, since Q is a constant.
- (b) $\ln \frac{A_0}{RT}$ where A_0 varies with temperature.

At the lower temperatures, A_0 is small in relation to Q and $\ln t$ tends to a straight line of slope Q/R . At higher temperatures the curve tends to longer times because A_0 increases rapidly, and so a retardation takes place of amount represented by $\ln \Delta t = \frac{A_0}{RT}$

$$\ln \Delta t = \frac{A_0}{RT}$$

The reciprocal rate plots for 10%, 50% and 90% of transformation in the upper C loop are shown in Fig. 7. The curves are continuous and do not display the discontinuity found with U-Cr alloy using electrical-resistivity data¹⁰ and attributed to the $C_1 \rightarrow C_2$ transition. The present plots support the previous evidence^{5,7,13} that dilatometric data do not show a subdivision of mechanisms in the upper C region. This may reflect the fact that dilatometric results on fairly massive specimens are not sufficiently sensitive compared to resistivity measurements on wire specimens.

The activation energy Q for diffusion was calculated from the slope of the straight-line portion of the reciprocal rate curves:

- Q for 10% transformation = 26,400 cal/mole.
- Q for 50% transformation = 26,200 cal/mole.
- Q for 90% transformation = 27,200 cal/mole.

The increase in activation energy with fraction transformed during the later stages of transformation is attributed to the greater contribution from the growth process as transformation proceeds. The activation energy for self-diffusion of β -U is 42,000 cal/mole.²⁰ It is known that the diffusion coefficient for Cr in β -U is very much larger than for self-diffusion, so that the lower activation energies found for this alloy are to be expected.

The precise significance of Q cannot be decided until the exact nature of the transformation modes in the upper C is known. For example, if there are C_1 and C_2 regions, Q needs to be redetermined for each region. There is therefore a need for further electrical-resistivity studies to supplement the dilatometry, although it may be that the temperature of zero resistance change on $\beta \rightarrow \alpha$ transformation¹¹ is in the critical range 520–480°C, in which case the sensitivity of electrical resistivity will also be too low to provide direct evidence one way or the other.

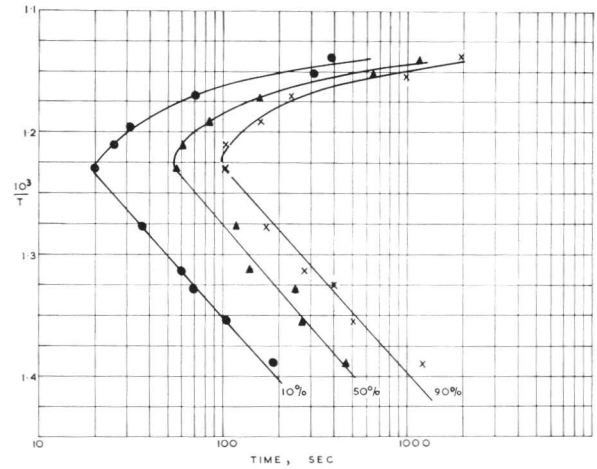


Fig. 7 Inverse rate plot in upper C loop for 10, 50, and 90% transformation.

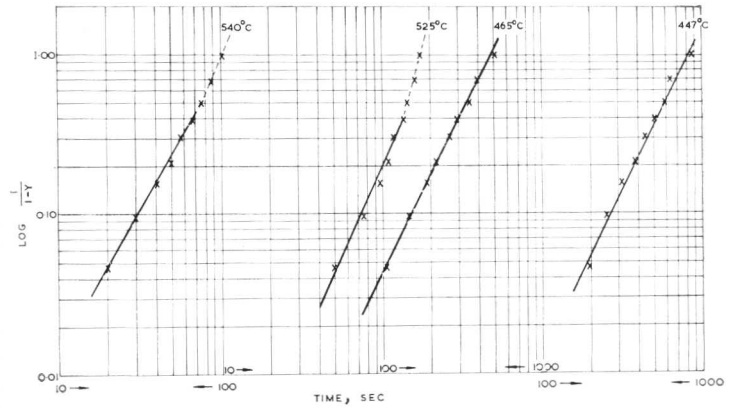


Fig. 8 Derived rate curves for U-Cr-Mo.

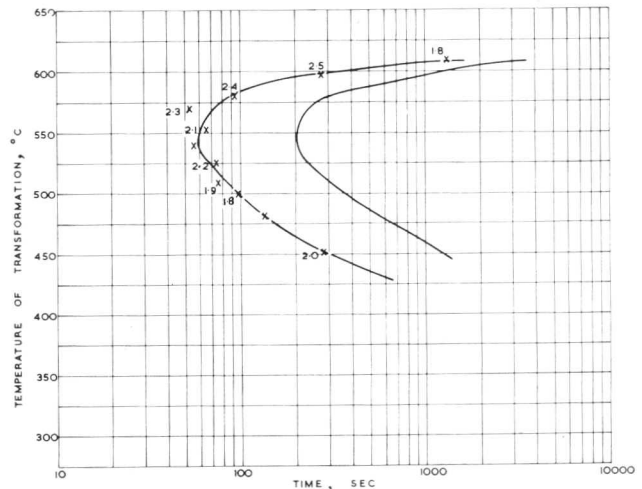


Fig. 9 Variation of exponent n with position on TTT diagram.

Time-Dependence of Transformation

The general empirical equation applied to isothermal rate processes is given as

$$y = 1 - \exp - \left(\frac{t}{K} \right)^n$$

where y is the fraction transformed.

By putting $n = 4$ and $1/K = G^3N/3$, where G is the rate of growth and N is the nucleation rate, one obtains the Johnson and Mehl equation for the rate of growth of a precipitate in the austenite \rightarrow pearlite reaction.²¹

Impingement can be allowed for by using the factor $(1-y)$ where y is the fraction transformed. Burke²² and Ham²³ applied the factor to the growth of a group of particles. The

resulting general equation $y = 1 - \exp - \left(\frac{t}{K} \right)^{3/2}$ was shape-

independent, and found to hold for values of y from 0 to 0.5.

Hence, without nucleation, a value of $n = 1.5$ will be obtained when the process is controlled by long-distance diffusion through the parent interface. Any excess of n over 1.5 can be attributed to nucleation. However, where the reaction rate is controlled not by long-distance diffusion but by the rate of transfer at the interface between parent and product, n will vary between 1.5 and 3 for the growth term alone, while the nucleation contribution will be additive to this.

Thus, differentiating the general equation for a thermally activated process,

$$\frac{dy}{dt} = n \left(\frac{t}{K} \right)^{n-1} \exp - \left(\frac{t}{K} \right)^n$$

Hence

$$\frac{dy}{1-y} = \frac{n}{K^{n-1}} t^{n-1} dt$$

Integrating and taking logs

$$\log \log \frac{1}{1-y} = n \log t - (n-1) \log K$$

Hence a plot of $\log \log \frac{1}{1-y}$ vs. $\log t$ should give a straight

line of slope n in the region where the above equation holds.

Typical derived rate curves are given in Fig. 8. The straight-line approximation from $y = 0$ to $y = 0.5$ suggested by Burke²² and Ham²³ appears to hold. The exponent n values are shown in relation to their position on the TTT diagram of the U–Cr–Mo alloy in Fig. 9.

The value $n = 1.8$ at the top of the upper C region indicates that the transformation in this region is diffusion-controlled with the small amount in excess of 1.5 due to nucleation. This nucleation contribution is small since there is only a slight degree of undercooling. As the transformation temperature is lowered towards the nose of the TTT curve, n increases to 2.4. This can be explained either by an increasing nucleation rate or by a slower reaction at the parent/product interface becoming the rate-controlling factor, rather than the long-range diffusion at the higher temperatures in the upper C region.

The decrease in n to 1.9 at 510°C could be attributed to a change in the transformation mechanism from that of a diffusion-controlled type to a bainitic type, as in U–Cr.¹¹ In the lower regions of the upper C curve (ie. possibly in a C₂ region), where the transformation could now be bainitic in character, the n index remains reasonably constant since with a bainitic transformation a constant rate of growth can be expected. Ideally, with no diffusion, n would equal 3 with a constant three-dimensional growth; hence the lower value of n obtained probably means the persistence of long-range diffusion as the predominant process.

Conclusions

The TTT curve for the U–Cr–Mo alloy, as derived dilatometrically, consisted of two C curves. The upper C curve represents a diffusion-controlled transformation, while the lower C curve apparently represents a martensitic-type transformation. The dilatometric results did not separate the $\beta \rightarrow \alpha$ transformation in the upper C region.

Associated metallographic, hardness, and X-ray results, together with kinetic analysis of the data, suggest indirectly a subdivision of the upper C region into a nucleation- and growth-C₁ region and a bainitic-type C₂ region where diffusion still plays a dominant role. A mixture of products existed over a temperature range of ~ 30 degC during transition from C₁ to C₂.

The effect of Mo was to depress and extend the range of the upper C loop compared with the binary U–Cr alloy. There was also an increase in incubation period for the $\beta \rightarrow \alpha$ transformation in both the upper and lower C loops.

References

- G. F. Slattery and J. A. McLeish, *J. Nuclear Mat.*, 1965, **17**, 192.
- J. H. Gittus, V. W. Eldred, A. Stuttard, G. F. Slattery, and E. Chatterley, "Proceedings of Conference on Radiation Damage in Reactor Materials" (Venice 1962), Vol. 4, p. 109. 1963: Vienna (Internat. Atomic Energy Agency).
- J. H. Gittus, "Uranium". 1963: London (Butterworths).
- D. J. Marsh, G. F. Slattery, and J. H. Gittus, *J. Inst. Metals*, 1964–65, **93**, 260.
- M. D. Jepson, R. B. Kehoe, R. W. Nichols, and G. F. Slattery, "Proceedings of the 2nd International Conference on Peaceful Uses of Atomic Energy". Vol. VI, p. 42. 1958: Geneva (United Nations).
- H. Aubert and C. Lelong, *Commissariat à l'Energie Atomique Rap.* (2956), 1966.
- D. W. White, *Trans. Amer. Inst. Min. Met. Eng.*, 1955, **203**, 1221.
- J. Beaudier, G. Cabane, and P. Mouturat, *Mém. Sci. Rev. Mét.*, 1961, **58**, 176.
- P. H. Dixon and J. Burke, "Uranium and Graphite", p. 9. 1962: London (Inst. Metals).
- P. H. Dixon and J. Burke, *Atomic Energy Research Estab. Rep.* (4431), 1964.
- R. D. Townsend and J. Burke, *Nature*, 1965, **205**, 794.
- I. Amity, A. Rosen, and A. Bar-Or, *J. Inst. Metals*, 1967, **95**, 48.
- W. J. Kitchingman, K. M. Pickwick, I. G. Brown, and R. J. Edwards, *J. Nuclear Mat.*, 1966, **18**, 219.
- G. F. Slattery, *J. Less-Common Metals*, 1965, **8**, 195.
- J. F. R. Ambler and G. F. Slattery, *J. Nuclear Mat.*, 1961, **4**, 90.
- W. J. Kitchingman and K. M. Pickwick, *J. Inst. Metals*, 1967, **95**, 61.
- R. Becker, *Z. Metallkunde*, 1937, **29**, 245.
- R. Becker, *Ann. Physik*, 1938, **32**, 128.
- H. K. Hardy and T. J. Heal, "Progress in Metal Physics", Vol. V, p. 143. 1954: London (Pergamon Press).
- Y. Adda, A. Kirianenko, and C. Mairy, *J. Nuclear Mat.*, 1959, **1**, 300.
- W. A. Johnson and R. F. Mehl, *Trans. Amer. Inst. Min. Met. Eng.*, 1939, **135**, 416.
- J. Burke, *Phil. Mag.*, 1960, **5**, 176.
- F. S. Ham, *J. Physics. Chem. Solids*, 1958, **6**, 335.

The $\beta' \rightarrow \zeta^\circ$ Transformation in the AgZn System

J. E. Kittl and A. Cabo

The $\beta' \rightarrow \zeta^\circ$ phase transformation in the AgZn system has been studied by means of electrical-resistivity measurements and hot-stage metallographic observations. Activation energies for the displacement of the transformation interface were determined in the hot stage by comparing velocities of the same interface at two temperatures in a single experiment. The results showed a small anisotropy in Q values as a function of orientation of the interface. It is proposed that the rate-controlling mechanism in this transformation is the diffusion necessary to attain the required changes in the degree of order at the transformation interface. Surface marks and deformation twins produced throughout the transformation are also discussed.

In recent years "massive" transformations have been studied in several non-ferrous¹⁻³ and ferrous systems.^{4,5} Following a study of the ζ (h.c.p.) \rightarrow β' (b.c.c. ordered) transformation in the AgCd system,² it was of interest to study another transformation where both the phases involved were ordered. On these grounds the AgZn $\beta' \rightarrow \zeta^\circ$ transformation was selected for the present work.

In the equatomic region of the AgZn system, the β phase (b.c.c. disordered) is present at temperatures above 274°C and the ζ° phase (hexagonal complex ordered) at temperatures below 274°C.⁶ The β phase becomes an ordered phase (β') by quenching from the β -phase field. Annealing of this β' phase in the range of existence of ζ° results in the $\beta' \rightarrow \zeta^\circ$ phase transformation. There is some previous work on the $\beta \rightarrow \zeta^\circ$ transformation that takes place on slow cooling from the β -phase field^{7,8} and a model for the $\beta \rightarrow \zeta^\circ$ and the $\beta' \rightarrow \zeta^\circ$ transformations has been proposed by Kitchingman⁹ which will be discussed in another section. In the present work the $\beta' \rightarrow \zeta^\circ$ transformation has been studied by means of electrical-resistivity measurements and hot-stage metallography.

Manuscript received 6 March 1968. J. E. Kittl, Chem. Ing., and A. Cabo, Lic. Physics, are in the Departamento de Metalurgia, Comisión Nacional de Energía Atómica, Buenos Aires, Argentina.

TABLE I

at.-% Zn	Q , kcal/mole
45	21 ± 2
47	25 ± 2
48	28 ± 2
49	34 ± 2
50	34 ± 2

Experimental Results

Resistometric Measurements

The isothermal transformation kinetics were represented in the usual way as $\ln \ln (1/1-x)$ vs. $\ln t$, where x is the fraction transformed and t is the time. The slope of the lines obtained corresponds to the exponent n of the Johnson-Mehl-Avrami equation

$$x = 1 - \exp\left(-\frac{t}{\tau}\right)^n \quad \dots (1)$$

where τ and n are constants. The isothermal results gave n values between 2 and 3, which according to Cahn¹⁰ correspond to a distribution of nuclei in grain boundaries and in the matrix. The metallographic observations described in the following section, made on specimens transformed isothermally, confirmed Cahn's predictions.

From the isothermal kinetics an activation energy (Q) was calculated by the usual methods.^{2,11} $(dx/dt)_{x_1}$ and $(1/t)_{x_1}$ were represented as a function of $1/T$ for the fraction transformed $x_1 = 0.30, 0.50, \text{ and } 0.80$, and Q was calculated from these plots using the Arrhenius equation

$$v = \frac{dx}{dt} = A \exp\left(-\frac{Q}{RT}\right) \quad \dots (2)$$

The activation energy was found to be dependent on the composition (Table I) and diminished with increasing departure of the alloy composition from stoichiometry. To confirm that Q does not depend on x , the change-of-rate method^{2,11} was also used to determine the activation energy. The measurements were made only with the 50% alloy and we assume that all other alloys behave similarly. Ten to fifteen changes in

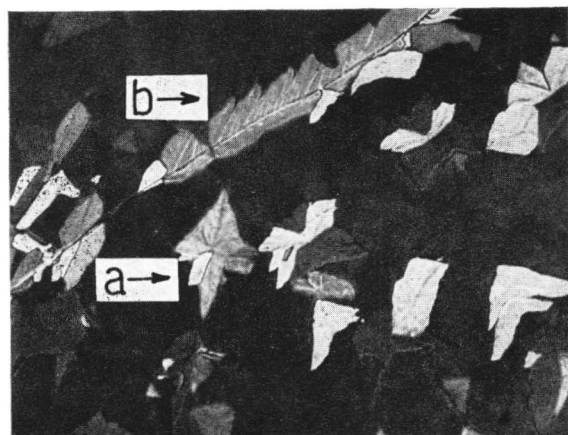


Fig. 1 Stoichiometric alloy annealed at 128 and 113° C. β' partially transformed to ζ° showing (b) grain-boundary allotriomorph and (a) star-shaped grain.

temperature were performed in each experiment. At each change of temperature, Q was calculated from the slopes of the resistivity/time curves at the two transformation temperatures, T_1 and T_2 . The temperature difference between T_1 and T_2 was ~ 15 degC. The value obtained for Q was the same for all the experiments and equal to that calculated from the isothermal work (Table I). This confirmed that Q does not depend on the fraction transformed.

From all the resistivity measurements we conclude that: (a) Q does not change with T (in the range 130–180° C); (b) Q does not depend on x ; (c) Q is strongly dependent on composition.

Hot-Stage Observations

Several isothermal experiments were conducted in the hot stage. A strong dependence of the ζ° grain size on composition was observed in the samples transformed, though the distribution and shape of the ζ° grain, did not change with composition. Isothermal experiments were carried out in the range 90–180° C for all these alloys and they did not show a significant dependence of the ζ° grain size on transformation temperature. The 50% alloy was selected for more detailed work in the hot stage since it was the one that showed the largest ζ° grain size. These results will be presented in more detail.

The shapes of the transformed ζ° grains were in some instances not comparable with systems studied before.^{1,2} We will describe the morphology of these grains making partial use of the morphological classification of Dubé.¹² Some of the principal shapes observed are shown in Fig. 1. Most of the shapes have both curved and straight edges but the total length of the curved edges was greater. Ledges in the straight edges were rarely observed. The straight edges appear to grow normally with velocities of the same order of magnitude as for curved edges, though in some cases ledges were observed to contribute to the growth mechanism.

Many grains of an intergranular star shape were observed during the growth process. They began to grow with random shapes but soon developed definite points. In most cases these stars are formed by a set of differently oriented grains growing together (Fig. 1). New orientations occasionally appear after the initial particle has achieved a certain size. In several cases an arrow shape formed by two ζ° grains growing together was associated with a star.

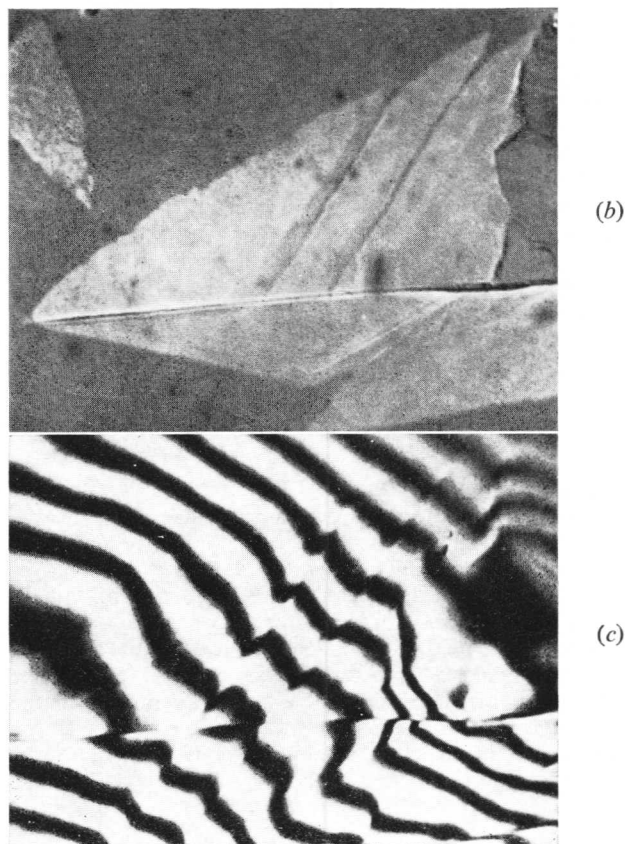
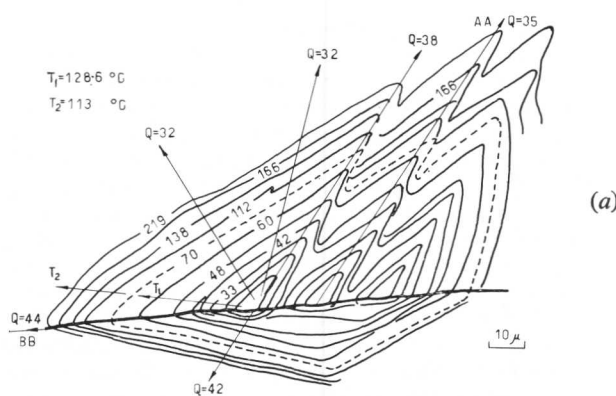


Fig. 2 Stoichiometric alloy transformed in the hot stage. (a) Transformation interface positions corresponding to a typical transformation sequence. The numbers at the interface positions indicate corresponding times in minutes. (b) Same region seen with polarized light after the transformation sequence. (c) Interferogram of the same region. $\lambda = 0.6\mu\text{m}$.

Some ζ° grains were observed to nucleate as grain-boundary allotriomorphs at β' matrix grain boundaries. In some cases the nucleation proceeded as a continuous ribbon of ζ° grains at a β' grain boundary. In other cases ζ° grains were independently nucleated at different points of the β' grain boundary and, in subsequent growth, they merged into a continuous ribbon with secondary sideplates or sawteeth (Fig. 2(a)). Differences in the morphologies observed in later stages of growth of the ζ° grain-boundary allotriomorphs resulted from these differences in nucleation.

Observed Relief Effect and Deformation Twinning

Special care was taken to detect signs of surface relief on the specimens. In the samples made out of thin sheets some relief was noticed but it was more pronounced in the thicker samples. Fig. 2(c) corresponds to a typical partially transformed area as seen by polarization interferometry. A general rumpling of the transformed area is apparent as well as some grooves or surface marks. These marks correspond to former positions of the transformation interface, Fig. 3, or to places where two grains of similar orientation impinge and continue growing together (Fig. 2). In the first case the groove is fairly straight and in the second it follows the contact interface between the two grains. The general roughness or rumpling of the transformed surfaces was observed to be different in areas of different orientation and also different for a single ζ° grain growing from a β' grain boundary into both β' grains.

There was no microscopic evidence of plastic deformation in the thin-sheet samples, but for samples of 3–4 mm thickness the results were different. Deformation twins were observed to grow in transformed ζ° grains (Fig. 4), which indicates that a high stress level is reached when the transformation is well advanced. Deformation traces in β' were not observed in the optical microscope.

In most cases the velocity of two interfaces did not change when they approached each other. However, when a portion of β' was enclosed or surrounded by ζ° the last part of the β' transformed at a much slower rate (Fig. 4). A similar phenomenon has been observed in previous work¹ where it was attributed to transformation stresses acting upon the untransformed material. The existence of a deformation twin in the area of ζ° supports this hypothesis in the present case.

Activation Energies

The velocity of an interface in a particular direction was obtained by plotting the positions of the interface as a function of time at constant temperature. Linear relationships were obtained, indicating that the velocity is a constant at constant temperature. For measurements of activation energy a change-of-rate method was used. After a certain degree of transformation, the temperature was changed to another preselected value, and held for a period of time until the desired amount of transformation was reached. Fig. 5 shows a typical plot of velocities obtained by this method. Q was evaluated from

$$Q = \frac{\ln \frac{v_1}{v_2}}{\frac{1}{R} \left(\frac{1}{T_1} - \frac{1}{T_2} \right)} \quad \dots (3)$$

where v_1 and v_2 are the measured interface velocities in a given direction at temperatures T_1 and T_2 , respectively. This calculation is valid if A (from equation (2)) is constant. A was found to be approximately a constant in the range 90–150°C by means of electrical-resistivity measurements. Furthermore, short temperature intervals were chosen between T_1 and T_2 (~ 15 degC) and this decreases the possibility of a change in A . This method was also used to make two successive changes of temperature within a single sequence; Q values obtained from both temperature changes were within the estimated experimental error. When a specific transformation shape was analysed in different directions it was considered that:

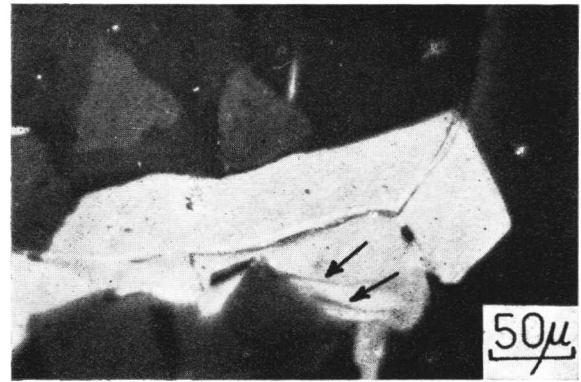


Fig. 3 Stoichiometric alloy partially transformed at $T_1 = 126^\circ\text{C}$ and $T_2 = 110^\circ\text{C}$. The arrows indicate surface marks.

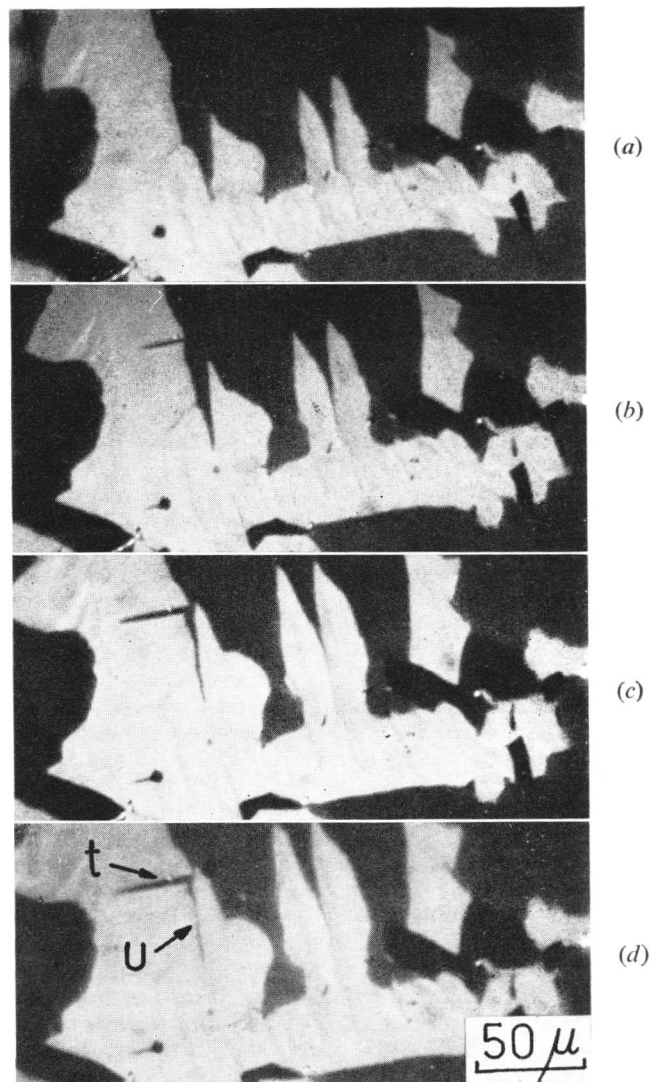


Fig. 4 Stoichiometric alloy partially transformed at 128.6°C for (a) 54 min, (b) 76 min, and at 112°C for (c) 121 min, (d) 158 min. t indicates a deformation twin, u indicates a region of delayed transformation.

(a) If the shape does not change after the temperature change, Q is the same when measured in all directions.

(b) If a shape change does take place in a growing grain, the plots of length vs. time would indicate whether this change of shape was due to a change of velocity along the different directions of the grain (giving a linear plot like Fig. 5) or whether it had another origin (giving a non-linear plot). Two possibilities in the latter case could be protrusion to the surface from the interior of the sample or sudden changes in the angle between the interface and the surface of observation.

Some results are presented in Figs. 2 and 6. In these figures the values of Q are indicated along the different directions. An average of 12 sets of Q values (each set corresponding to a separate area like Fig. 2 or Fig. 6) gave $Q = 35$ kcal/mole. Sequences were found where Q did not change with direction but in other sequences Q did change by amounts between 3 and 10 kcal/mole. From these experiments we conclude that the activation energy for growth is slightly anisotropic. Values of Q were found to change from one ζ° grain to another ζ° grain of different orientation (Fig. 6) or even for a single ζ° grain nucleated at a grain boundary and growing into two adjacent β' grains (Fig. 2).

Discussion

Surface-Relief Effects

Surface marks have already been observed in previous work on the CuGa and AgCd^{1,2} systems. These marks differed in appearance in the optical microscope: in the CuGa $\beta \rightarrow \zeta_M$ transformation they looked like slip markings and in the AgCd $\zeta \rightarrow \beta'$ transformation like smooth grooves. Slip was presumed to be the origin of the marks in the CuGa transformation, while in the AgCd transformation the marks were thought to be due to an anisotropic annihilation of vacancies. Neither of these arguments can be used to explain the marks in the AgZn $\beta' \rightarrow \zeta^{\circ}$ transformation, since their appearance makes it very unlikely that they have any link with slip and no extra vacancies are produced by the transformation that occurs with a volume expansion ($\Delta V/V = +0.6\%$). All the marks found in the present work appear to correspond to a boundary between grains or subgrains of small misorientation. Their origin could be sliding along these grains or subgrains produced by the anisotropy of the volume change occurring during transformation. This anisotropy has recently been confirmed by Clark.¹³

The observed rumpling can be explained if the volume expansion on transformation is readily transmitted to the free surface.¹³

Transformation Stresses

It is well known that changes in volume during transformation can result in plastic deformation in both the matrix and the product phase. No slip was observed in the untransformed β' phase or in the ζ° phase using optical microscopy; however, slip could have existed since, as pointed out by Christian,¹⁴ if this effect is produced on a sufficiently fine scale it might not be detected. Moreover, the surface rumpling indicates that plastic deformation did take place and the presence of deformation twins in ζ° grains indicates that high stress concentrations are produced during the transformation.

The presence of transformation stresses did not affect the movement of the transformation interface except when the interfaces were very close to each other (Fig. 4). This seems to indicate that these stresses have an influence on the movement of the transformation interface only at short-range distances where they probably reach high stress levels. The presence of differently oriented groups of ζ° grains during nucleation and

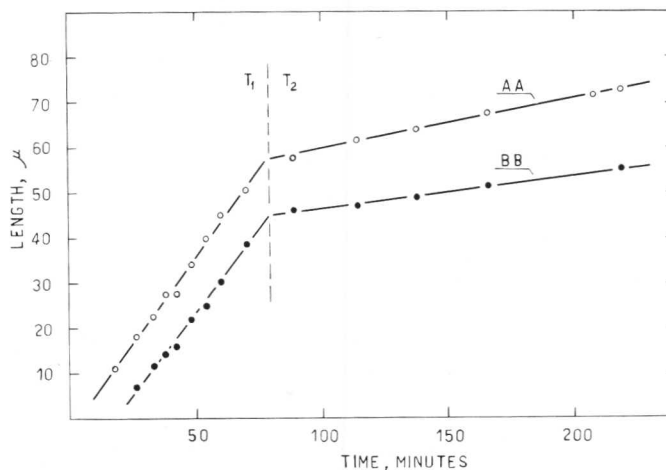


Fig. 5 Plots of length as a function of time used for the calculation of Q in the two directions indicated in Fig. 2(a). $Q^{AA} = 38$ kcal/mole; $Q^{BB} = 44$ kcal/mole.

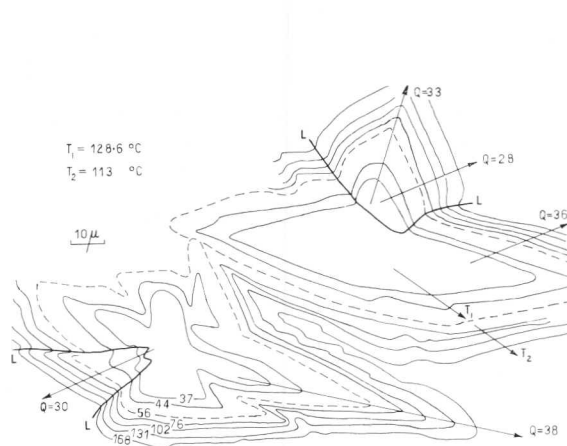


Fig. 6 Interface positions corresponding to another transformation sequence. Lines LL indicate grain boundaries $\zeta^{\circ}/\zeta^{\circ}$.

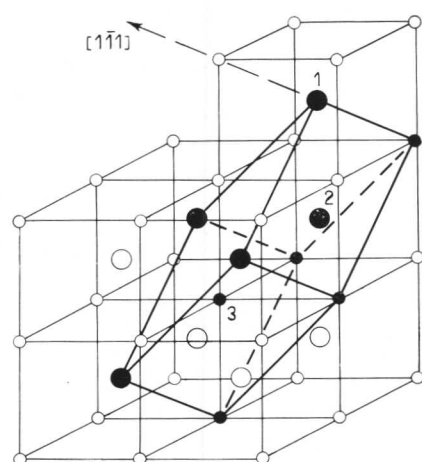


Fig. 7 β' structure in which $1/3$ of a hexagonal unit cell equivalent to the unit cell of ζ° is shown.

TABLE II

System	$A' \exp(\Delta S^*/R)$	Q , kcal/mole
AgCd	0.4	16
CuZn	10	16
AgZn	10^3	28
	10^9	37

growth could originate in a minimization of the stresses produced by the volume change resulting from a suitable oriented set of ζ° grains.

It can therefore be concluded that stresses are important in both nucleation and growth only during the final stages of the transformation when only a small part of the matrix remains untransformed.

Activation Energy and Pre-Exponential Factor for Interface Movement

Important changes in nucleation behaviour and in the measured values of activation energy were observed with change of composition. Departure from stoichiometry considerably decreases the order in β' and since Q also decreases, it seems that Q depends on order in this transformation. Small but consistent differences in Q were also measured for different growth directions in a single experiment. The origin of this anisotropy could be the anisotropy of diffusion at the transformation interface, since it is quite possible that interface diffusion is the controlling factor during this kind of transformation.^{2,3} Speich¹⁵ also noticed differences in Q in edgewise and sideways growth rates of bainite plates.

The pre-exponential factor of equation (2) can be analysed using absolute reaction rate theory.² This gives

$$A' \exp\left(\frac{\Delta S^*}{R}\right) = \frac{v}{\frac{kT}{h} D \exp\left(-\frac{Q}{RT}\right) \left[1 - \exp\left(-\frac{\Delta G^{\beta \rightarrow \zeta^\circ}}{RT}\right)\right]}$$

where A' is the fraction of atoms at reactive sites on the interface, k and h are Boltzmann's and Planck's constants, D is the average jump distance, Q and ΔS^* are the enthalpy and entropy of activation, and $\Delta G^{\beta \rightarrow \zeta^\circ}$ is the free-energy change of the reaction.

The value of $\Delta G^{\beta \rightarrow \zeta^\circ}$ was taken as 35 kcal/mole in the range of reaction temperatures from 110 to 140°C¹⁶ and D was taken as the interatomic distance. Table II shows the present data compared with previous values calculated for the $\zeta^\circ \rightarrow \beta'$ transformation in the AgCd system² and the $\beta \rightarrow \alpha_M$ transformation in the CuZn system.³ It is clear that $A' \exp(\Delta S^*/R)$ for the $\beta' \rightarrow \zeta^\circ$ transformation in AgZn is several orders of magnitude greater than for the AgCd or CuZn transformations. In addition the value of $A' \exp(\Delta S^*/R)$ is larger for directions where Q is larger. This explains the small difference in growth velocity observed for various directions despite differences in measured Q values.

The high values of $A' \exp(\Delta S^*/R)$ give $\Delta S^* = 40$ cal/mole/degC when $A' = 1$, which is of the order of 20 times the entropy of melting in metals. Early data on recrystallization of metals gave similarly high values and it was later demonstrated that this was due to impurities.¹⁷ In the present case the alloy was of similar purity to the alloys used for previous work in other systems,^{2,3} which did not give such high $A' \exp(\Delta S^*/R)$ values. Hence impurities are probably not the

origin of the high pre-exponential factor and a detailed analysis of this phenomenon remains to be done.

The Q and $A' \exp(\Delta S^*/R)$ values can be compared with some data on diffusion in intermetallic phases. The only data available for AgZn are the values of Q for the β phase of stoichiometric composition. ($Q^v = 27$ kcal/mole for Zn and $Q^v = 16.6$ kcal/mole for Ag.¹⁸) If we take $Q^{\beta'} \simeq 2Q^{\beta}$ and $Q^{gb} \simeq 1/2 Q^v$, where Q^{gb} is the activation energy for grain-boundary diffusion and Q^v is the activation energy for lattice diffusion, then the measured value of Q (34 kcal/mole) for the transformation lies between that for grain-boundary diffusion (27 kcal/mole for Zn and 16.6 kcal/mole for Ag) and that for lattice diffusion (54 kcal/mole for Zn and 33 kcal/mole for Ag). It is often considered that $Q^v = Q^f + Q^m$, where Q^f is the energy for vacancy formation and Q^m is the activation energy for atomic migration, and that Q^{gb} is equal to Q^m since vacancies are thought to be available at grain boundaries. However, in the present case any excess vacancies created at the interface will be annihilated close to the interface since the transformation is associated with a volume expansion. Hence Q^{gb} for this transformation could be higher than the normal Q^{gb} .

Concerning the pre-exponential factor, it should also be mentioned that in ordered and disordered β phase in the CuZn system there is a difference of several orders of magnitude between the measured pre-exponential factors for the β disordered phase ($D_0 = 10^{-2}$ – 10^{-3}) and the β' ordered phase ($D_0 = 10^2$ – 10^4).¹⁸ It is interesting that this difference in D_0 is of the same kind as the difference in $A' \exp(\Delta S^*/R)$ in Table II between disordered and ordered phases. The origin of these effects is probably similar since the transformations are diffusion-controlled. Further discussion is precluded since there is no satisfactory model for D_0 in ordered alloys.

Atomistic Model

The model for the $\beta \rightarrow \zeta^\circ$ transformation discussed by Kitchingman and Buckley⁸ was extended by Kitchingman⁹ to the $\beta' \rightarrow \zeta^\circ$ transformation with the necessary allowances for the ordering in β' . This model used the orientation relationship between β' and ζ° determined by Bergman and Jaross,⁷ namely that each β' crystal gave rise to a set of ζ° grains oriented with their respective [001] ζ° axes parallel to the four possible [111] β' axes. The model indicated that volumetric changes take place on transformation which require some shuffling of atoms over distances less than the interatomic distances, and that some atom exchange is also needed to fulfil order requirements.

Fig. 7 shows a view of the β' ordered structure. The thick lines correspond to 1/3 of a hexagonal unit cell based on β' which can be compared with the corresponding 1/3 of the ζ° unit cell oriented with [111] $\beta' \parallel$ [0001] ζ° . It is clear that alternate layers of Ag and Zn parallel to [111] β' make up the unit cell. Thus each layer of atoms in the β' structure contains only one kind of atom (in a perfectly ordered lattice) and the corresponding (0001) layers in the ζ° phase contain different proportions of atoms. The transformation therefore requires atom exchange between the (111) layers and it can be shown that one half of the atoms of a ζ° unit cell need to exchange places on passing from β' to ζ° . This exchange should take place at the transformation interface. Most of the active transformation interfaces are somewhat incoherent, hence we must not only consider what happens in a perfect lattice (which was the view taken by Kitchingman⁹ when considering his model for the transformation) but also what happens at an incoherent transformation interface. At such an interface the following events should take place:

- (i) A volumetric expansion of +0.6%.
- (ii) Exchange of places of one-half of the atoms involved in the transformation to fulfil order requirements.
- (iii) Shuffling of two atoms per unit cell along the $[111]_{\beta'} \parallel [0001]_{\zeta^\circ}$ direction.

Present observations on the effect of (i) on a macroscopic scale and the small movement required by (iii) indicate that neither factor is probably rate-controlling. However, (ii) requires extensive diffusion and it is probably the rate-controlling factor. If a transformation interface is parallel to the $(111)_{\beta'}$, $(0001)_{\zeta^\circ}$ planes then it is possible that a small contribution to the required atom exchange will be made via interface diffusion involving exchange between atoms lying on the interface and their neighbours away from the interface or else exchange of atoms across the interface. On the other hand, an interface that intersects the $(111)_{\beta'}$, $(0001)_{\zeta^\circ}$ planes will have atoms of Ag and Zn present at the interface in more favourable positions for diffusion along the interface to contribute to the atom exchange needed for the fulfilment of the order requirements. If this is correct, it can be deduced that transformation interfaces parallel to the $(111)_{\beta'}$, $(0001)_{\zeta^\circ}$ planes, if they exist, will move at a slower rate than interfaces lying at an angle to this plane.

The anisotropy of the activation-energy data could result from a different contribution to the atomic exchange made by diffusion along or perpendicular to the interface. These are the limiting cases and, depending upon the interface orientation, a variety of intermediate Q values would be possible.

The effect described will depend on the structure of the transformation interface. The model of a grain boundary due to Mott¹⁹ has recently been discussed by Gifkins.²⁰ This model predicts grain boundaries made out of islands of good fit, crystallographically oriented, surrounded by channels of material saturated with defects. If this model applies to the present transformation interface, then the islands will transform via "submicroscopic ledge growth" since, for these islands, the atom exchange could be more difficult for the $(111)_{\beta'}$, $(0001)_{\zeta^\circ}$ planes as described above. The number of islands of good fit will change with orientation; hence this will contribute to the measured anisotropy of Q as a function of interface orientation.

We conclude that the grain-boundary model of Mott¹⁸ is compatible with the idea that anisotropy in Q results from different contributions to atom exchange made by pure "interface" or pure "volume" diffusion. This effect could be enhanced by the volume expansion taking place during transformation, which would tend to diminish the vacancy concentration at and near the transformation interface. Measurements of the self-diffusion parameters in the phases involved and determinations of the crystallographic orientation and nature of the transformation interfaces are necessary to complement the present results and provide further understanding of some of the problems considered.

Conclusions

- (1) The change-of-rate method was used for the determination of the activation energy of a phase transformation. The results were consistent with electrical-resistivity determinations in the same alloy.
- (2) From the pre-exponential factor and Q values it appears that the reaction is controlled by diffusion at the transformation interface. The model of Kitchingman⁹ satisfactorily explains the transformation behaviour if the transformation interface is considered. The atom exchange needed to fulfil order requirements is probably the rate-controlling step.
- (3) Anisotropy in interface diffusion at the transformation interface is thought to play a role in determining the small anisotropy detected in the activation-energy values of the transformation along different growth directions.

Acknowledgements

The authors wish to acknowledge constant support and encouragement received from Professor J. Sabato and valuable comments regarding the manuscript from J. Mazza. Helpful discussions with J. Abriata and C. Rodriguez were maintained during the course of this study. Acknowledgement is also made of the partial financial support from the National Research Council of Argentina and the Deutsche Forschungsgemeinschaft, which made this work possible.

References

1. J. E. Kittl and T. B. Massalski, *Acta Met.*, 1967, **15**, 161.
2. J. E. Kittl, H. Serebrinsky, and M. P. Gomez, *ibid.*, 1967, **15**, 1703.
3. D. A. Karlyn, Ph.D. Thesis, Massachusetts Inst. Technology, 1967.
4. W. S. Owen and E. A. Wilson, "Physical Properties of Martensite and Bainite" (Special Rep. No. 93), p. 53. 1965: London (Iron Steel Inst.).
5. R. H. Goodenow and R. F. Hehemann, *Trans. Met. Soc. A.I.M.E.*, 1965, **233**, 1777.
6. M. Hansen and K. Anderko, "Constitution of Binary Alloys", p. 63. 1958: New York and London (McGraw-Hill).
7. G. Bergman and R. W. Jaross, *Acta Cryst.*, 1955, **8**, 232.
8. W. J. Kitchingman and J. I. Buckley, *Acta Met.*, 1960, **8**, 373.
9. W. J. Kitchingman, *ibid.*, 1962, **10**, 799.
10. J. W. Cahn, *ibid.*, 1956, **4**, 449.
11. M. Hillert, *ibid.*, 1959, **7**, 653.
12. H. I. Aaronson, "Decomposition of Austenite by Diffusional Processes" (edited by V. F. Zackay and H. I. Aaronson), p. 391. 1962: New York and London (John Wiley).
13. H. McL. Clark, private communication.
14. J. W. Christian, Ref. 12, p. 383.
15. G. R. Speich, Ref. 12, p. 359.
16. A. Cabo, J. E. Kittl, and J. Abriata, "Phase Stability of AgZn 50 at.-% Zn". Paper presented at the annual meeting of the Argentine Physical Association, 1967.
17. P. Gordon and R. A. Vandermeer, "Recrystallization, Grain Growth, and Textures", p. 230. 1966: Metals Park, Ohio (Amer. Soc. Metals.)
18. W. C. Hagel, "Intermetallic Compounds" (edited by J.H. Westbrook), p. 378. 1967: New York and London (John Wiley).
19. N. F. Mott, *Proc. Phys. Soc.*, 1948, **60**, 391.
20. R. C. Gifkins, *Mat. Sci. Eng.*, 1967, **2**, 181.

The Effect of Small Additions of Copper on the Transformation Characteristics of β' -Phase AuCd Alloys

M. E. Brookes and R. W. Smith

It has been reported that when Ag replaces Au in β' -phase AuCd alloys, the β' phase is stabilized to lower temperatures (F. Rothwarf and L. Muldrew, *J. Appl. Physics*, 1962, 33, 2531). However, as the Ag content of AgAuCd⁵⁰ alloys is increased beyond 5 at.-%, the transformation product is no longer trigonal but orthorhombic. When Cu is added to β' -phase AuCd alloys the transformation pattern is reversed. As the Cu content of CuAuCd^{47.5} is increased, M_s falls rapidly. Beyond 0.5 at.-% Cu the product of the transformation is the trigonal phase and M_s is lower than 77° K at the 2.5 at.-% Cu concentration. Additions of Cu to AuCd⁴⁹ similarly reduce M_s but the transformation product is invariably trigonal. These results are discussed and it is concluded that the marked difference in transformation characteristics observed on the substitution of Cu for Au in β' -phase AuCd alloys, compared with the effect of Ag, is due to the increased ordering forces arising in the case of the Cu addition.

The binary systems resulting from the alloying of a noble metal with one of higher valency are characterized by the appearance of a so-called "electron compound" around an electron/atom ratio (e/a) of 3/2. The several structures in which this phase is seen have been studied by Hume-Rothery, Reynolds, and Raynor.¹ The most common of the possible structures are the body-centred cubic (ordered β' , or disordered β) the hexagonal close-packed (ζ' or ζ) and the β' -manganese type (μ). It would appear that the fundamental structure for the 3/2 electron compound is the hexagonal close-packed structure.²

Such phases are formed only when size-factors are reasonably favourable. Increasing the valency of the solute favours the μ or ζ phases at the expense of the β or β' structures, while increasing the temperature favours the β form at the expense of the others. An increase in size-factor displaces the β phases in the direction of lower e/a and narrows the range of composition in terms of e/a and temperature. The tendency to form β' structures on alloying a solute with a noble-metal solvent follows the series Cu < Ag < Au, i.e. in order of increasing electrochemical factor. A high electrochemical factor leads to ordering right up to the melting point as in the systems AuMg, AuCd, and AuZn. Thus,

ordered b.c.c. phases are favoured by a high electrochemical factor and the larger this factor, the more the electron compound will assume the character of a normal valency compound. However, as pointed out by Warlimont³, a large size-factor may also promote stable superlattice formation even in the absence of a marked electrochemical factor.

The b.c.c. phases tend to instability at low temperatures. This tendency has been analysed by Zener,⁴ who has noted that a shear in the $[110]$ direction in the (110) plane of a b.c.c. lattice leaves nearest-neighbour atoms unchanged to a first approximation and should, therefore, occur unimpeded in a b.c.c. packing of hard spheres. Now the equilibrium state of an alloy is characterized by a minimum value of the free energy, ΔG , which is given by

$$\Delta G = \Delta H - T\Delta S$$

where ΔH is the enthalpy, T the absolute temperature, and ΔS the entropy.

The amplitude of the thermal vibration resulting from such a low value of the shear modulus is large, and an entropy which is large compared with other structures is associated with the b.c.c. structures at high temperatures. Any increase in temperature produces a rapid decrease in ΔG because of the comparatively large $T\Delta S$ term. Thus the b.c.c. structure is stabilized at high temperatures, but may have a high energy relative to other close-packed structures at low temperatures. At low temperatures, therefore, mechanical instability would be expected involving a (110) $[110]$ shear mechanism.

As predicted by Zener,⁴ metals and alloys with the b.c.c. structure are often observed to transform at low temperatures in a diffusionless manner to a more closely packed structure. This phenomenon has evoked considerable interest and many investigations have been made to uncover the factors promoting this instability. The earlier work has been reviewed by King and Massalski.⁵ In particular it has been observed that M_s , the temperature at which transformation spontaneously begins, decreases as e/a increases.⁶ As mentioned earlier, a large size factor tends to displace the β -phase field to lower e/a concentrations; a large size factor has also been reported to favour the β phase over other structures.¹ In this connection the present authors⁷ have recently shown that as small ternary additions of various metals are made in replacement of cadmium in Au⁵⁰Cd alloys,* M_s decreases if

Manuscript received 26 February 1968. M. E. Brookes, B.Sc., and R. W. Smith, B.Sc., Ph.D., A.I.M., are in the Department of Physical Metallurgy and Science of Materials, University of Birmingham.

* Alloy compositions given in this paper as A^xB mean x at.-% A in B. In ternary alloys of varying compositions the figure is given for the component which is kept constant.

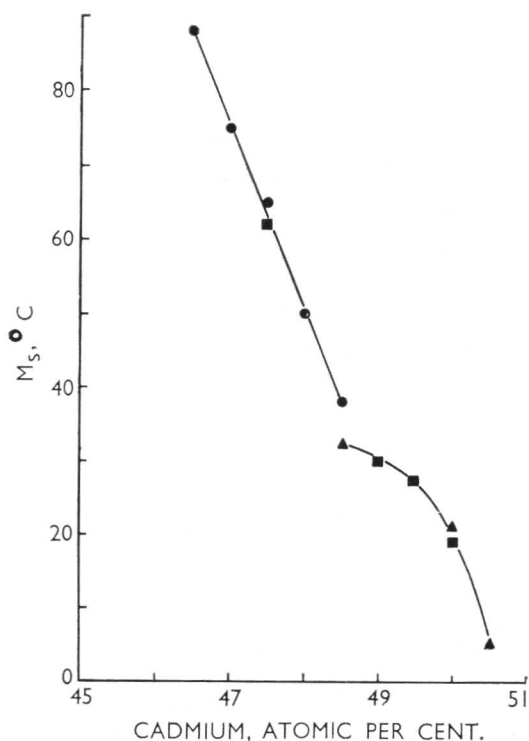


Fig. 1 The variation of the cubic \rightarrow orthorhombic and cubic \rightarrow trigonal M_s temperatures with composition for binary AuCd β' -phase alloys. After Nakanishi and Wayman.¹³

● Ahmed ▲ Mullendore ■ Nakanishi and Wayman

the atomic size of the ternary solute addition is smaller than that of the binary divalent constituent. However, it was also observed that electrochemical effects appeared to predominate and so, at times, M_s was actually reduced when the electronegativity between the ternary addition and gold was larger than that between cadmium and gold, although the atomic size of the ternary atom was larger. In view of this, the experiments to be described involving the replacement of the noble metal in AuCd alloys were undertaken, so as to further examine electrochemical influences on β -phase stability.

Long-range order persists to the melting point in the "3/2 electron compound" of AuCd.⁸ On simple cooling this ordered b.c.c. phase (β') transforms martensitically at all compositions.⁹ Alloys having compositions near AuCd^{47.5} transform at $\sim 60^\circ\text{C}$ on slow cooling to an orthorhombic phase.¹⁰ However, transformation of the AuCd⁴⁹ alloy occurs at $\sim 30^\circ\text{C}$ to give a phase which was earlier classified as tetragonal¹¹ but has more recently been identified as trigonal.¹² Fig. 1 shows the variation with composition of the cubic \rightarrow orthorhombic and cubic \rightarrow trigonal M_s temperatures for binary AuCd β' -phase alloys.¹³

Investigation of the β' phase occurring in the ternary AgAuCd system has recently been carried out by Rothwarf and Muldrew.¹⁴ A general depression of the cubic \rightarrow orthorhombic and cubic \rightarrow trigonal transformation temperatures was observed on replacing Au by Ag in AuCd^{47.5} and AuCd⁵⁰; this was interpreted in terms of ion-core overlap effects.

Experimental

The influence of Cu on the transformation characteristics of AuCd^{47.5} and AuCd⁵⁰ was carried out by measuring the electrical resistivity of polycrystalline samples over the range 78–400° K.

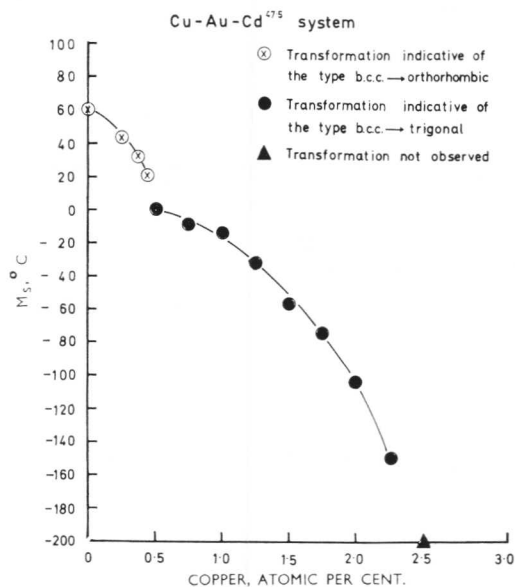


Fig. 2 The depression of M_s in AuCd^{47.5} on replacing Au by Cu.

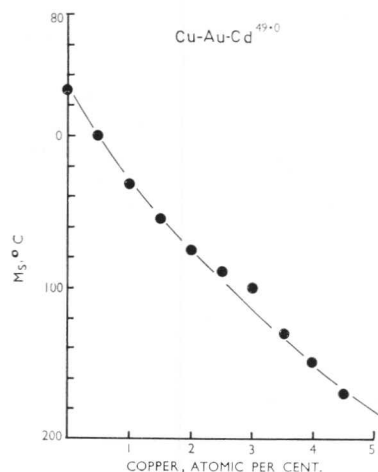


Fig. 3 The depression of M_s in AuCd^{49.0} on replacing Au by Cu.

To prepare the resistivity specimens, 2–3-g charges of accurately weighed constituent metals were sealed under argon in 5-mm-dia. silica tubes, melted, well shaken, and finally water-quenched. These small ingots were resealed in argon-filled silica tubes of similar dimension to which a 2-mm silica capillary was attached. On remelting, the molten alloy could be forced into the capillary by the differential pressure attained by cooling the far end of the capillary. Homogenization was carried out by annealing at 50 degC below the melting point of the alloy for 10 days, after which the alloys were furnace-cooled. Even with recasting, the loss in weight was < 1 part in 2000.

The cryostat used was of simple design and has been described elsewhere.¹⁵ The standard four-probe technique was used in conjunction with a constant-current source¹⁶ to determine resistivity. This arrangement, in conjunction with an X–Y recorder, permitted transformation curves to be plotted directly. The general depression of the M_s in AuCd alloys by the addition of Cu is shown in Figs. 2 and 3.

At.-% Cu	Temp., °C				Hysteresis, deg C
	M_s	M_f	A_s	A_f	
0.25	45	34	38	56	7.5
0.75	- 8	- 28	- 30	- 10	2.0
1.25	- 32	- 55	- 53	- 31	1.5
1.75	- 75	- 97	- 97	- 75	0

The nature of the transformation product forming in the CuAuCd alloys was established in two ways. In the binary AuCd alloy, transformation when $< 48.5\%$ Cd was present (to give an orthorhombic phase) was accompanied by a marked reduction in electrical resistivity; an opposite effect was observed for alloys containing $> 48.5\%$ Cd. Thus, the structure of the transformation product could easily be concluded from the shape of the resistivity vs. temperature plots. These conclusions were verified by X-ray diffraction.

It was also observed that the transformation hysteresis, $\frac{1}{2}[(A_s - M_f) + (A_f - M_s)]$, decreased as M_s fell (Table I).

Discussion

During any martensitic transformation "accommodation stresses" arise which promote reversibility. However, apart from "stabilization" effects, annealing can take place to reduce these stresses and so increase the transformation hysteresis. Because thermally activated redistribution of stresses would be negligible at low temperatures but would increase appreciably with temperature, transformation hysteresis would be expected to decrease as M_s decreases. This was observed in the present work, as also reported earlier for single-crystal studies.¹³

The change from orthorhombic to trigonal transformation product with increasing Cu content in alloys containing 47.5% Cd appears to be discontinuous. This is shown clearly in Fig. 2. The resistivity vs. temperature plots obtained for alloys with compositions near the transition region were always one or other of the characteristic forms, never in any case suggesting that transformation had taken place to a mixed product. However, Nakanishi and Wayman¹³ have examined the transformation characteristics of single crystals of AuCd^{47.5}, containing up to 1.5% Cu, using the resistivity technique. They observed mixed transformation characteristics for the 1.0% Cu alloy. The present authors consider that this result is attributable to macrosegregation during the growth of the crystals. Since virtually the whole of the as-grown crystal was used, significant macrosegregation would be expected and would be little affected by prolonged annealing. It may be seen from Fig. 2 that the transition from an orthorhombic product to the trigonal form took place over a composition range of $< 0.025\%$ Cu. Such a variation could result quite easily from the simple crystal-growing technique employed.

On thermodynamic grounds, the coexistence of both transformation products might be expected over a small temperature range since local changes in free energy would occur due to variations in the local state of strain. Swann

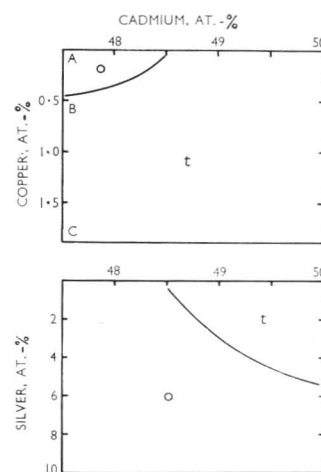


Fig. 4 The transformation fields of AgAuCd and CuAuCd alloys.

and Warlimont,¹⁷ using transmission electron microscopy, observed that two transformation products could coexist in a single martensitic plate of CuAl. This occurred over a composition range of 1 at.-%. However, in comparing these results with those of the CuAuCd alloys it is important to remember that the critical temperature for long-range order is only ~ 250 degC above the M_s , whereas in the CuAuCd alloys ordering persists to the melting point and, as will be discussed later, the ordering forces are considered to change markedly with Cu content. Thus the role of non-chemical factors is expected to be smaller in CuAuCd alloys.

It is convenient to represent the earlier results for AgAuCd alloys¹⁴ and the present results for CuAuCd alloys as the transformation fields shown in Fig. 4. The cubic \rightarrow orthorhombic transition temperature in AuCd^{47.5} is depressed at the rate of 80 degC/at.-% Cu (region AB), while M_s for the cubic \rightarrow trigonal change is reduced by ~ 60 degC/at.-% Cu (region BC) for both the AuCd^{47.5} and AuCd⁴⁹. In comparison, the M_s of AuCd^{47.5} is depressed by only 10 degC/at.-% Ag. Thus copper is considerably more potent than silver in increasing the structural stability of β' -AuCd.

It is seen from Fig. 4 that the transformation characteristics of the AgAuCd alloys are very different from those observed in the CuAuCd alloys. The clue to the different behaviour is presumed to lie with the different ordering forces present in the various alloys, particularly with respect to the occurrence of ordering at the noble-metal atom lattice sites. The electronegativity difference between Cu and Au promotes long-range order in binary CuAu, whereas no long-range order is found in AgAu alloys. This suggests that the ordering forces will be greater in CuAuCd alloys than in AgAuCd alloys. Unfortunately little ordering information is available for CuAuCd alloys, although AgAuCd alloys have been examined in this respect.¹⁴ However, the analogous situation involving the addition of Ag and Cu to AuZn alloys has been examined by Muldrew,¹⁸ who showed that long-range order persists to a relatively higher temperature when Cu is the ternary addition. He also noted that quenching partially suppresses AgAu ordering in AgAuZn₂ but not CuAu ordering in CuAuZn₂, and that cold work completely destroys noble-metal order in AgAuZn₂ but only partially affects CuAu ordering in CuAuZn₂. All this would support the contention that greater ordering forces exist in CuAuCd alloys than in AgAuCd alloys.